

AD-A059 526

TEXAS A AND M UNIV COLLEGE STATION MECHANICS AND MAT--ETC F/G 11/4
STUDIES ON THE MECHANICAL RESPONSE AND FRACTURE OF VISCOELASTIC--ETC(U)
JUL 78 R A SCHAPERY, J H SCHMIDT

AFOSR-74-2697

UNCLASSIFIED

MM-3064-78-6

AFOSR-TR-78-1257

NL

1 of 2
AD
A059 526



AFOSR-TR- 78 - 1257



Mechanics and Materials Research Center
TEXAS A&M UNIVERSITY
College Station, Texas

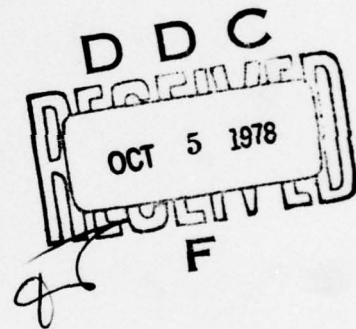
2

LEVEL II

STUDIES ON THE MECHANICAL RESPONSE AND FRACTURE OF
VISCOELASTIC COMPOSITE MATERIALS

R. A. SCHAPERY

J. H. SCHMIDT, JR.



AIR FORCE OFFICE OF SCIENTIFIC RESEARCH
OFFICE OF AEROSPACE RESEARCH
UNITED STATES AIR FORCE
GRANT NO. AFOSR 74-2697

MM 3064-78-6

JULY, 1978

APPROVED FOR PUBLIC RELEASE : DISTRIBUTION UNLIMITED

78 09 05 051

AD A059526

DDC FILE COPY

REPORT DOCUMENTATION PAGE		READ INSTRUCTIONS BEFORE COMPLETING FORM
1. REPORT NUMBER AFOSR TR-78-1257	2. GOVT ACCESSION NO.	3. RECIPIENT'S CATALOG NUMBER
4. TITLE (and Subtitle) STUDIES ON THE MECHANICAL RESPONSE AND FRACTURE OF VISCOELASTIC COMPOSITE MATERIALS.	5. TYPE OF REPORT & PERIOD COVERED FINAL Rept. 1 Jun 74 - 31 May 78	
7. AUTHOR(s) R. A. SCHAPERY J. H. SCHMIDT, JR	6. PERFORMING ORG. REPORT NUMBER MM-3064-78-6	
9. PERFORMING ORGANIZATION NAME AND ADDRESS TEXAS A & M UNIVERSITY MECHANICS AND MATERIALS RESEARCH CENTER COLLEGE STATION, TEXAS 77843	14. CONTRACT OR GRANT NUMBER(s) AFOSR-74-2697	
11. CONTROLLING OFFICE NAME AND ADDRESS AIR FORCE OFFICE OF SCIENTIFIC RESEARCH/NA BLDG 410 BOLLING AIR FORCE BASE, D C 20332	10. PROGRAM ELEMENT, PROJECT, TASK AREA & WORK UNIT NUMBERS 2307B2 B2 61102F	
14. MONITORING AGENCY NAME & ADDRESS (if different from Controlling Office)	12. REPORT DATE July 1978	
	13. NUMBER OF PAGES 140	
	15. SECURITY CLASS. (of this report) UNCLASSIFIED	
	15a. DECLASSIFICATION/DOWNGRADING SCHEDULE	
16. DISTRIBUTION STATEMENT (of this Report) (12) 144 p. Approved for public release; distribution unlimited.		
17. DISTRIBUTION STATEMENT (of the abstract entered in Block 20, if different from Report)		
18. SUPPLEMENTARY NOTES		
19. KEY WORDS (Continue on reverse side if necessary and identify by block number) FRACTURE SOLID PROPELLANT VISCOELASTICITY CRACK PROPAGATION COMPOSITES BONDING		
20. ABSTRACT (Continue on reverse side if necessary and identify by block number) This final report describes research activities conducted during the course of the grant. They were concerned generally with the analysis of cracks in particulate and fibrous viscoelastic media and the effect of cracks on the mechanical behavior of composites. The work is presented in five sections: 1) Elastostatic Fields in a Crack Tip Neighborhood-Measurements and Uniqueness; 2) On the Mechanical Behavior of Solid Propellant under Transient Temperatures; 3) Some Viscoelastic Crack Growth Relations for Orthotropic and Prestrained Media; 4) A theory of Time-Dependent Bonding for Viscoelastic Media; and 5) A method for Predicting Crack Growth in		

Nonhomogeneous Viscoelastic Media. Only abstracts and conclusions are given in the last three sections as the studies were previously published in separate reports.

UNCLASSIFIED

SECURITY CLASSIFICATION OF THIS PAGE(When Data Entered)

FOREWORD

Two studies completed during the final year of the grant are reported herein. The first one is entitled "Elastostatic Fields in a Crack Tip Neighborhood - Measurements and Uniqueness," which is essentially the doctoral dissertation submitted by J. H. Schmidt to Texas A&M University. The second study, which starts on page 110, is entitled "On the Mechanical Behavior of Solid Propellant under Transient Temperatures." Both investigations deal in part with the influence of small flaws or cracks on the mechanical behavior of solid propellant.

Work completed and published during prior years of the grant is then summarized on pages 126 - 133. Abstracts and conclusions are given for each of the three studies covered on these pages.

ACCESSION for	
NTIS	White Section <input checked="" type="checkbox"/>
DDC	Buff Section <input type="checkbox"/>
UNANNOUNCED	<input type="checkbox"/>
JUSTIFICATION	
BY	
DISTRIBUTION/AVAILABILITY CODES	
SPECIAL	
PA	

78 09 05 051

ELASTOSTATIC FIELDS IN A CRACK TIP NEIGHBORHOOD —
MEASUREMENTS AND UNIQUENESS.*

J. H. Schmidt, Jr.

ABSTRACT

Theoretical and experimental investigations of stress and displacement distributions in cracked solids are described. The effect of damaged material in the small highly stressed zone around a crack tip on maximum shear stress trajectories is first shown. Discussed next is experimental work consisting of tensile tests conducted with long rectangular strips of solid propellant clamped along the long edges and containing a central crack; displacements of the strip were obtained through speckle diffraction interferometry. These results are compared to predicted displacements using a finite element technique. Finally, a uniqueness theorem for weak elastostatic traction problems is proved; hypotheses in Kirchoff's uniqueness theorem are relaxed, and uniqueness is proved for a variety of singular problems including the crack problem.

*Based on a Ph.D. Dissertation submitted to Texas A&M University,
May, 1978.

TABLE OF CONTENTS

	Page
LIST OF FIGURES.	iv
INTRODUCTION	1
A REVIEW OF LINEAR ELASTIC FRACTURE MECHANICS.	4
General Development	4
Limitations of the Linear Elastic Solution.	12
AN ANALYSIS OF THE FINITE STRESS CRACK PROBLEM	17
General Discussion.	17
The Barenblatt Problem.	17
The Williams Problem.	21
The Combined Problem.	22
FINITE ELEMENT SOLUTIONS OF THE BIAXIAL STRIP.	33
Motivation.	33
Finite Element Analysis	33
FRACTURE TESTS	36
Samples and Equipment	36
Displacement Measurement Methods.	39
Speckle Diffraction Interferometry.	41
Results	51
Discussion of Results	53
COMPARISON OF THEORY AND EXPERIMENT.	60
A QUESTION OF UNIQUENESS	72

	Page
Motivation.	72
Classical Elastostatic Results.	73
Mathematical Preliminaries.	77
Uniqueness of Solution to the Traction Problem for Weak Elastostatic States.	83
CONCLUSIONS AND RECOMMENDATIONS.	95
REFERENCES	97
APPENDIX A	102
APPENDIX B	105
APPENDIX C	107
ACKNOWLEDGMENTS.	109

LIST OF FIGURES

	Page
Figure 1. Particulate composite, PBAN Propellant (300X).	2
Figure 2. Three modes of crack surface displacements; (a) Mode I, (b) Mode II, (c) Mode III.	6
Figure 3. Cross-section of an idealized crack.	15
Figure 4. Normal stresses acting along the crack plane.	16
Figure 5. Normalized grid deformations of the combined (finite stress) problem and Williams' problem for a constant failure stress.	24
Figure 6. Normalized grid deformations of the combined (finite stress) problem and Williams' problem for a ramp failure stress.	25
Figure 7. Nondimensionalized normal stresses of the combined problem along the crack plane for constant and ramp failure zone distribution.	26
Figure 8. Nondimensionalized normal stresses of the combined (finite stress) problem along the crack plane for constant and ramp failure zone distributions normalized to the constant failure zone stress intensity factor.	28
Figure 9. Far field isochromatic fringes for a constant failure zone stress.	29
Figure 10. Near field isochromatic fringes for a constant failure zone stress.	30
Figure 11. Far field isochromatic fringes for a ramp failure zone stress.	31
Figure 12. Near field isochromatic fringes for a ramp failure zone stress.	32
Figure 13. (a) Painted specimen (b) unpainted specimen.	37
Figure 14. Top (a) and side (b) views of bonding jig.	38
Figure 15. Speckle pairing (100x).	44
Figure 16. A schematic of laser speckle photography [57].	46

	Page
Figure 17. Specklegram recording equipment.	47
Figure 18. Specklegram interrogation equipment.	48
Figure 19. Modulated diffraction halo.	49
Figure 20. Fringe pattern recording equipment.	50
Figure 21. Crack tip before stress (a) 150X, (b) 60X. . . .	54
Figure 22. Crack tip after stresses 5% (a) 150X, (b) 60X.	55
Figure 23. Tensile stage and specimen used in SEM study. . .	58
Figure 24. Williams' grid deformations (solid curves) for the quarter biaxial strip compared to experimentally obtained results (O contains data points).	61
Figure 25. Williams' grid deformations (TEXGAP solution) for the quarter biaxial strip superposed with with Barenblatt's grid deformations for the infinite sheet compared with measured deformations (O contains data points) for both constant (dashed curves) and ramp (solid curves) failure stresses.	62
Figure 26. Modified Williams' grid deformations (TEXGAP solutions) for the quarter biaxial strip compared with measured deformations (O contains data points) for both constant (dashed curves) and ramp (solid curves) failure stresses.	63
Figure 27. Modified Williams' displacements for the quarter biaxial strip compared with measured displacements @ $y = .1$ inches with the vertical scale expanded by a factor of 10.	64
Figure 28. Modified Williams' displacements for the quarter biaxial strip compared with measured displacements @ $y = .2$ inches with the vertical scale expanded by a factor of 10.	65
Figure 29. Modified Williams' displacements for the quarter biaxial strip compared with measured displacements @ $y = .4$ inches with the vertical scale expanded by a factor of 10.	66

Page

- Figure 30. Modified Williams' displacements for the quarter biaxial strip compared with measured displacements @ $y = .6$ inches with the vertical scale expanded by a factor of 10. 67
- Figure 31. Modified Williams' displacements for the quarter biaxial strip compared with measured displacements @ $y = .8$ inches with the vertical scale expanded by a factor of 10. 68
- Figure 32. Modified Williams' displacements for the quarter biaxial strip compared with measured displacements @ $y = 1.0$ inches with the vertical scale expanded by a factor of 10. . . . 69

INTRODUCTION

There are two broad divisions of composite materials, particulate and fibrous [1]. This study is concerned primarily with the applicability of linear elastic theory in predicting elastostatic states near cracks in solid rocket propellant, a particulate composite material (Figure 1).

One's ability to predict these states and crack growth is essential when predicting the service life of particulate composite materials [2-4].

The relevance of this research becomes readily apparent when the effects of large cracks in rocket motors are investigated. Cracks in rocket motors increase propellant burning surfaces, thereby increasing the products of combustion with possible motor over pressurization resulting in catastrophic failure. Additionally, propagation of the crack through the propellant and motor exposing the motor casing to hot gases can also lead to failure [5].

A large number of investigators have studied crack propagation in linear materials with excellent reviews of these investigations given in [6,7].

Schapery [2-4] has investigated crack growth in a linear viscoelastic material. Swanson [8] indicated a reasonable measure of success in the use of Schapery's theory in predicting both initiation and subsequent velocity of crack propagation in PBAN solid propellant.

The format of this dissertation follows the style of the International Journal of Fracture.

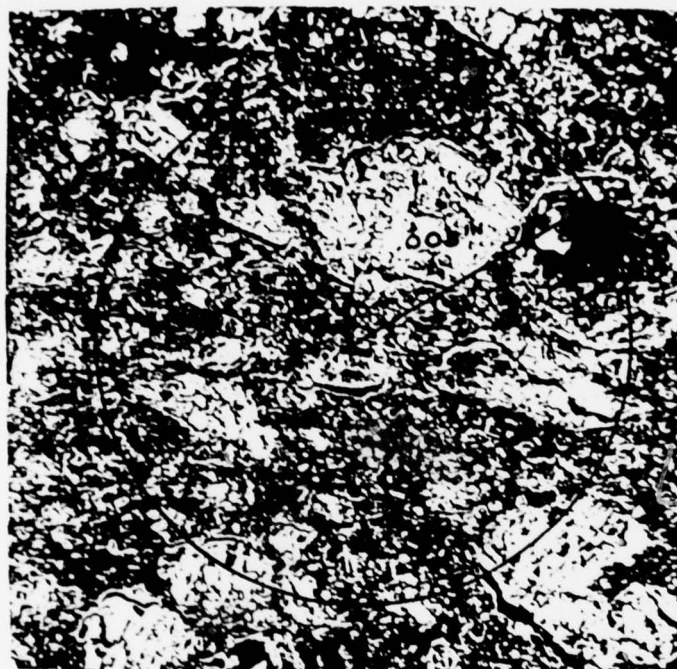


Figure 1. Particulate composite, PBAN Propellant (300X).

Previous investigators [9-11] have documented the nonlinear behavior of solid propellant; however, little or no work has been done to explain why, in some cases, a globally linear theory of fracture apparently predicts initiation and velocity of crack propagation in a globally nonlinear material.

The theories of fracture mechanics can be utilized to investigate, in part, this phenomenon. The work presented here begins with the classical works of Barenblatt [12] and Williams [13]. Displacements are then obtained, through a finite element code, by solving the classical linear elastic equations applied to a cracked biaxial strip — a long rectangular strip clamped along the long edges and containing a central crack. These numerically obtained displacements are compared to displacements measured on a cracked biaxial strip of PBAN propellant through a relatively new laser scheme, speckle diffraction interferometry.

Questions about uniqueness of solutions to elastostatic traction boundary value problems are addressed. A uniqueness theorem for bounded, locally star-shaped, regular domains is proven. The boundary value problem is cast in a "weak" sense (to be explained in a following chapter) requiring continuous displacements and absolutely integrable (in the Lebesgue sense) tractions over the boundary.

A REVIEW OF LINEAR ELASTIC FRACTURE MECHANICS

General Development

Since the beginning of the twentieth century there has been an increase in the number of articles published on fracture. There are three basic types of stress fields near crack tips [14], each associated with a specific mode of deformation, as illustrated in Figure 2. It is Mode I that we are concerned with in this work. For completeness, however, the stresses (σ_x , σ_y , τ_{xy}) and displacements (u , v , w) for all three modes are listed below as given by Irwin [15] (with r, θ the local polar coordinates in the x - y plane).

MODE I

$$\begin{aligned}
 \sigma_x &= \frac{K_I}{(2\pi r)^{1/2}} \cos \frac{\theta}{2} \left[1 - \sin \frac{\theta}{2} \sin \frac{3\theta}{2} \right] + \sigma_{ox} + \dots \\
 \sigma_y &= \frac{K_I}{(2\pi r)^{1/2}} \cos \frac{\theta}{2} \left[1 + \sin \frac{\theta}{2} \sin \frac{3\theta}{2} \right] + \dots \\
 \tau_{xy} &= \frac{K_I}{(2\pi r)^{1/2}} \sin \frac{\theta}{2} \cos \frac{\theta}{2} \cos \frac{3\theta}{2} + \dots \\
 \sigma_z &= \nu(\sigma_x + \sigma_y), \quad \tau_{xz} = \tau_{yz} = 0 \\
 u &= \frac{K_I}{\mu} \left[\frac{r}{2\pi} \right]^{1/2} \cos \frac{\theta}{2} \left[1 - 2\nu + \sin^2 \frac{\theta}{2} \right] + \dots \\
 v &= \frac{K_I}{\mu} \left[\frac{r}{2\pi} \right]^{1/2} \sin \frac{\theta}{2} \left[2 - 2\nu - \cos^2 \frac{\theta}{2} \right] + \dots \\
 w &= 0
 \end{aligned}
 \tag{1}$$

MODE II

$$\begin{aligned}\sigma_x &= -\frac{K_{II}}{(2\pi r)^{1/2}} \sin \frac{\theta}{2} \left[2 + \cos \frac{\theta}{2} \cos \frac{3\theta}{2} \right] + \dots \\ \sigma_y &= \frac{K_{II}}{(2\pi r)^{1/2}} \sin \frac{\theta}{2} \cos \frac{\theta}{2} \cos \frac{3\theta}{2} + \dots \\ \tau_{xy} &= \frac{K_{II}}{(2\pi r)^{1/2}} \cos \frac{\theta}{2} \left[1 - \sin \frac{\theta}{2} \sin \frac{3\theta}{2} \right] + \dots \\ \sigma_z &= \nu(\sigma_x + \sigma_y), \quad \tau_{xz} = \tau_{yz} = 0 \\ u &= \frac{K_{II}}{\mu} \left[\frac{r}{2\pi} \right]^{1/2} \sin \frac{\theta}{2} \left[2 - 2\nu + \cos^2 \frac{\theta}{2} \right] + \dots \\ v &= \frac{K_{II}}{\mu} \left[\frac{r}{2\pi} \right]^{1/2} \cos \frac{\theta}{2} \left[-1 + 2\nu + \sin^2 \frac{\theta}{2} \right] + \dots \\ w &= 0\end{aligned}\tag{2}$$

MODE III

$$\begin{aligned}\tau_x &= \frac{-K_{III}}{(2\pi r)^{1/2}} \sin \frac{\theta}{2} + \dots \\ \tau_{yz} &= \frac{K_{III}}{(2\pi r)^{1/2}} \cos \frac{\theta}{2} + \dots \\ \sigma_x &= \sigma_y = \sigma_z = \tau_{xy} = 0 \\ w &= \frac{K_{III}}{\mu} \left[\frac{2r}{\pi} \right]^{1/2} \sin \frac{\theta}{2} + \dots \\ u &= v = 0\end{aligned}\tag{3}$$

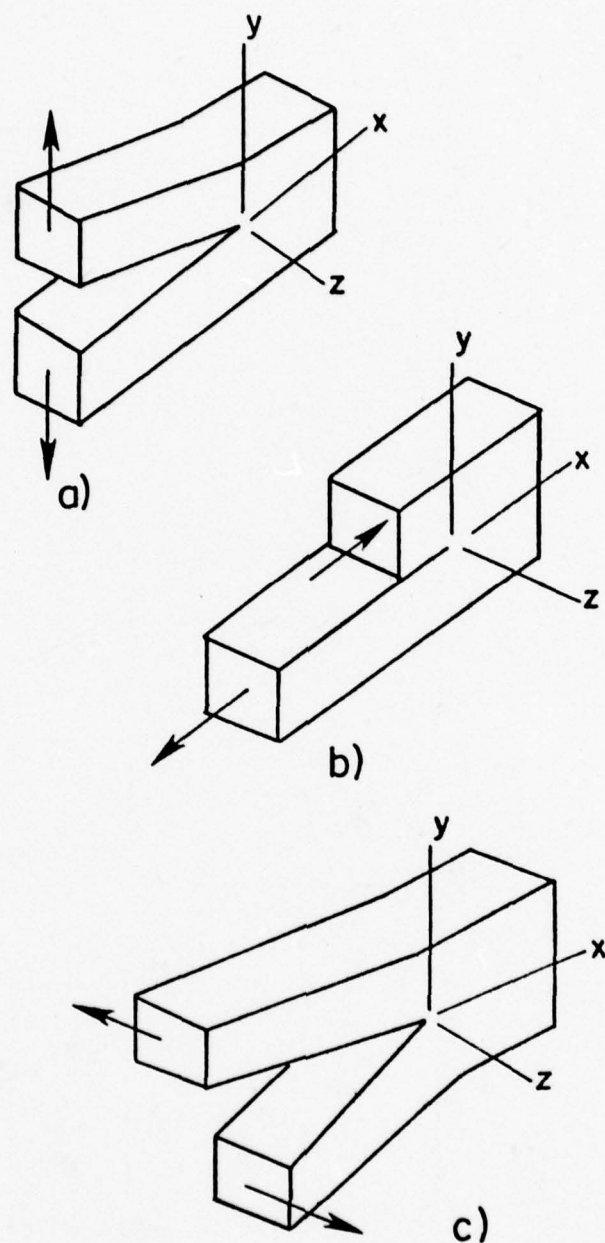


Figure 2. Three modes of crack surface displacements;
(a) Mode I, (b) Mode II, (c) Mode III.

The parameters K_I , K_{II} , and K_{III} are the stress intensity factors corresponding to the three modes of deformation while ν is Poisson's ratio and μ is the modulus of rigidity (shear modulus). It is important to note that while the stress intensity factors are independent of the coordinates r and θ , they are proportional to the loading forces and also depend on the configuration of the body [14].

There are two physically distinct types of plane elastostatic problems that we shall be concerned with; plane stress and plane strain (plane deformation).

The underlying assumption of the plane stress problem is that the surfaces of the object are stress free. This assumption together with the equilibrium equation implies $\frac{\partial \sigma_z}{\partial z} = 0$ along the strip surface (where the z -axis is normal to the surface). This suggests that, for a thin strip ($t/\beta \ll 1$ where t = strip thickness and β = any in-plane geometric dimension), $\sigma_z = 0$ [16].

The plane strain or plane deformation problem is characterized by $u = u(x,y)$, $v = v(x,y)$ and $w = 0$ where u , v , and w represent the displacements [16].

Displacements given by equations (1), (2), and (3) are for the case of plain strain and can be regarded as a good approximation in the region defined through $r/\beta \ll 1$ where β is the distance from the crack tip to the nearest geometric feature [17].

In the cracked plane problem, the stress field away from the crack tip can often be considered to be in a state of plane stress, while the stress field in the crack tip neighborhood suggests a state of plane strain [4, 17]. The plane stress and plane strain solutions differ only in the displacement fields; i.e., the in-plane stress

fields are identical [18]. In obtaining equations (1) — (3), Irwin [15, 20-22] used complex stress functions Z and $Z' = \frac{dZ}{dz}$ based on the method of Westergaard [19] that satisfy

$$\begin{aligned}\sigma_x &= \operatorname{Re} Z - y \operatorname{Im} Z' \\ \sigma_y &= \operatorname{Re} Z + y \operatorname{Im} Z' \\ \tau_{xy} &= -y \operatorname{Re} Z'\end{aligned}\tag{4}$$

Westergaard [19], using complex stress functions (for a modern treatise of complex stress functions, see for example, Timoshenko and Goodier [18], who closely follow Muskhelishvili [23]), solved the two-dimensional problem of a finite through-crack in an infinite sheet with $\sigma_x = \sigma$ at $|z| = \infty$.

It was shown by Sih [24] and by Eftis and Liebowitz [25] that the formulation by Westergaard, which was subsequently used by Irwin, was invalid for a class of problems dealing with an infinite medium containing finite cracks with loads applied at infinity. Both Sih, and Eftis and Liebowitz, proved that both σ_x and σ_y (equation (4)) must be modified by an additive constant. For example, in the opening mode problem, with the following boundary conditions applied to an infinite sheet containing a stress free interior crack [25],

$$\begin{aligned}\sigma_y(\infty) &= \sigma, \quad \sigma_x(\infty) = k\sigma, \quad \sigma_{xy}(\infty) = 0 \\ \text{at } |z| &= \infty,\end{aligned}\tag{5}$$

the following approximations for the plane strain crack tip stress and displacement fields are obtained [25]

$$\begin{aligned}
 \sigma_x &\approx \frac{K_I}{(2\pi r)^{1/2}} \cos \frac{\theta}{2} \left[1 - (\sin \frac{\theta}{2})(\sin \frac{3\theta}{2}) \right] - (1 - k)\sigma \\
 \sigma_y &\approx \frac{K_I}{(2\pi r)^{1/2}} \cos \frac{\theta}{2} \left[1 + (\sin \frac{\theta}{2})(\sin \frac{3\theta}{2}) \right] \\
 \sigma_{xy} &\approx \frac{K_I}{2\pi} (\sin \frac{\theta}{2})(\cos \frac{\theta}{2})(\cos \frac{3\theta}{2}) \\
 \mu u &\approx K_I \left[\frac{r}{2\pi} \right]^{1/2} \cos \frac{\theta}{2} \left[(1 - 2\nu) + \sin^2 \frac{\theta}{2} \right] \\
 &\quad - \frac{\sigma}{E} (1 - \nu^2)(1 - k)r \cos \theta \\
 \mu v &\approx K_I \left[\frac{r}{2\pi} \right]^{1/2} \sin \frac{\theta}{2} \left[(2 - 2\nu) - \cos^2 \frac{\theta}{2} \right] \\
 &\quad + \frac{\sigma}{E} \nu(1 + \nu)(1 - k)r \sin \theta.
 \end{aligned} \tag{6}$$

For the equal biaxial stress field, $k = 1$, it is clear that the additive constant term in the σ_x , u , and v equations (equation (6)) are zero.

Inglis [26], also in the context of classical elasticity theory presented the solution of an infinite sheet containing an elliptical cavity with the sheet subjected to a uniform stress field applied at infinity normal to the ellipse major axis. Inglis [26] then obtained the solution to the crack problem by requiring the minor axis of the ellipse to approach zero. Muskhelishvili [23] — also in the

framework of classical elasticity—solved, among others, the two-dimensional problem of a semi-infinite straight cut in an infinite sheet with the faces of the cut subjected to internal pressure.

A. A. Griffith [27], in a fundamental paper on the theory of cracks in brittle fracture, treated the problem of a finite crack in an infinite sheet acted upon by a uniform tensile stress, σ , at infinity. A critical stress, σ_0 , was determined at which the crack began to expand. Griffith's results were based on the work of Inglis [26] and an extension of the "theorem of minimum potential energy" by taking into account the increase in surface energy which occurs during crack growth.

Williams [13] studied the elastic stress distribution in the neighborhood of a crack under arbitrary loadings and showed the stresses to be of order $O(r^{-1/2})$ as $r \rightarrow 0$. Williams' solution was based on his earlier work [28] dealing with singularities in angular corners. In [28], Williams, using an Airy's stress function and a displacement function in the sense of Coker and Filon [29], solved the angular corner problem with stress free surfaces. In his later work, Williams [13] allowed the included angle of the angular corner to approach 2π . The resulting stress and displacement fields for the opening mode (Mode I) are given for plane strain in polar coordinates by the following expressions. (Williams solved the plane stress problem; however, as noted earlier, in the crack tip neighborhood a condition of plane strain exists.)

$$\begin{aligned}
\sigma_r(r, \theta) &= \frac{a_1}{4r^{1/2}} \left[-5 \cos \frac{\theta}{2} + \cos \frac{3\theta}{2} \right] + 4a_2 \cos^2 \theta + O\left(\frac{r}{\beta}\right)^{1/2} \\
\sigma_\theta(r, \theta) &= \frac{a_1}{4r^{1/2}} \left[-3 \cos \frac{\theta}{2} - \cos \frac{3\theta}{2} \right] + 4a_2 \sin^2 \theta + O\left(\frac{r}{\beta}\right)^{1/2} \\
\tau_{r\theta}(r, \theta) &= \frac{a_1}{4r^{1/2}} \left[-\sin \frac{\theta}{2} - \sin \frac{3\theta}{2} \right] - 2a_2 \sin 2\theta + O\left(\frac{r}{\beta}\right)^{1/2} \\
2\mu u_r(r, \theta) &= a_1 r^{1/2} \left[\left(-\frac{5}{2} + 4\nu\right) \cos \frac{\theta}{2} + \frac{1}{2} \cos \frac{3\theta}{2} \right] + O\left(\frac{r}{\beta}\right) \\
2\mu u_\theta(r, \theta) &= a_1 r^{1/2} \left(\frac{7}{2} - 4\nu \right) \left[\sin \frac{\theta}{2} - \frac{1}{2} \sin \frac{3\theta}{2} \right] + O\left(\frac{r}{\beta}\right)
\end{aligned} \tag{7}$$

where the quantity β represents the distance from the crack tip to the nearest geometric feature. It should be emphasized that Williams' solution (equation (7)) yields a square root singularity in stress regardless of external loadings and shape of the crack and body.

Williams' solution (equation (7)) and the corrected Irwin solution (equation (6)) are equivalent in the crack tip neighborhood for symmetric loadings when the constants a_1 and K_I are related through $a_1 = \frac{-K_I}{\sqrt{2\pi}}$ and $a_2 = -\frac{(1-\nu)\sigma}{4}$. Similarly, Williams' antisymmetric stress case (not shown here) is equivalent to Irwin's Mode II in the crack tip neighborhood under the substitution $b_1 = \frac{K_{II}}{\sqrt{2\pi}}$. These equivalences are shown in Appendix A for reference purposes.

Although Williams' expansion is not suitable for internal cracks, the method employed by Williams is readily extended to this case when the complex variable form is used [30, 31].

Limitations of the Linear Elastic Solution

In these early investigations the equations of linear elasticity were solved; i.e., Hooke's law and small displacement gradient theory were assumed. In the linear theory, particles close together relative to the size of geometric features are assumed to remain close together after deformation; however, when cracking occurs, this close neighborhood relation fails to hold. The solution to the linear elastic problem in these early investigations led to strains and stresses which were no longer small compared to unity; indeed, the strains and stresses become unbounded as the crack tip is approached, and the solution is simply not valid in this region [32].

There are three conditions which lead to singular solutions in an elastic medium [33]; geometric discontinuities, material discontinuities, and load discontinuities. Geometric discontinuities are of principal concern in this work and for discussions of this type of singularity the reader is referred to the work of Sternberg [33], Sternberg and Koiter [34], and England and Spencer [35].

The application of linear elastic solutions to the crack problem is validated by the exclusion of a small zone of such size and shape that the remaining region satisfies linearity. This zone is commonly referred to in the literature as the plastic, failure, process, or damage zone. This dissertation will refer to this zone, when in the form of a thin layer, as the failure zone of length α as shown in Figure 3.

A criterion (e.g. Griffith's energy criterion [26]) is needed to determine when crack growth occurs; i.e. when the crack boundary

undergoes a change. In this work we will be interested in stationary cracks.

To date, the modelling of crack tip material has been restricted to two approaches: a) the "particle approach" where individual atoms and interatomic forces are idealized through some mathematical model, and b) the "continuum approach" where mass is not concentrated in particles, but rather in small volumes. This latter model filters out many of the complexities of the former approach; however, in dealing with cracks, the microstructure behavior is helpful in the crack tip neighborhood in the interpretation of stress behavior in the failure zone. It is in this crack tip neighborhood that the continuum model falls short. Barenblatt [12] combines these two models.

We shall begin by following the lead of Barenblatt [12], Dugdale [36], and others, and postulate that the stresses in the elastic medium must remain finite—a physical condition. Following Schapery [2] we designate the stress in the failure zone as the failure stress distribution, σ_f .

Schapery [2-4] and Goodier [32] proposed a crack tip model mathematically similar but conceptually different—in the interpretation of the finite stress condition—to Barenblatt's crack tip model. Dugdale [36], in a study of the plastic zone at the end of a finite slit in an ideal elastic-plastic material, used the finite stress postulate in obtaining the plastic (failure) zone length.

It is interesting to note that Schapery [2] proved the equivalence of the cohesive force model and the elastic model of Williams [13] when the "failure zone" length of the cohesive force model

approaches zero. Rice [37] indicated that the energy criterion for fracture of the cohesive model reduced to the Griffith theory, regardless of the force attraction law, whenever the "failure zone" was small compared to characteristic dimensions.

Referring to Figure 3, the "apparent crack tip", following Schapery [2], is located by definition, at the point $x = -\alpha$, (though this location is often called the crack tip in the literature), while the crack tip is located at $x = 0$. All theoretical crack equations referred to in this work are written with respect to a coordinate system located at the crack tip; however, because of the difficulty in experimentally locating the crack tip, all experimental data is recorded relative to the apparent crack tip (cf. the chapter comparing theory and experiment). In order to study the effect of the failure zone on the stress and displacement fields we shall follow Schapery [2], who removed the stress singularity by considering a failure zone ahead of the apparent crack tip. The model used was obtained by superposing the solutions of Williams [13] and Muskhelishvili [23].

Schapery further extended the elastic solution to that of a viscoelastic medium via the correspondence principle. Although the undamaged portion of the continuum was assumed to be a linear, isotropic, viscoelastic medium, the material within the zone could be highly nonlinear; indeed, it need not even be a continuum, in that it could consist of strands of material as in Figure 3.

In Figure 4 the reaction of the failure zone on the linear continuum is shown, and is designated the "failure stress", σ_f .

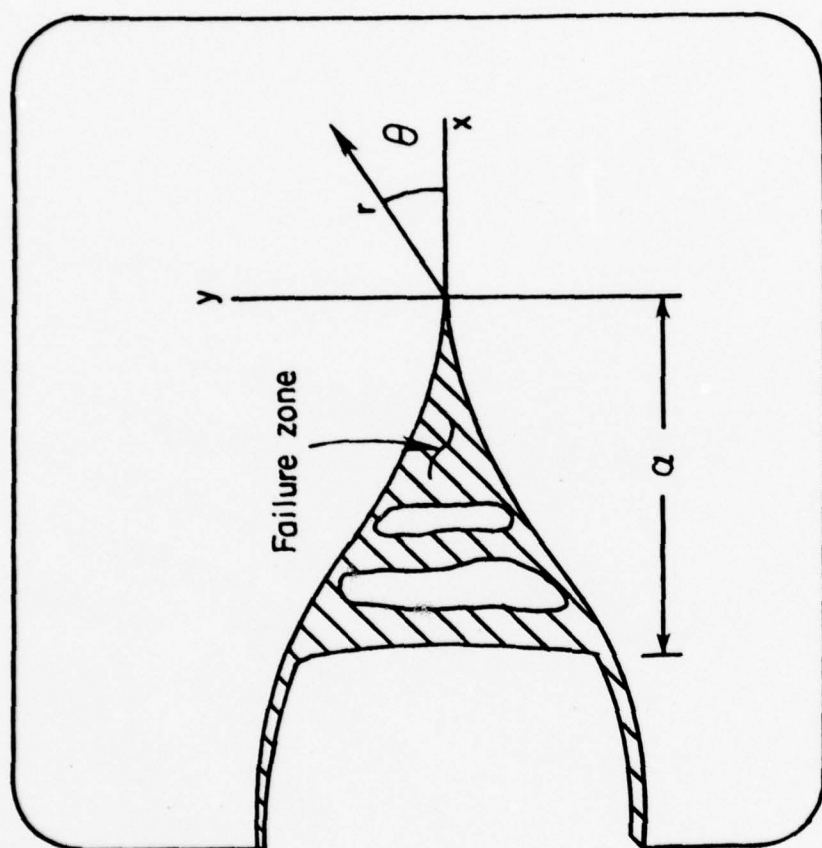


Figure 3. Cross-section of an idealized crack.

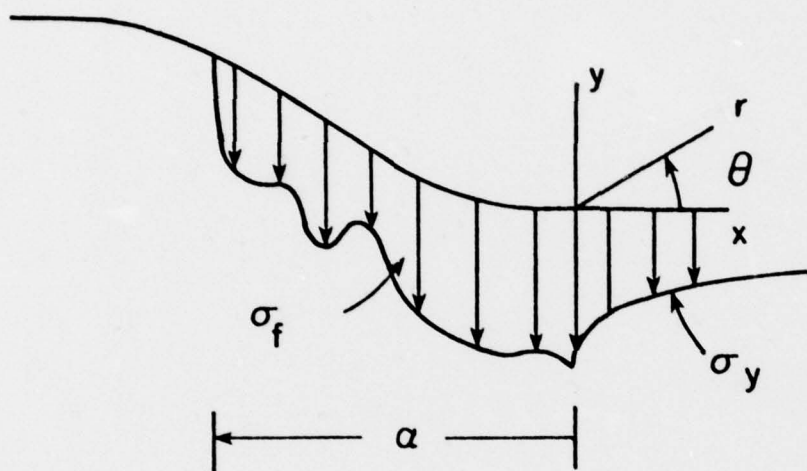


Figure 4. Normal stresses acting along the crack plane.

AN ANALYSIS OF THE FINITE STRESS CRACK PROBLEM

General Discussion

A detailed analysis of the combined Barenblatt and Williams problem will now be presented so that the effects of the failure zone on the stress and displacement fields can be determined.

Since closed form solutions to the crack problem only exist for the case of an infinite body, we will restrict our study to this case. In order to analyze the finite stress problem we shall first consider the stress and displacement fields of two singular problems. The first problem, solved by Barenblatt, involves an infinite body with a semi-infinite cut that is symmetrically loaded with normal stress, σ_f , along the surface of the cut. The second one is the elastic solution to the crack problem, given by Williams [13].

The Barenblatt Problem

From Barenblatt [12] we obtain the solution to the first. The solution is essentially that given by Muskhelishvili [23] restricted to normal stresses acting along the surface of the cut,

$$\sigma'_x + \sigma'_y = 4 \operatorname{Re} \phi(z) \quad (8)$$

$$\sigma'_y - i\sigma'_{xy} = \phi(z) + \Omega(z) + (z - \bar{z}) \overline{\phi'(z)}$$

with displacements

$$2\mu(u' + iv') = k \phi(z) - \omega(\bar{z}) - (z - \bar{z}) \overline{\phi'(z)} \quad (9)$$

where for plane strain, $k = 4 - 3\nu$.

The analytic functions ϕ , ω , Φ , and Ω are expressed through

$$\phi(z) = \Omega(z) = \phi'(z) = \omega'(z) = \frac{1}{2\pi i \sqrt{z}} \int_0^{\infty} \frac{\sqrt{t} \sigma_f(t)}{t - z} dt \quad (10)$$

$$\phi(z) = \omega(z) = \frac{1}{2\pi i} \int_0^{\infty} \sigma_f(t) \ln \left(\frac{\sqrt{t} + \sqrt{z}}{\sqrt{t} - \sqrt{z}} \right) dt$$

The following failure stress distributions, σ_f , will be considered.

$$\begin{aligned} \text{a) } \sigma_f(t) &= \sigma_m \quad t \in [0, \alpha] \\ &= 0 \quad \text{otherwise} \end{aligned} \quad (11a)$$

$$\begin{aligned} \text{b) } \sigma_f(t) &= -\frac{\sigma_m}{\alpha} t + \sigma_m \quad t \in [0, \alpha] \\ &= 0 \quad \text{otherwise} \end{aligned} \quad (11b)$$

These stress distributions are for a crack along the positive real axis since Barenblatt's [11] and Muskhelishvili's [23] work are cast in this way. The solution of Williams [13] is for the crack along the negative real axis

For a crack along the positive real axis, the branch cut for the "multivalued" functions $\ln(\cdot)$ and $(\cdot)^{1/2}$ is also along the positive real axis. This poses no real problem, even though we need to superpose the two solutions. We can define $z = -x + iy$ which in effect places the crack, and thereby the branch cut, along the negative real

axis. Additionally, by physical reasoning, the shear stresses and the displacements in the x-direction of the Barenblatt solution must undergo a sign change.

We seek the elastostatic state corresponding to the failure stress distribution of equation (11a). We need to find the analytic function, $\phi(z)$. Towards this end consider

$$\frac{\partial}{\partial t} \left\{ (t - z) \ln \left(\frac{\sqrt{t} + \sqrt{z}}{\sqrt{t} - \sqrt{z}} \right) + 2\sqrt{z} \sqrt{t} \right\} = \ln \left(\frac{\sqrt{t} + \sqrt{z}}{\sqrt{t} - \sqrt{z}} \right) \quad (12)$$

whenever $z \neq t$. Equation (12) implies

$$\int_0^\alpha \ln \left(\frac{\sqrt{t} + \sqrt{z}}{\sqrt{t} - \sqrt{z}} \right) dt = (\alpha - z) \ln \left(\frac{\sqrt{\alpha} + \sqrt{z}}{\sqrt{\alpha} - \sqrt{z}} \right) + 2\sqrt{z} \sqrt{\alpha} + i\pi z. \quad (13)$$

It can be shown that equation (13) is valid for all $z \neq \alpha$, by using the usual definition of the improper integral. The function ϕ defined by

$$\phi(z) = \frac{\sigma_m}{2\pi i} \left[\left(1 - \frac{z}{\alpha}\right) \ln \left(\frac{1 + \sqrt{z/\alpha}}{1 - \sqrt{z/\alpha}} \right) + 2\sqrt{z/\alpha} + i\pi z/\alpha \right] \quad (14)$$

can be shown to be analytic everywhere in the complex plane except along the branch cut (the positive real axis). Because of the analyticity of ϕ we may write

$$\phi'(z) = \frac{\sigma_m}{2\pi i} \left[\frac{2}{\sqrt{z/\alpha}} - \ln \left(\frac{1 + \sqrt{z/\alpha}}{1 - \sqrt{z/\alpha}} \right) + i\pi \right] \quad (15)$$

$$\phi''(z) = -\frac{\sigma_m}{2\pi i} \left(\frac{1}{\alpha} \right) \left[\frac{1}{(z/\alpha)^{3/2}} + \frac{1}{(z/\alpha)^{1/2}} \left(\frac{1}{1 - z/\alpha} \right) \right] \quad (16)$$

Equations (8), (9), (14), (15), and (16) give the state of stress for the Barenblatt problem when σ_t is defined as in equation (11a).

Now we turn our attention to the Barenblatt problem when the failure stress distribution is given by equation (11b).

As before, we must find ϕ for the given failure stress distribution. Consider the following,

$$\begin{aligned} \frac{\partial}{\partial t} \left\{ (t - z) \ln \left(\frac{\sqrt{t} + \sqrt{z}}{\sqrt{t} - \sqrt{z}} \right) - \frac{(t^2 - z^2)}{2\alpha} \ln \left(\frac{\sqrt{t} + \sqrt{z}}{\sqrt{t} - \sqrt{z}} \right) + 2\sqrt{z}\sqrt{t} \right. \\ \left. - 1/3 \frac{\sqrt{z}t^{3/2}}{\alpha} - \frac{z^{3/2}\sqrt{t}}{\alpha} \right\} = (1 - \frac{t}{\alpha}) \ln \left(\frac{\sqrt{t} + \sqrt{z}}{\sqrt{t} - \sqrt{z}} \right) \end{aligned} \quad (17)$$

whenever $z \neq t$. Clearly

$$\begin{aligned} \int_0^\alpha (1 - \frac{t}{\alpha}) \ln \left(\frac{\sqrt{t} + \sqrt{z}}{\sqrt{t} - \sqrt{z}} \right) dt = \alpha \left[(1 - \frac{z}{\alpha}) \ln \left(\frac{1 + \sqrt{z/\alpha}}{1 - \sqrt{z/\alpha}} \right) \right. \\ \left. - \left(\frac{1 - (z/\alpha)^2}{2} \right) \ln \left(\frac{1 + \sqrt{z/\alpha}}{1 - \sqrt{z/\alpha}} \right) + \frac{5}{3} \sqrt{z/\alpha} - \left(\frac{z}{\alpha} \right)^{3/2} \right. \\ \left. + i\pi \left(\frac{z}{\alpha} - \frac{1}{2} \left(\frac{z}{\alpha} \right)^2 \right) \right] \end{aligned} \quad (18)$$

whenever $z \neq \alpha$. The resulting function ϕ is

$$\begin{aligned} \phi(z) = \frac{\sigma_m \alpha}{2\pi i} \left[\left(1 - \frac{z}{\alpha} \right)^2 \ln \left(\frac{1 + \sqrt{z/\alpha}}{1 - \sqrt{z/\alpha}} \right) + \frac{5}{3} \sqrt{z/\alpha} - \left(\frac{z}{\alpha} \right)^{3/2} \right. \\ \left. + i\pi \left(\frac{z}{\alpha} - \frac{1}{2} \left(\frac{z}{\alpha} \right)^2 \right) \right] \end{aligned} \quad (19)$$

which is analytic everywhere in the complex plane except along the

branch cut (the positive real axis). Because of the analyticity of ϕ ,

$$\phi'(z) = \frac{\sigma_m}{2\pi i} \left[\left(\frac{z}{\alpha} - 1 \right) \ln \left(\frac{1 + \sqrt{z/\alpha}}{1 - \sqrt{z/\alpha}} \right) + \frac{4}{3} \frac{1}{\sqrt{z/\alpha}} - 2\sqrt{z/\alpha} + i\pi \left(1 - \frac{z}{\alpha} \right) \right] \quad (20)$$

$$\phi''(z) = \frac{\sigma_m}{2\pi i} \left(\frac{1}{\alpha} \right) \left[\ln \left(\frac{1 + \sqrt{z/\alpha}}{1 - \sqrt{z/\alpha}} \right) - 2 \left(\frac{1}{\sqrt{z/\alpha}} \right) - \frac{2}{3} \left(\frac{1}{(z/\alpha)^{3/2}} \right) - i\pi \right] \quad (21)$$

Equations (8), (9), (19), (20) and (21) completely define the stress and displacement fields to the Barenblatt problem with a failure stress distribution given as the ramp function in equation (11b).

The Williams Problem

The polar stresses and displacements (equation (7)) given by Williams must now be written as rectangular components of stress and displacement so that they may be superposed with the rectangular stress and displacement components given in the Barenblatt solution.

We seek u and v , the rectangular components of the Williams solution (equation (7)). By a coordinate transformation we obtain

$$\begin{aligned} u &= (\cos \theta) u_r - (\sin \theta) u_\theta \\ v &= (\sin \theta) u_r + (\cos \theta) u_\theta \end{aligned} \quad (22)$$

Timoshenko and Goodier [18] related the rectangular stresses, $(\sigma_x, \sigma_y, \tau_{xy})$, to the polar stresses $(\sigma_r, \sigma_\theta, \tau_{r\theta})$ through

$$\begin{aligned}
\sigma_x &= \sigma_r(\cos^2\theta) + \sigma_\theta(\sin^2\theta) - 2\tau_{r\theta} \sin\theta \cos\theta \\
\sigma_y &= \sigma_r(\sin^2\theta) + \sigma_\theta(\cos^2\theta) + 2\tau_{r\theta} \sin\theta \cos\theta \\
\tau_{xy} &= (\sigma_r - \sigma_\theta)\sin\theta \cos\theta + \tau_{r\theta}(\cos^2\theta - \sin^2\theta)
\end{aligned} \tag{23}$$

by equilibrium considerations. Equation (23) can also be obtained through a coordinate transformation of the second order stress tensor.

The Combined Problem

Next, we add the solution of Williams [13] (equations (7), (22), (23)), for the case of equal biaxial loading, i.e. $a_2 = 0$ in equation (7), and Barenblatt [12] (equations (8), (9), (10)). The stress state obtained from the addition of two stress states is an application of the method of superposition. Superposition is possible as a result of the linearity of the system of governing partial differential equations, cf. Sokolnikoff [16]. This addition, together with the finite stress postulate, yields a relatively simple expression relating K_I and σ_f [4,32],

$$K_I = \left(\frac{2}{\pi}\right)^{1/2} \int_0^\alpha \frac{\sigma_f(\xi)}{\xi^{1/2}} d\xi. \tag{24}$$

For the failure stresses considered in this work (equations (11)), the relationship between K_I and σ_f (equation (24)) results in

$$K_I = 2\left(\frac{2}{\pi}\right)^{1/2} \sigma_m \tag{25a}$$

for the failure stress in equation (11a), and

$$K_I = \frac{4}{3} \left(\frac{2\alpha}{\pi} \right)^{1/2} \sigma_m \quad (25b)$$

for the failure stress associated with equation (11b).

The elastostatic state corresponding to the stress distributions of equations (11) is obtained through the superposition of equations (7), (8), (9) (where $a_1 = -K_I/2\pi$ in equation (7)) together with the finite stress conditions of equations (25a) and (25b). Figures 5 and 6 compare the grid deformations for these combined problems, corresponding to equations (11a) and (11b) respectively, to the grid deformations given by the Williams' solution. Particular attention is drawn to the deformations near the crack tip, which show the opposite faces of the crack surface closing smoothly in a cusp-like fashion, a result due to the finite stress condition (13). The nondimensionalized normal stresses acting along the crack plane are shown in Figure 7, which graphically illustrates the continuity of $\frac{\sigma_y}{\sigma_m}$ at the crack tip.

Since the stress intensity factor is determined by geometry (including crack size) and loading conditions [14], it is reasonable to normalize the stress fields corresponding to the different failure stress distributions (equations (11a) and (11b)) with respect to the same stress intensity factor. This is accomplished for the ramp and constant failure stress distributions by equating equations (24) and (25) and by associating σ_m with a specified maximum strength.

This results in different failure zone lengths which are related through $\alpha \Big|_{\text{ramp}} = \frac{9}{4} \alpha \Big|_{\text{constant}}$. The effect of the two failure stress distributions are displayed

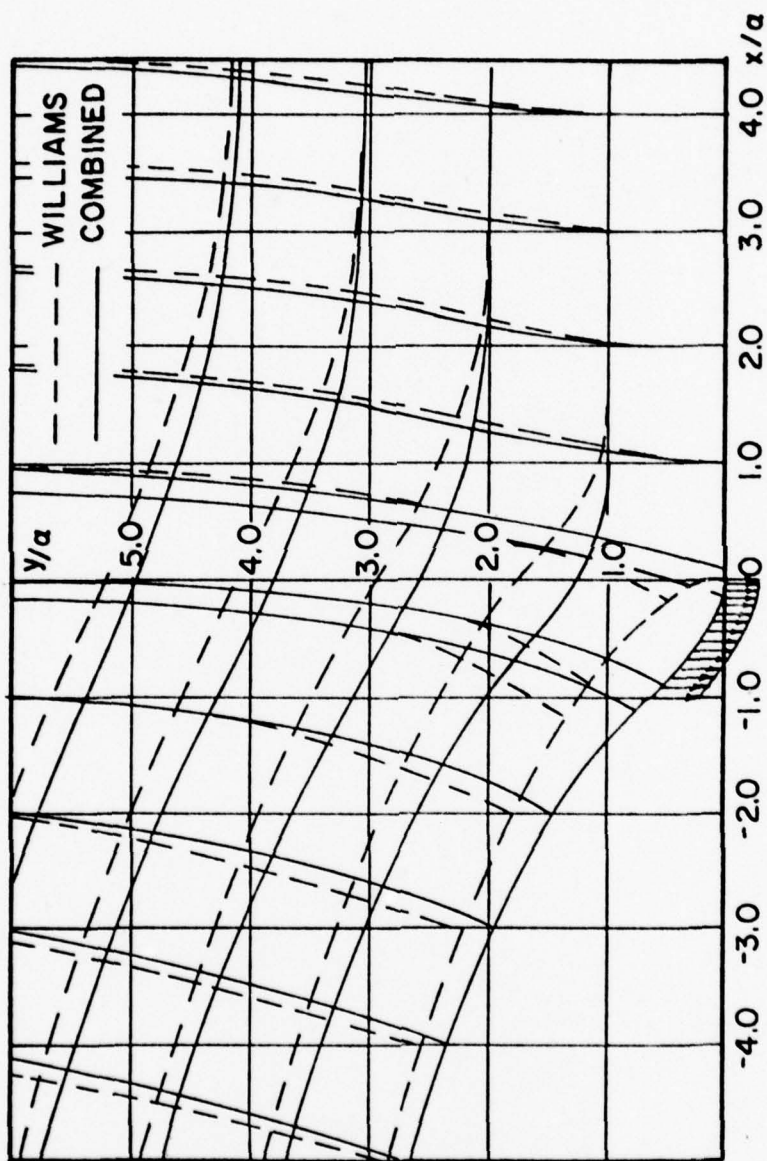


Figure 5. Normalized grid deformations of the combined (finite stress) problem and Williams' problem for a constant failure stress.

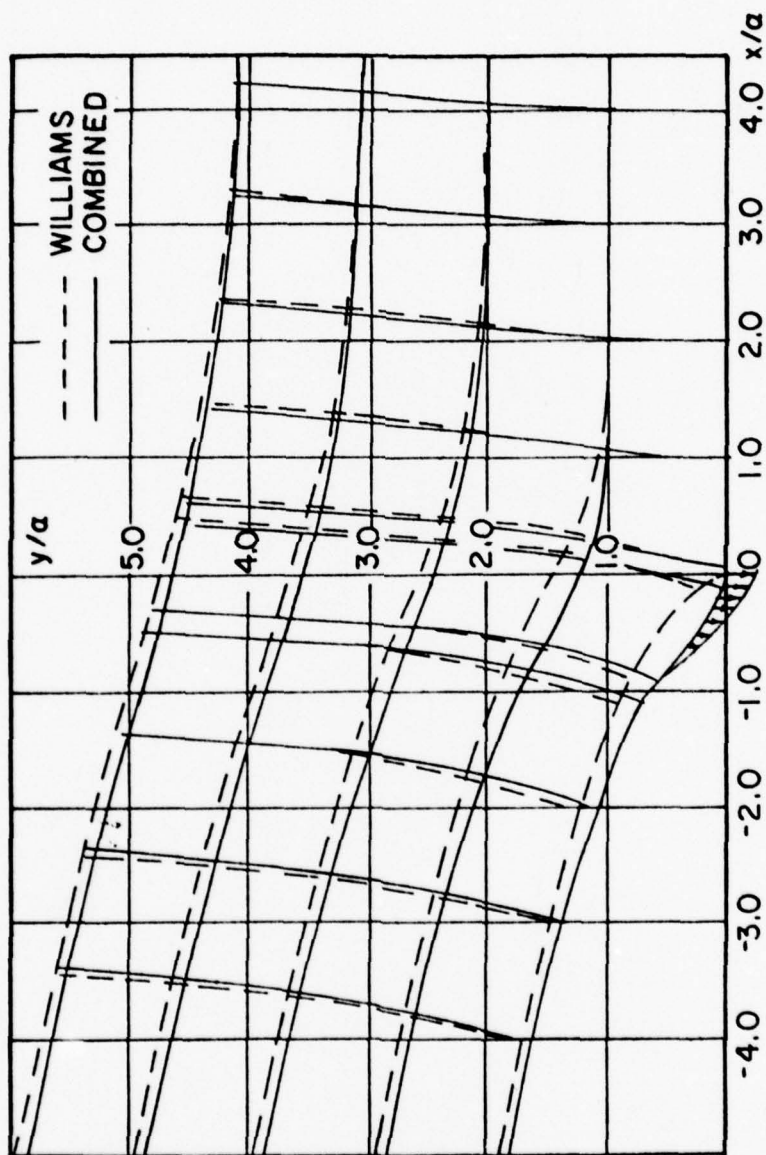


Figure 6. Normalized grid deformations of the combined (finite stress) problem and Williams' problem for a ramp failure stress.

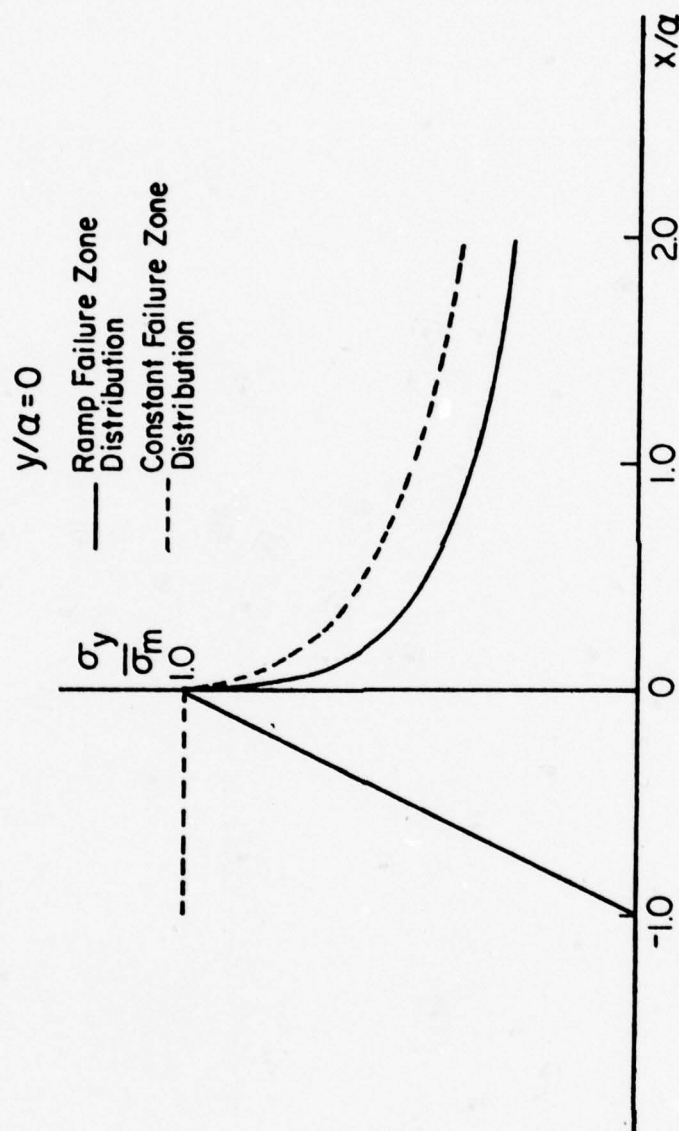


Figure 7. Nondimensionalized normal stresses of the combined problem along the crack plane for constant and ramp failure zone distributions.

in Figure 8, which indicates the dominance of the Williams singularity term along the plane of the crack after a distance of approximately 5α .

Figures 9-12 compare the isochromatic fringe patterns* of the singular Williams solution to that of the combined problem for both the constant and ramp failure zone stresses. The tilting of the isochromatic lines is due solely to the cohesive zone and cannot theoretically be answered through the addition of a constant term to the singular term in Williams' σ_x expansion, since, as previously discussed, this term is zero for equal biaxial loadings.

For the case of uniaxial tension applied to a plate with an edge crack, the tilting effect of the isochromatic fringes was explained by previous investigators [38-40] through the addition of a constant to the singular term of the Williams' σ_x expansion. That the constant term in the σ_x expansion must be included is a theoretical reality [24, 25]; however, whether or not the isochromatic fringe tilting is due exclusively to this term with no regard to the cohesive zone depends on the scale of this zone.

In Figures 9 and 10 the isochromatic fringes touch the crack plane at $x/\alpha = -1.0$ because of the finite stress discontinuity ($\frac{\sigma_y}{\sigma_m} \rightarrow 0$ as $x/\alpha \rightarrow -1.0$ from the left and $\frac{\sigma_y}{\sigma_m} \rightarrow 1$ as $x/\alpha \rightarrow -1.0$ from the right) of the constant failure stress distribution. These illustrations show that the shape of the isochromatic fringes in the crack tip neighborhood is very dependent on the failure stress distribution.

*These patterns are the maximum shear stress trajectories.

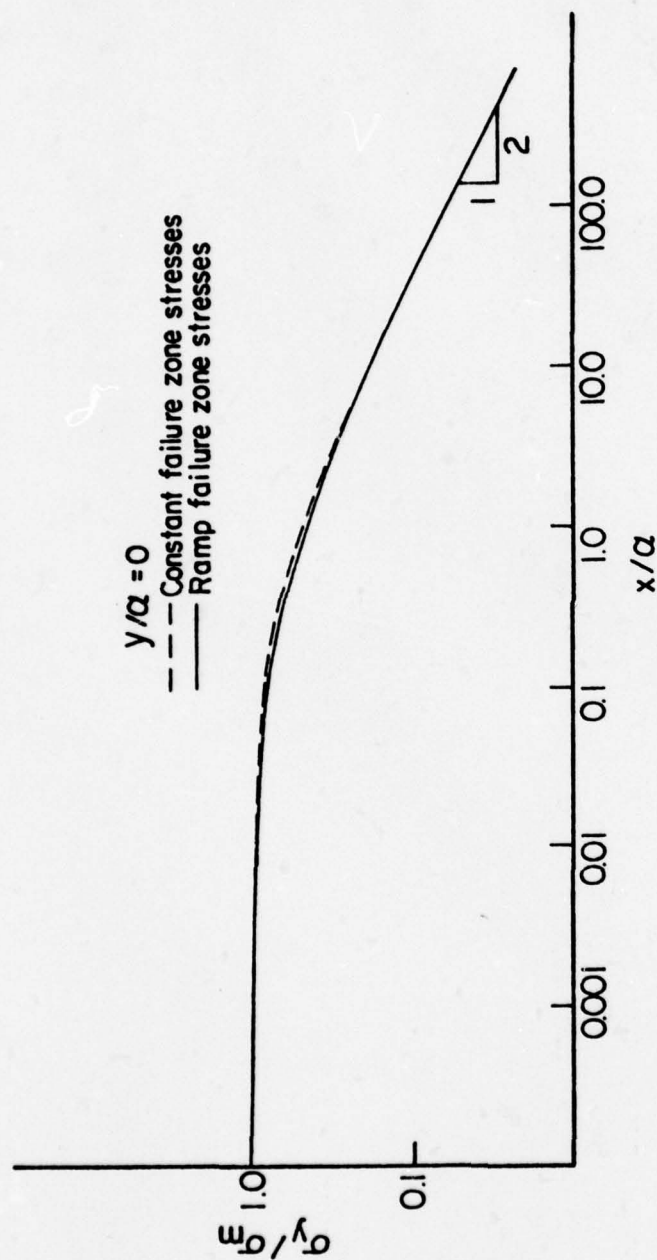


Figure 8. Nondimensionalized normal stresses of the combined (finite stress) problem along the crack plane for constant and ramp failure zone distributions normalized to the constant failure zone stress intensity factor.

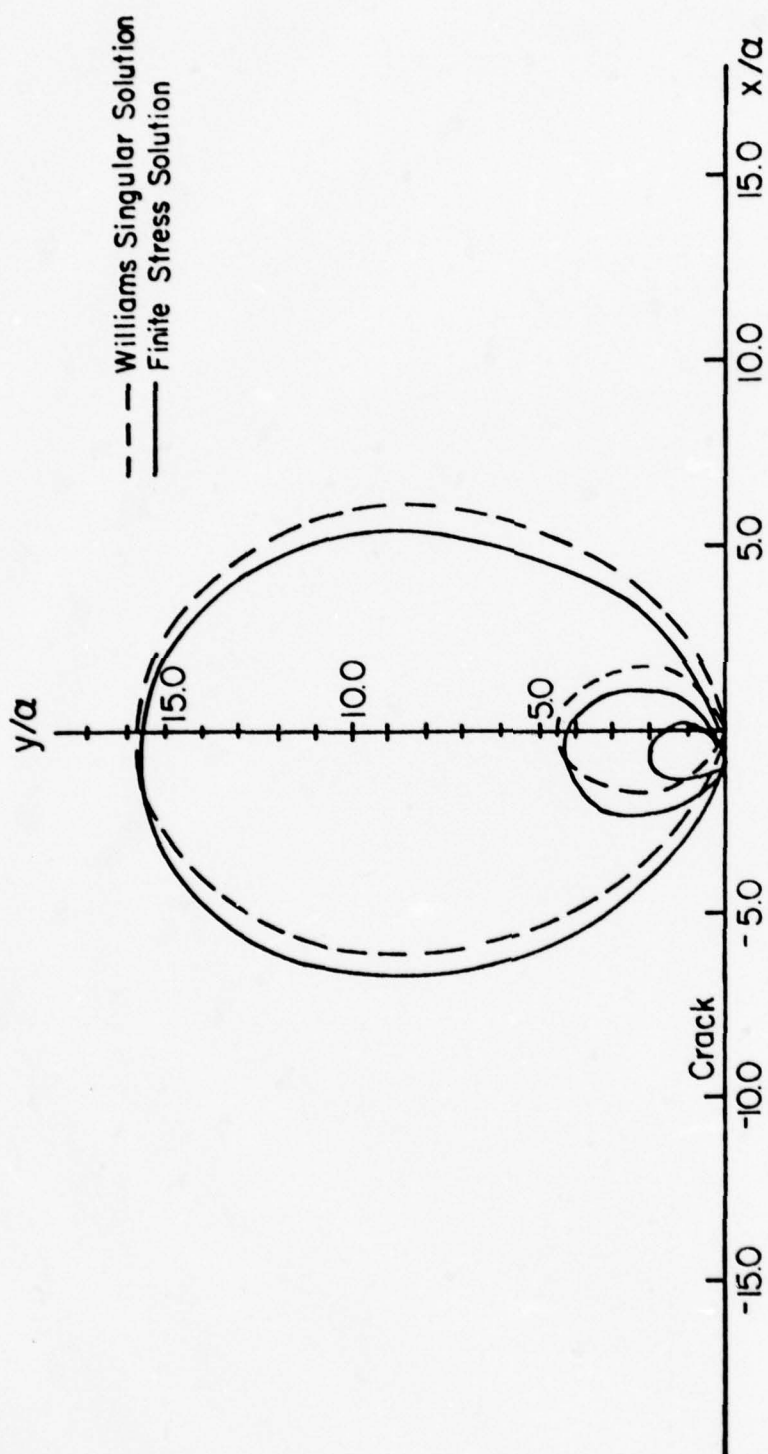


Figure 9. Far field isochromatic fringes for a constant failure zone stress.

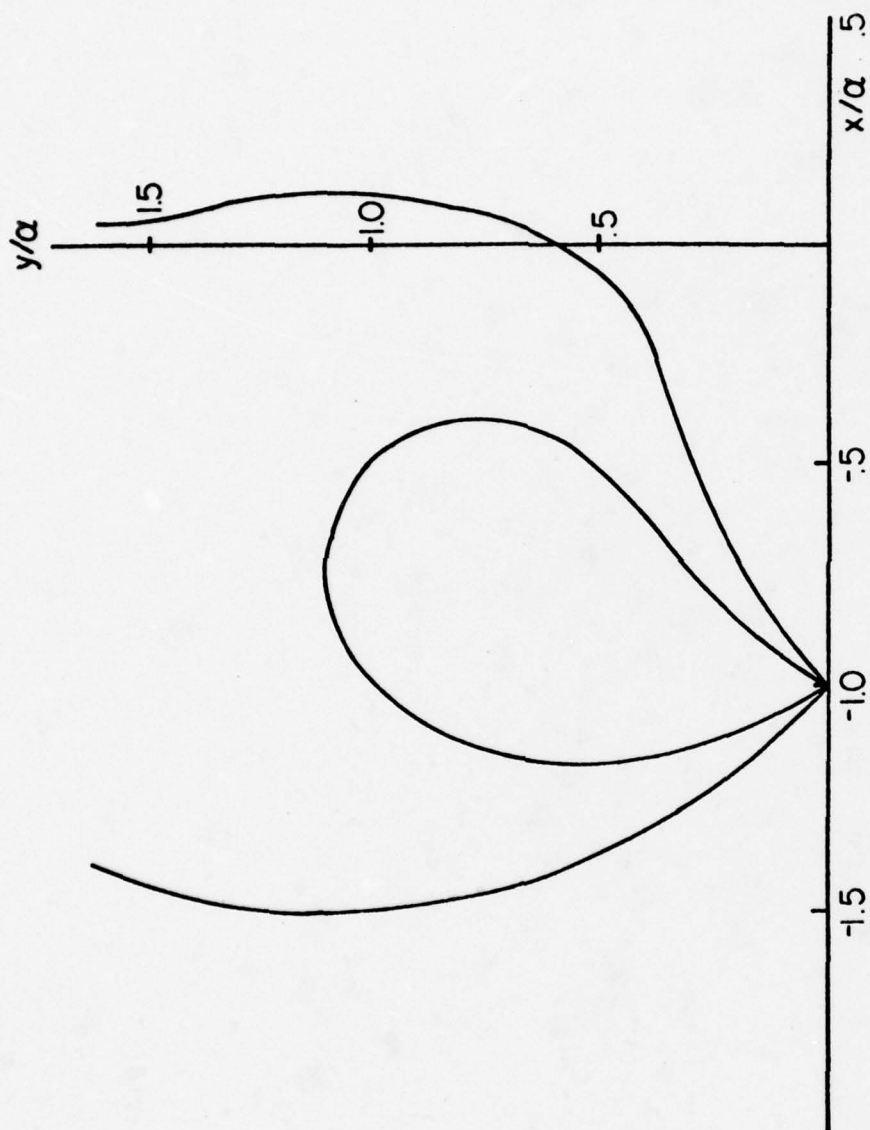


Figure 10. Near field isochromatic fringes for a constant failure zone stress.

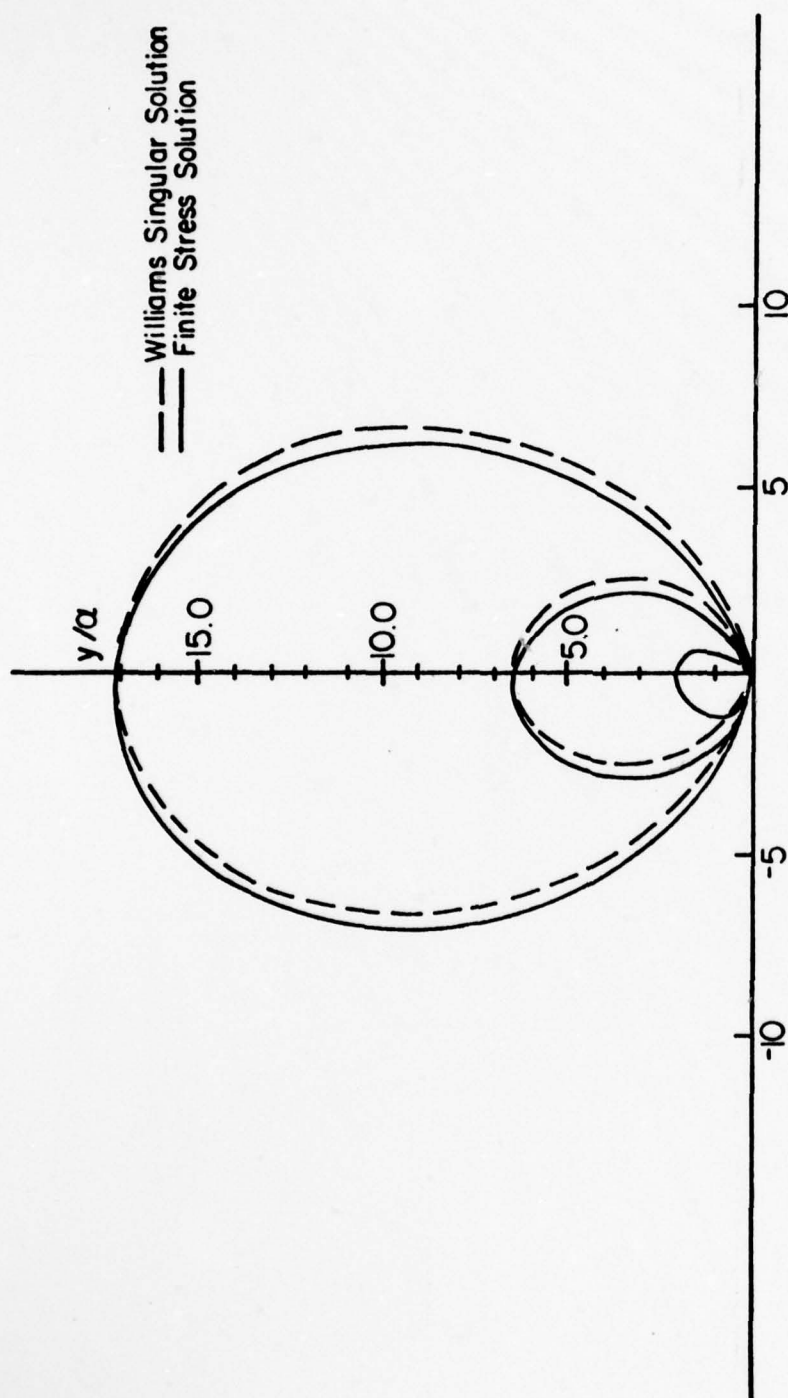


Figure 11. Far field isochromatic fringes for a ramp failure zone stress.

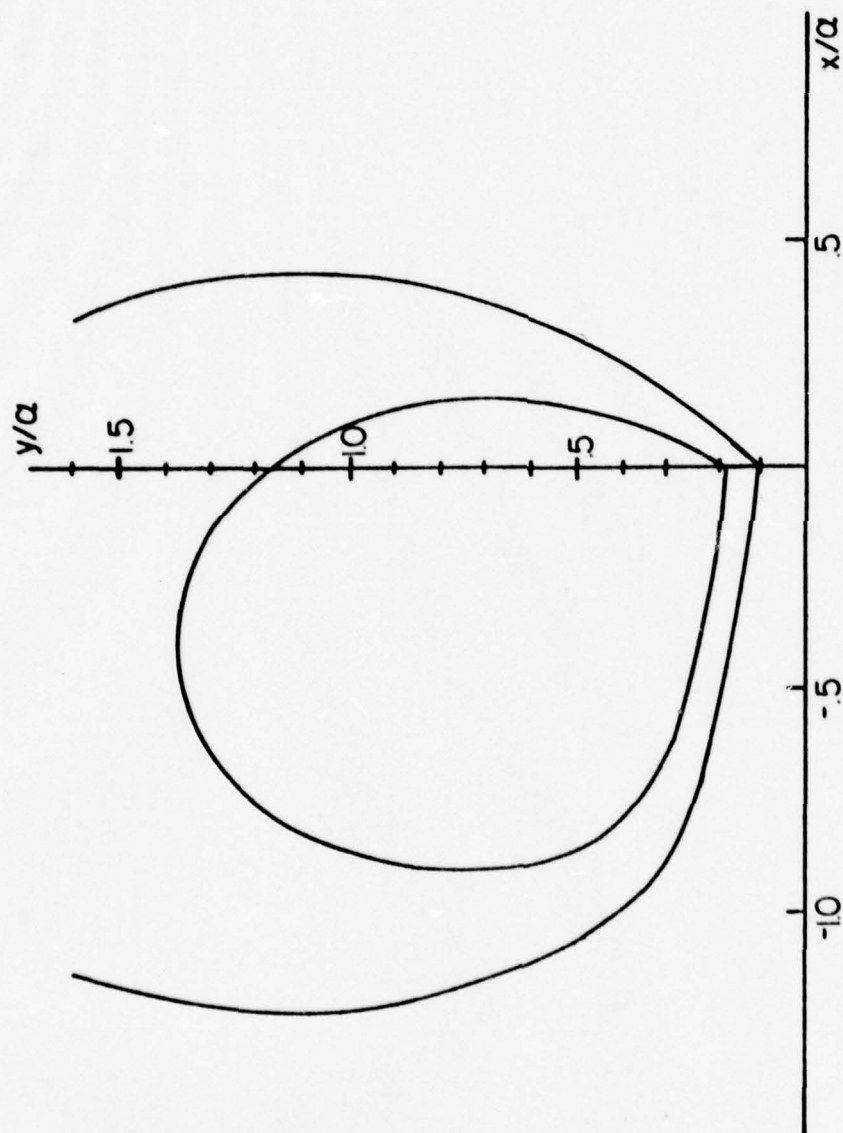


Figure 12. Near field isochromatic fringes for a ramp failure zone stress.

FINITE ELEMENT SOLUTIONS OF THE BIAXIAL STRIP

Motivation

The most crucial part of this work is the experimental verification of analytical results. Inasmuch as linear theory is used we come to the question of its validity in the practicing engineering environment.

The cracked infinite sheet problem could, in principle, be approximated in the laboratory. This approach would be, at best, cumbersome. An alternative to this approach is the numerical solution to a more easily handled geometry with more readily applied boundary conditions.

The exact solution to many boundary value problems of elasticity in engineering often presents formidable mathematical difficulties, due to the complicated form of the physical boundary conditions. It is noteworthy, in technical applications of the theory of elasticity, that for many problems only a mathematical approximation to the physical boundary conditions exist. The resulting solution then represents only an approximation to the physical problem. The finite element method can provide solutions based on an improved approximation of the physical boundary conditions.

Finite Element Analysis

Numerically obtained displacement fields and grid deformations were compared to experimentally determined displacement fields and grid deformations. These numerical solutions were calculated

by means of an existing finite element code.

Due to the symmetry of the chosen test geometry only a quarter of the biaxial strip was analyzed. Following Conrad [41], The Texas Grain Analysis Program (TEXGAP) [42] (a finite element program originally developed for analyzing solid rocket propellant), was used to numerically analyze the quarter biaxial strip. There are standard texts which discuss the finite element method (cf. Prenter [43], Strang and Fix [44], Oden and Reddy [45]). For many boundary value problems, an energy inner product exists (related to the potential energy of an appropriate physical system) whose minimum with respect to some admissible class of functions is the solution to the boundary value problem. This energy formulation, when applied to a body which is approximately using discrete volume or area elements, is referred to as the finite element method.

Three numerical problems were solved for a cracked biaxial strip with dimensions of 2 inches by 7 inches. A comparison of each of the three numerical problems with experimental data is recorded and discussed following a discussion of the experimental work.

First, the problem of a 1.5 inch crack in a biaxial strip with no failure zone (the square root singular solution) was solved. The second type of problem investigated was a superposition of the solution to the first problem (with crack lengths of 1.7 inches and 1.9 inches), and the solution to the Barenblatt infinite sheet problems discussed previously (with failure zone lengths of .1 inches and .2 inches respectively). At this point it was felt that a more refined numerical problem not requiring the superposition of a geometrically

finite problem with that of a geometrically infinite problem should be solved. Therefore, the third problem was solved by linking the failure stress distribution with the TEXTGAP solution through the finite stress condition (equation (24)) as shown in Appendix B.

The plane stress mode of the TEXTGAP code was used since, as previously indicated, the sheet, except for a small neighborhood about the crack tip, is approximated by the plane stress hypothesis.

The generation of the crack elements by the TEXTGAP program is discussed by Conrad [41] and also by Dunham and Becker [42]. The elements generated by TEXTGAP in solving the quarter biaxial strip problem in this work are rectangular and are shown later when a comparison of theory and experiment is made.

FRACTURE TESTS

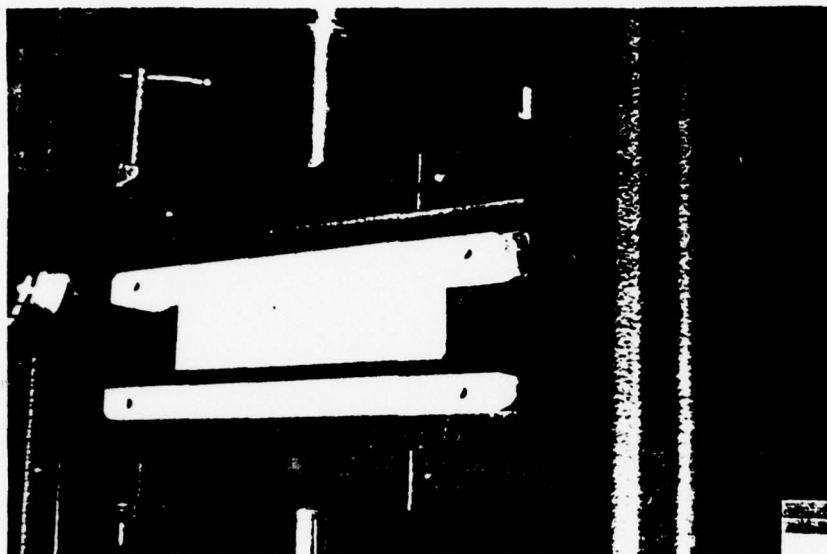
Samples and Equipment

Composite solid propellant consists of a rubber matrix filled with hard particles. The propellant used in this investigation was polybutadiene acrylonitrile (PBAN) containing 66% by volume ammonium perchlorate with a particle size range of 20-100 microns and 10% by volume aluminum powder with particle size on the order of 10 microns. The samples were provided by the Air Force Rocket Propulsion Laboratory. They were stored in a controlled climatic environment of 75°F and 25% relative humidity prior to testing.

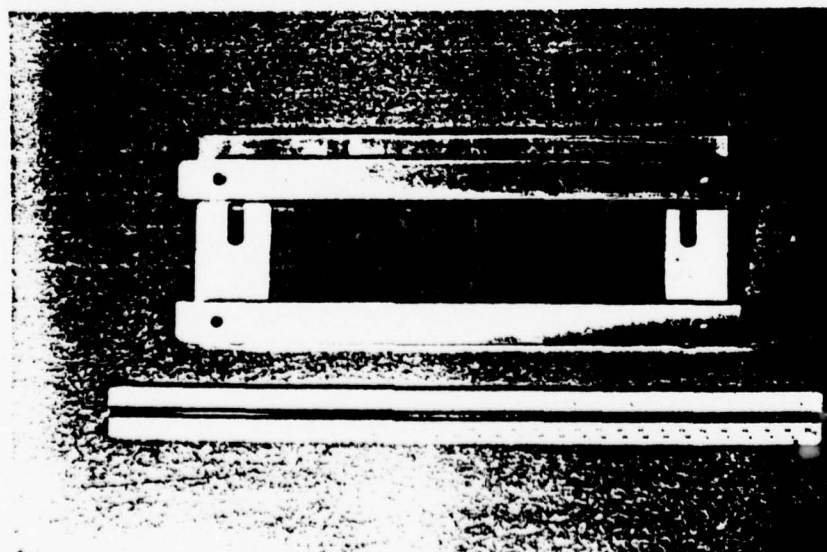
The geometry of the test specimen chosen for the experiments reported herein was that of the biaxial strip as shown in Figure 13. The nominal sizes of the specimen were 2 inches X 7 inches with thicknesses of .125 and .2 inches.

Samples were bonded between two stainless steel bars. The bonding jig used to position the sample relative to the steel bars is shown in Figure 14. The jig was designed so that a micrometer could be used to center the sample to within $\pm .002$ of an inch.

One face of the sample was bonded to one bar and allowed to cure; then, the sample was removed from the jig, turned up side down, and the opposite face bonded to the remaining stainless steel bar. The two steel bars were kept from compressing the sample during this second bonding operation by two precision 1/2 inch X 2 inch pins placed between the two opposing steel bars. The epoxy used through-

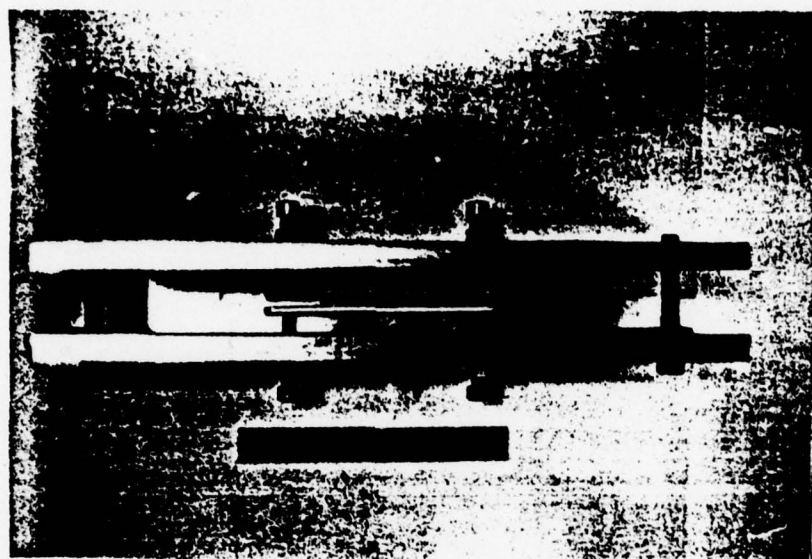


a)



b)

Figure 13. a) Painted specimen b) unpainted specimen.



a)



b)

Figure 14. Top (a) and side (b) views of bonding jig.

out this work was Versamid 125 hardener and R-815 resin with a hardener to resin mixing ratio of 2 to 3 (by volume). All specimens had a curing time of over 24 hours. Prior to bonding, the stainless bars were cleaned with acetone and then treated with M-Prep Conditioner A and B.

After samples were bonded, a rigid aluminum plate was attached to the steel bars preventing premature sample straining.

Flat white Krylon paint was sprayed on the specimen surface prior to testing to enhance interferometric fringes—the experimental method employed to measure displacements. During the painting process the paint can was held approximately 30 inches from the specimen surface in an attempt to minimize the paint thickness by mist spraying the specimen. The effect of the painting technique is addressed in a later section.

Finally, a crack was cut using a vertical milling machine to press a razor blade through the sample. A crack cut in this fashion could be placed within .005 of an inch from the specimen center.

Displacement Measurement Methods

We now address the experimental problem of displacement field measurements. Of the methods used for measuring displacements, the following were considered most promising: (i) Moire', (ii) a pattern recognition technique utilizing a microdensitometer, and (iii) speckle diffraction interferometry.

A close examination of the Moire' technique reveals some obvious disadvantages, the foremost being the need to apply a grid to the

specimen surface. The grid pattern must be of the highest quality with regard to line straightness, uniformity of pitch, contrast, and uniformity of line to space ratio. At the same time, the pattern must have the necessary line density to achieve required sensitivity [46].

There are several methods available for grid application, among them are photographic etching, machine ruling, and transferable grids.

Photoetching is a delicate procedure, and imperfect photographic reproduction of the master grid can produce large errors in strain. Moreover, sensitizers, developing materials, and dyes used in the photoetching procedure (e.g. ammonia perchlorate) act as desiccants, altering the chemical and/or physical properties of the sample. However, Hart [47] employed a method which for propellant samples apparently overcomes these difficulties by using a diazo-type photo-sensitive material together with ammonia vapors. Hart, using a grid of 500 lines/in, found that an average strain of 9.2% was required to obtain meaningful fringes. By comparison, using speckle diffraction interferometry, the present tests had average strains of .2%.

The most promising grid application is that of grid transfer. The best available grid transfers have grid densities on the order of 2000 lines/in. [48], resulting in a displacement sensitivity of 500 μ inches. On the other hand, the interferometric technique has a displacement sensitivity of 40 μ inches. Additionally, excessive specimen distortion can occur due to adhesion between the transfer grid and specimen when the adhesion modulus is on the order

or greater than the specimen modulus.

The microdensitometer technique at first seems very promising; however, it is very expensive both in initial expense and subsequent computer expense. Furthermore, it does not appear to be as accurate as the interferometry technique. Essentially, two film negatives are needed, one before and one after deformation. The microdensitometer is used to digitize the film negatives by assigning numbers ranging from 1 to 400 ($\pm 1\%$) corresponding to light intensity transmitted through the negative [49]. The instrument records approximately 300 density units per second, with software permitting incremental step sizes between 1 μm and 255 μm ($\pm 2 \mu\text{m}$) [49]. A pattern recognition technique is then used to obtain displacements.

The method ultimately chosen was that of speckle diffraction interferometry, which will now be described.

Speckle Diffraction Interferometry

A brief review of some basic concepts of light will define the terms needed to describe the interferometric process. Light may be regarded as an electromagnetic disturbance, as characterized through Maxwell's equations [50]. A disturbance moving in the z -direction with velocity c has the form [51]:

$$A \sin \left(\frac{2\pi}{\lambda} (z - ct) + \phi \right)$$

where A is the amplitude (A^2 is called the intensity), λ the wave length, t the time, and ϕ the phase angle of the disturbance. The receiver of the electromagnetic disturbance (retina, photographic

plate, photomultiplier, etc.) responds only to intensity and is insensitive to variations of phase [52]. A continuous series of sinusoidal cycles is called a wave train. Two wave trains are said to add constructively when the peaks and valleys of the two trains coincide in the spatial dimension, and are said to add destructively when the peaks of one coincide with the valleys of the other. Constructive addition of wave trains reinforces and increases brightness (intensity), while destructive interference tends to cancel the disturbances with an apparent reduction in brightness (intensity).

When a wave train is divided by a beam splitter and reunited, it can form interference fringes provided the difference between the two path lengths is less than the effective length of the characteristic wave train. Light which is capable of interference is called "coherent", and the characteristic wave train length is called the "coherent length".

The coherent length of lasers is several feet, while that of a typical light source is on the order of 1 mm [51]. This explains why holography did not become an important tool until after lasers became readily available in the 1960's. An excellent review of holography is given by Gabor [53], while a good physical introduction to holography is given by Brown [54]. Reviews of interferometry can be found in [55-57].

Consider a diffuse surface illuminated by highly coherent light. Any point in front of the surface receives contributions of light reflected from all illuminated points on the surface. When such a surface is viewed by an observer, it appears to have a grainy or

speckled appearance due to random interference. If the surface is then allowed to undergo a displacement, a new speckle pattern is formed corresponding to the displaced material points of the surface. If a double exposure of a photonegative is made, and the negative then developed, we have a recording of the two speckle patterns resulting in the speckle pairing shown in Figure 15. The speckle size is proportional to the wave length of the illuminating light and the numerical value of the recording device's lens aperture [58]. The governing relationship of the speckle diameters is given by [59]:

$$d \approx \lambda F (1 + M) \quad (26)$$

where λ is the illuminating light wave length, F the camera f- stop number, and M the camera lens magnification. For the helium-neon laser used in this work ($\lambda = 6328 \text{ \AA}$) the resolving power of the emulsion on the photographic plate had to be at least $1300/F$ lines per mm [58, 59]. In photographic film (plate), the higher the resolving power of the film (plate), the longer the exposure time required [60].

The interrogation of a double exposure "specklegram" (photonegative) consists of illuminating the specklegram with coherent light from the laser and observing the light intensity distribution on a screen placed so as to collect light transmitted through the specklegram. The resulting intensity distribution collected on the screen can be shown to be numerically equal to the diffraction halo from a single exposure transparency, modulated by



Figure 15. Speckle pairing (100x).

Young's fringes [61]. A schematic of the interferometric technique is shown in Figure 16, while the equipment used in the specklegram recording and interrogation are shown in Figures 17 and 18 respectively. The specklegram was made at Texas A&M, while the interrogation of the specklegram was done on equipment at the Flight Dynamics Laboratory in Ohio. Notice that recording is performed on an optical steady table to isolate the test system from surrounding noises.

The modulated diffraction halo (Figure 19) is predicted by the Fraunhofer diffraction integral which is, apart from a multiplicative factor, a Fourier transform [61]. The Fraunhofer diffraction integral applies to parallel light rays and is a specialization of the more general Fresnel-Kirchoff integral [55].

The magnitude of the displacement field of the specklegram at the point of interrogation is then obtained through the simple algebraic equation

$$\delta = \frac{(n - 1/2)\lambda M}{\sin \alpha} \quad (27)$$

where n is the number of intensity minimums, M the magnification of the specklegram, λ the wave length of the interrogating beam and α the fringe minimum angular displacement.

The fringe pattern was recorded by a linear silicon diode (9 inches by 1 inch) and plotted with the Varian F80A x-y plotter shown in Figure 20. Two stepping motors moved the specklegram past a rigid laser beam in a scanning process. Data point locations on the specklegram were recorded with an accuracy of $\pm .01$ inches (.02 inches on the specklegram since $M = 1/2$).

LASER SPECKLE PHOTOGRAPHY

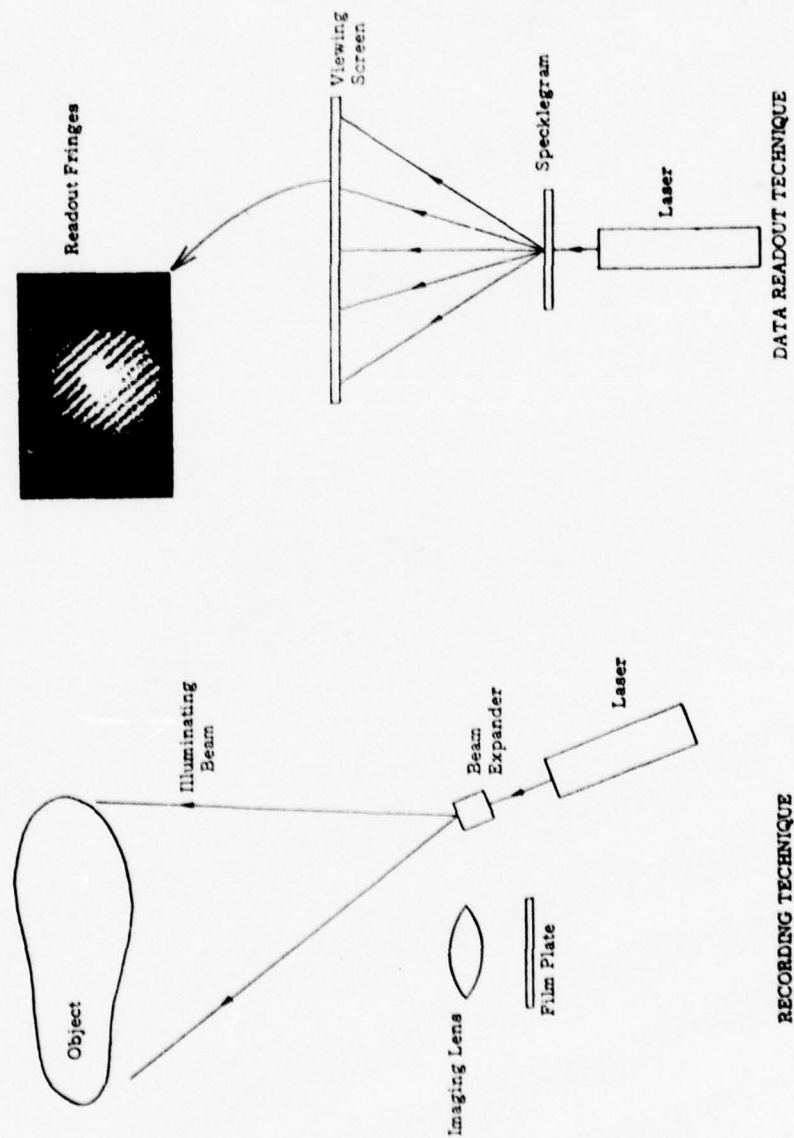


Figure 16. A schematic of laser speckle photography [57].

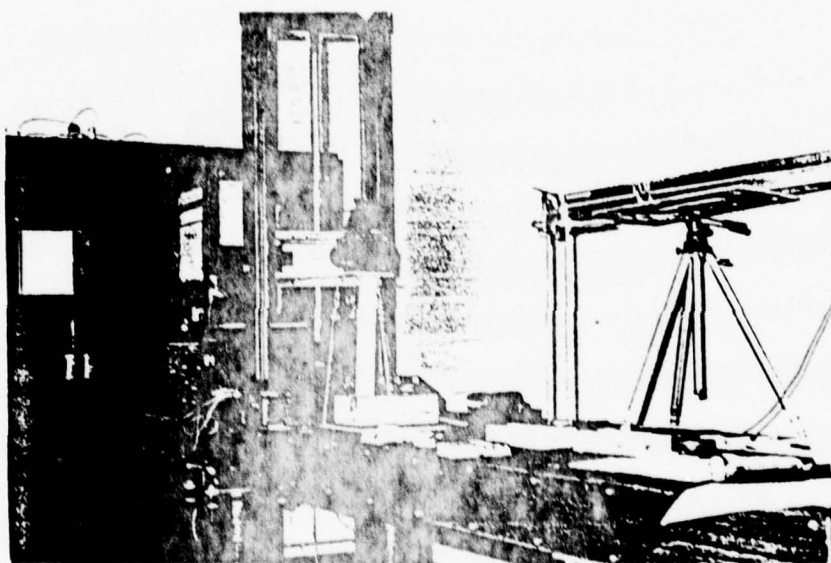


Figure 17. Specklegram recording equipment.

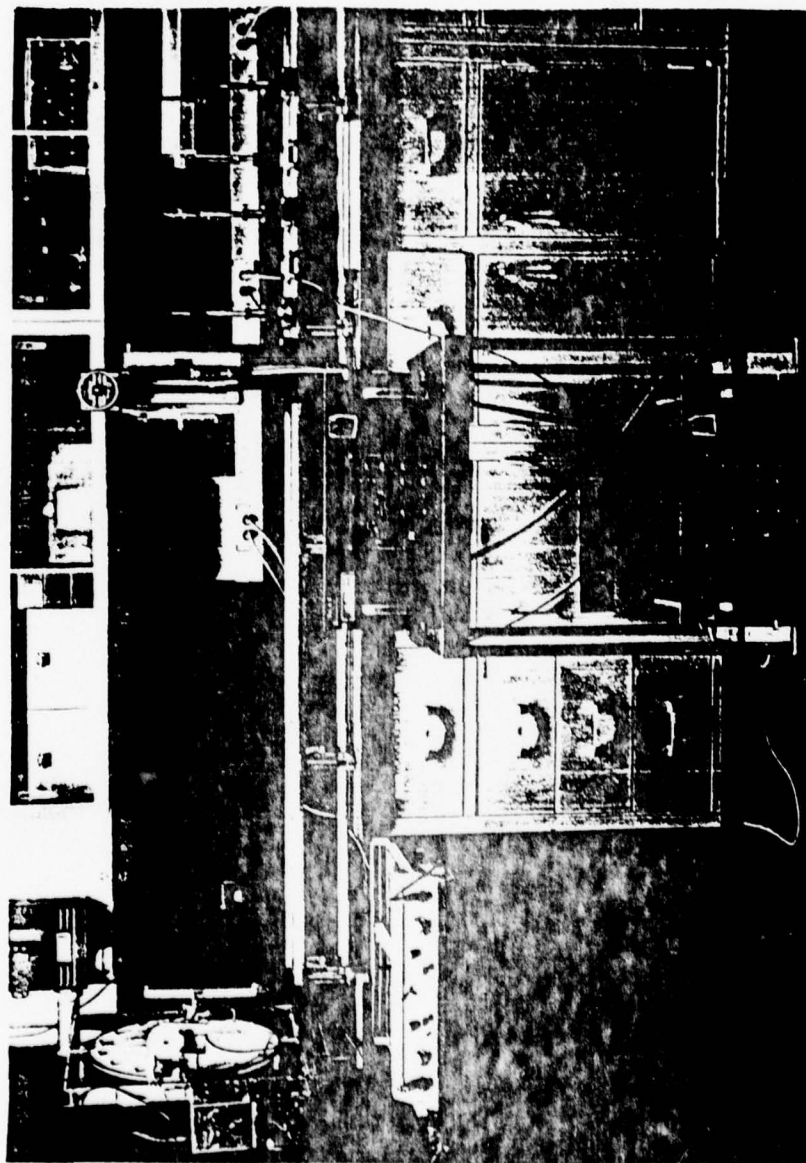


Figure 18. Specklegram interrogation equipment



Figure 19. Modulated diffraction halo.

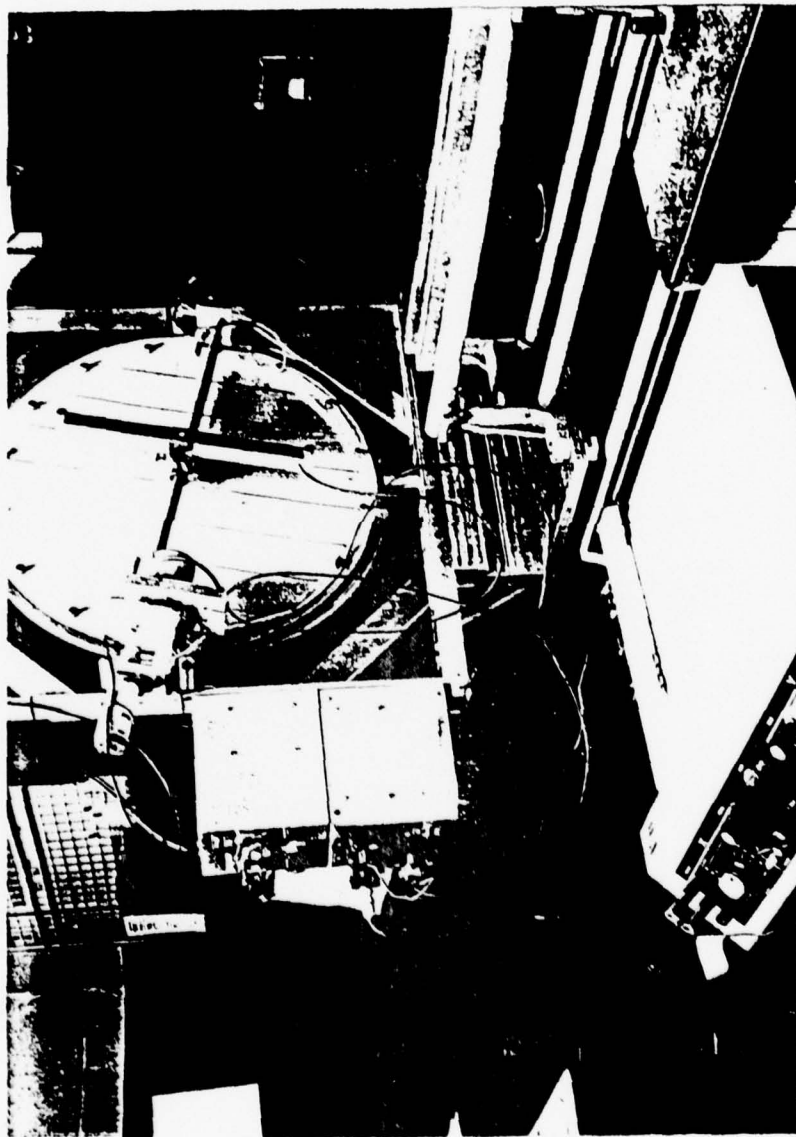


Figure 20. Fringe pattern recording equipment.

A Mamiya RB67 single lens reflex camera with a 90 mm lens was used in specklegram recordings. Specklegrams were recorded on Agfa Gavaert 10E75, a high resolution emulsion on a glass plate. The emulsion thickness on the plate was $10\text{ }\mu\text{m}$ with a resolving power of 2500 lines/mm. It can be shown (Archbold, Burch, and Ennos [58]) that with an emulsion thickness of $10\text{ }\mu\text{m}$, an f-stop number of at least 2 must be used so that the speckle pattern does not change appreciably with depth; an f-stop number of 3.8 was used in this work. It is easily shown through equation (26) that a resolution of 277 lines/mm is the minimum resolution tolerable for an f-stop number of 3.8 and light wave length of 6328\AA .

A 15 milliwatt Spectra-Physics 124A Helium-Neon laser was used to illuminate the specimen with a 10X Bausch and Lomb microscope objective acting as a beam diffuser. The relatively low power of the laser restricted the area of illumination on the specimen to a circle with approximately a 2.5 inch diameter. After double exposure of the photographic plate, the negative was developed in Kodak D-19.

Results

Six specimens were tested: one natural unfilled rubber, one uncracked propellant, and four cracked specimens (two .2 inches thick and two .125 inches thick). A table model Instron was used to apply a constant overall strain increment with nominal grip displacement of .004 inches for each increment. The total overall grip displacement of .012 inches was reached. A specklegram was made corresponding to each applied strain increment and designated according to

specimen and grip displacement; e.g., 6-2 was the designation accorded sample 6 undergoing the second strain increment. It should be noted that in all cases the first applied grip displacement gave ambiguous readings, perhaps due to a healing effect between the two precut crack surfaces.

The rubber sample and uncracked propellant samples were used to determine experimental procedures. The rubber sample produced fringe patterns of high contrast. Although the uncracked propellant sample produced fringes that were detectable to the human eye; there was not sufficient contrast for use with the semi-automated interrogation equipment.

An examination of the stressed unpainted propellant sample of Figure 1 (p. 2) indicates a large amount of microcracking, which causes decorrelation due to relatively large local displacements and particle rotations.

As previously mentioned, the interrogating process is accomplished by passing a 1mm laser beam through the specklegram. The fringe pattern produced is due to all speckle pairs illuminated by the interrogating beam. The fewer the number of correlated pairs, the weaker the fringe pattern contrast.

PBAN propellant was found to exhibit significant decorrelation outside the displacement range of 1-100 μm . When a natural unfilled rubber was tested, the upper displacement limit was extended to 250 μm . At the Flight Dynamics Laboratory, under ideal conditions, a pure translation of 750 μm has been recorded.

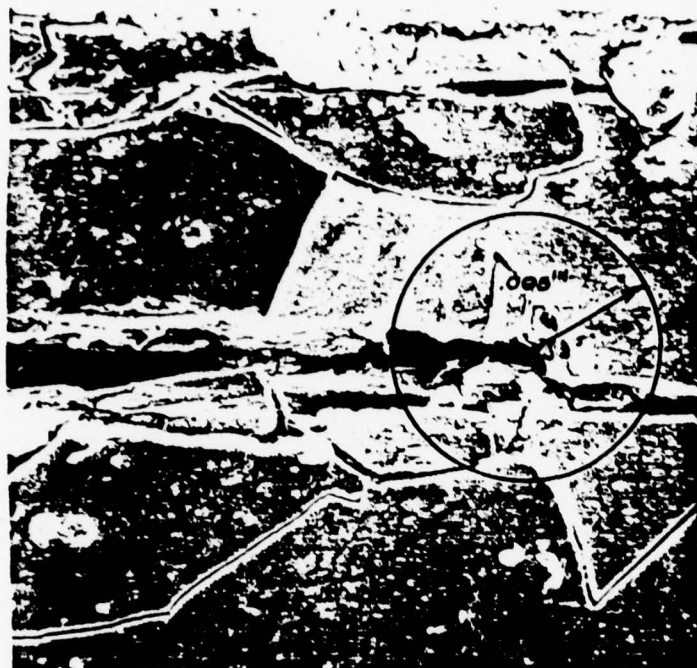
As previously mentioned, the effects of microcracking and

particle rotation were overcome by the application of a thin film of flat white Krylon spray paint applied to the sample surface. The effect of the paint film on the displacement field was investigated.

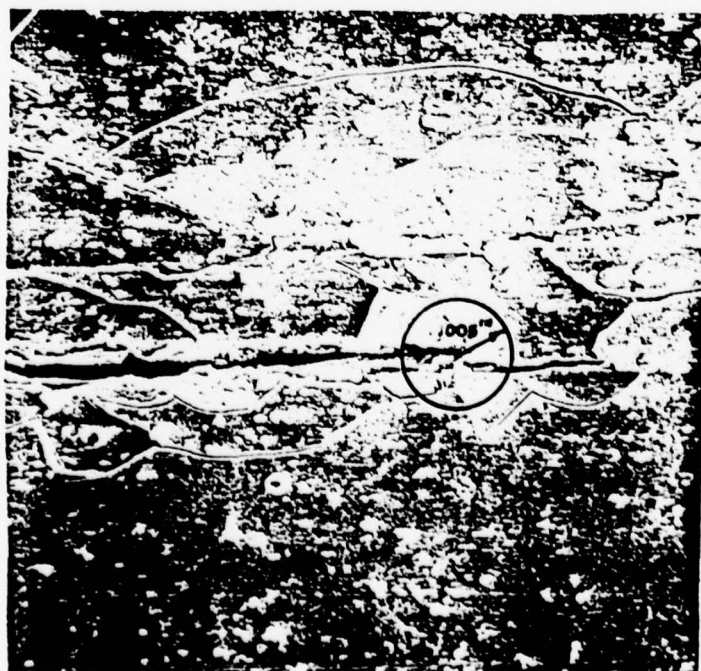
To test the effect of the paint on the displacement field, the upper half of the uncracked specimen was masked before painting. After painting, the mask was removed, leaving a distinct paint line. A specklegram of the specimen under load was made. A scan across the paint line in the specklegram proved the paint film had negligible effects. This was to be expected, since the interrogating laser beam has an averaging effect over the area of the beam (1mm diameter) and the effect of the paint was to average displacements. The averaging effect of the paint can be seen in the SEM study shown in Figures 21 and 22.

Discussion of Results

A comparison between the numerically obtained displacement field and the measured displacement field was made. A comparison of strain was attempted, requiring a differentiation of the displacement fields. A two-dimensional cubic spline technique was used in an attempt to obtain the strains associated with the measured displacement fields. Data scatter, albeit nominally within 6% of theoretical results, was apparently not small enough for the successful use of the spline technique. It was felt data scatter was due in part to the facilities used to run the experiment and in part due to local failure in the propellant, i.e., large movement in the paint caused by paint fracture (the interferometric technique has displacement measurement accuracies of 1 micron \pm 2% [62]). In order to

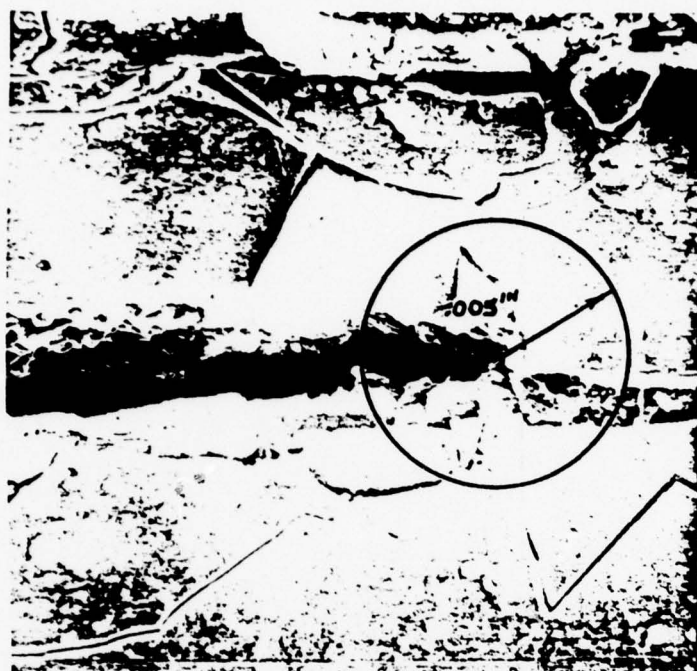


a)

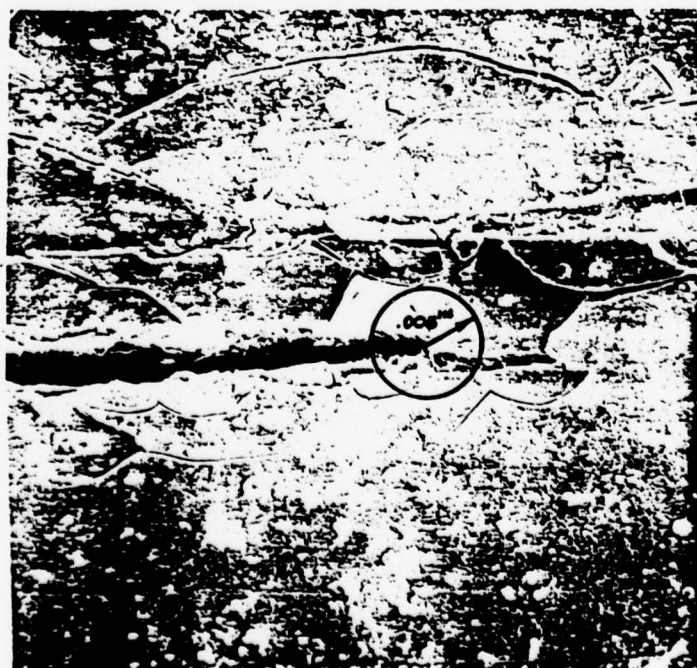


b)

Figure 21. Crack tip before stress a) 150X, b) 60X.



a)



b)

Figure 22. Crack tip after stresses 5% a) 150X, b) 60X.

check on the accuracy of the spline technique itself, in fracture problems, strain fields associated with rigid body displacements, affine displacements, Williams' singular crack problem, Barenblatt's singular crack problem, and the combined Williams-Barenblatt problem were calculated from theoretical displacements. All were in agreement with the analytically derived strain fields.

Of the four cracked specimens, only specimen 6 (.2 inches thick) and specimen 8 (.125 inches thick) had fringe patterns with sufficient contrast to interrogate. The other two specklegrams (each cracked sample was tested only once due to material damage suffered by propellant under strain) had poor contrast due to overexposure and/or over development.

The specklegram interrogation revealed still another problem. The crack tip neighborhood enclosed by the lines $x=-0.1$, $x=0.2$, $y=0.0$, $y=0.1$ was consistently absent of fringe patterns in all specklegrams.

There are seemingly two features in the interferometric technique which may be violated in this neighborhood, causing speckle pair decorrelation: time dependent motion of the specimen and/or rotational movement of the specimen (paint cracking was not considered a problem since paint flakes were considered large enough to interrogate, e.g., those shown in Figures 21 (p. 54) and 22 (p. 55)).

It can be shown, through the governing field equations, that for an incompressible elastic body with displacement boundary conditions on part or all of the boundary and zero tractions

specified over the remaining portion of the boundary, that the strain and displacement distributions are independent of the modulus; therefore, in the nonaging linear viscoelastic case, the correspondence principle implies that a similarly loaded viscoelastic material has strain and displacement distributions which are independent of the relaxation modulus. As previously indicated, that portion of the quarter biaxial strip boundary located between the apparent crack tip and the crack tip is acted on by a non-zero stress, which implies the displacements are modulus dependent.

Rather than directly treating the problem of the non-zero boundary tractions, the second limiting feature of the interferometric technique was investigated.

While pure translatory motion can be measured over a considerable range by the interferometric technique, the degree of rotational movement that can be tolerated is more severely limited [63]. Archbold and Ennos [63] record fringe patterns with rotations of .02 radians.

A scanning electron microscope (SEM) study was performed on a cracked specimen under 5% loadings to qualitatively determine paint flake rotations. These strains, 5%, though considerably higher than those applied to the test specimen (.2%), were the lowest that could be applied using the relatively insensitive tensile stage (Figure 23) furnished with the JOEL JSM - U3 scanning electron microscope. The samples were ion sputter coated with 60:40 Gold Paladium alloy to insure good secondary electron imaging and to minimize charging effects of the electron beam on

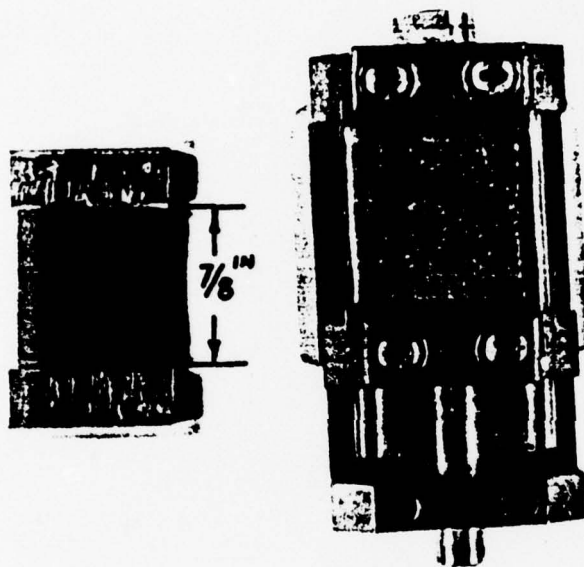


Figure 23. Tensile stage and specimen used in SEM study.

the sample.

The study, as recorded in Figures 21 (p. 54) and 22 (p. 55), indicates paint flake rotations are appreciably reduced away from the crack tip after a distance of .01 inches. Since the SEM sample was strained approximately 25 times higher than the interferometric test samples, one is led to conclude decorrelation is not an effect of paint flake rotation outside of .01 inches from the tip.

COMPARISON OF THEORY AND EXPERIMENT

All grip displacement increments applied to the samples were nominally .004 inches. To better visualize experimental grid deformations, these results were normalized to a grip displacement of .1 inches.

Figure 24 compares the singular crack solution as obtained through TEXGAP (where the failure zone length, a , is equal to zero) with normalized experimentally obtained data. Figures 25 and 26 compare the experimentally obtained data to finite stress solutions having failure zone lengths of .1 inches. The elements generated by the TEXGAP code are shown in Figures 24-26 as solid vertical and horizontal lines.

The theoretical solutions shown in Figure 25 were obtained by superposing previously derived Barenblatt solutions for the cracked infinite sheet problem for both the constant and ramp failure stress distributions to Williams' singular solution (TEXGAP solution) for the quarter biaxial strip.

Figure 26 illustrates the TEXGAP solution obtained by linking the failure stress distribution with the singular Williams' solution through the finite stress condition (Appendix B).

The trend throughout most of the strip is that of higher experimentally measured vertical displacements relative to theoretically predicted displacements. This discrepancy is more readily recognized in Figures 27 through 32, which expands the vertical scale by a factor of 10 and displays the displacements of Figure 26 (with the addition of test run 8-2). There were no horizontal displacements recorded because a horizontal shift of the loading frame when loads were applied completely masked specimen horizontal displacements. The horizontal load-

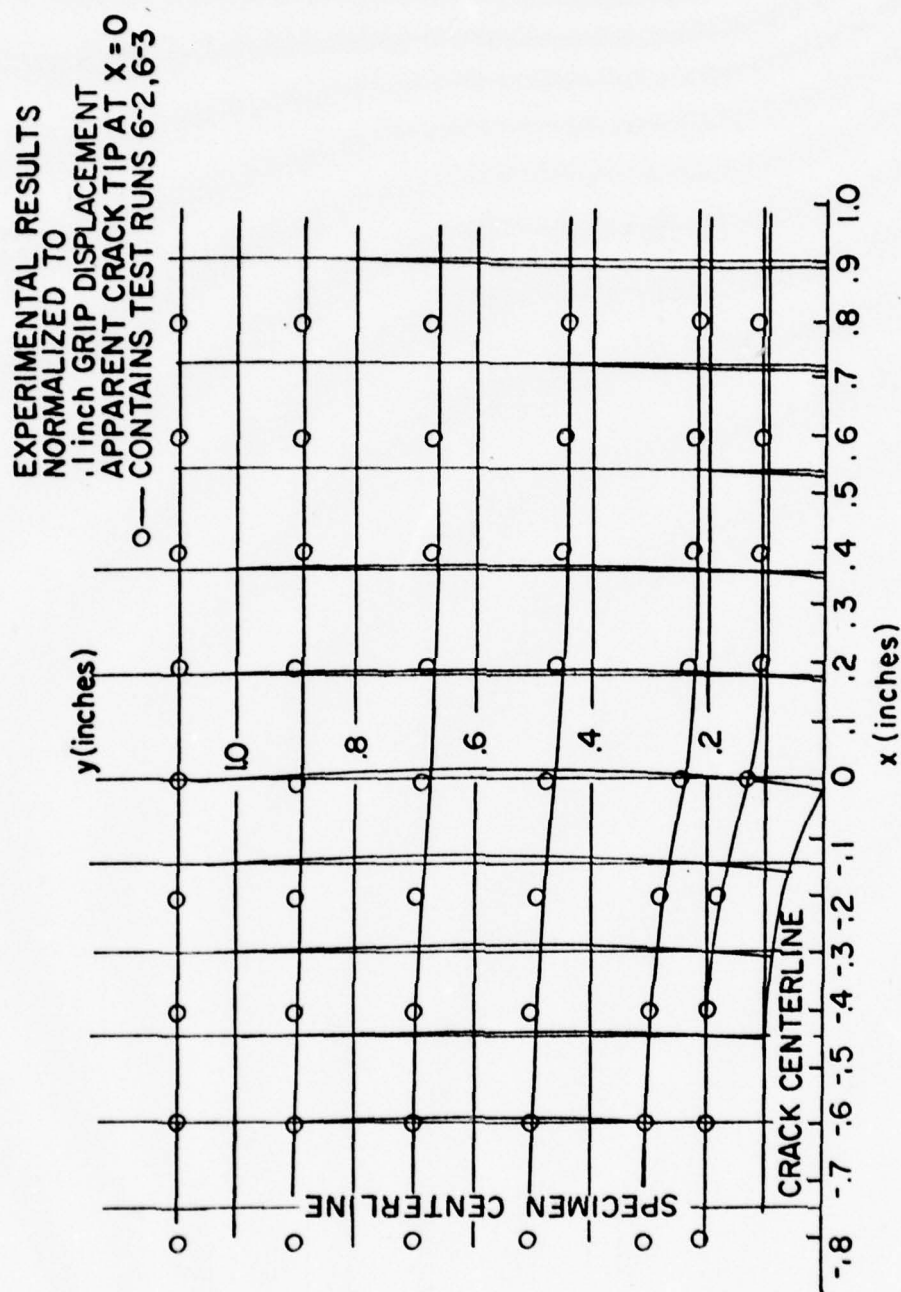


Figure 24. Williams' grid deformations (solid curves) for the quarter biaxial strip compared to experimentally obtained results (O contains data points).

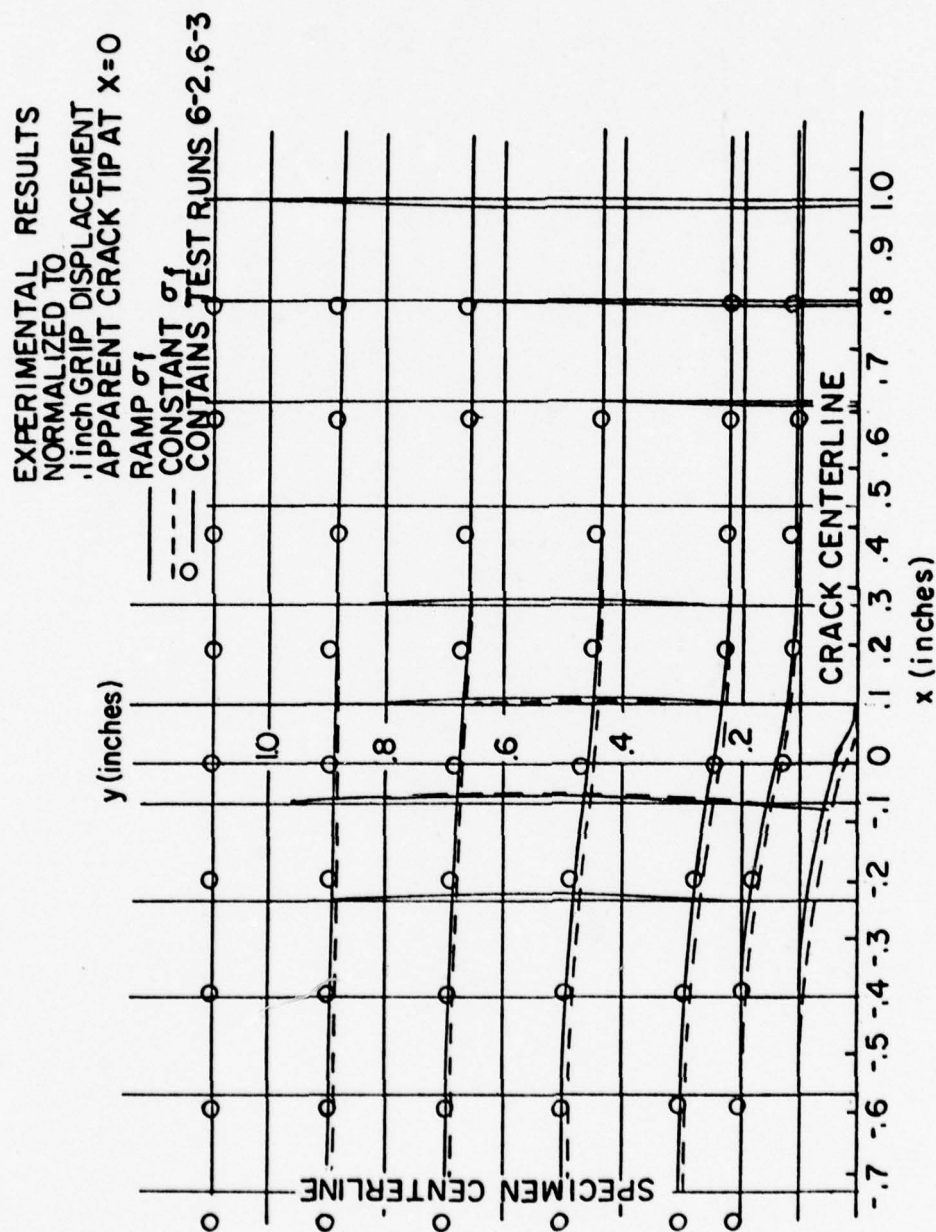


Figure 25. Williams' grid deformations (TEXGAP solution) for the quarter biaxial strip superposed with Barenblatt's grid deformations for the infinite sheet compared with measured deformations (O contains data points) for both constant (dashed curves) and ramp (solid curves) failure stresses.

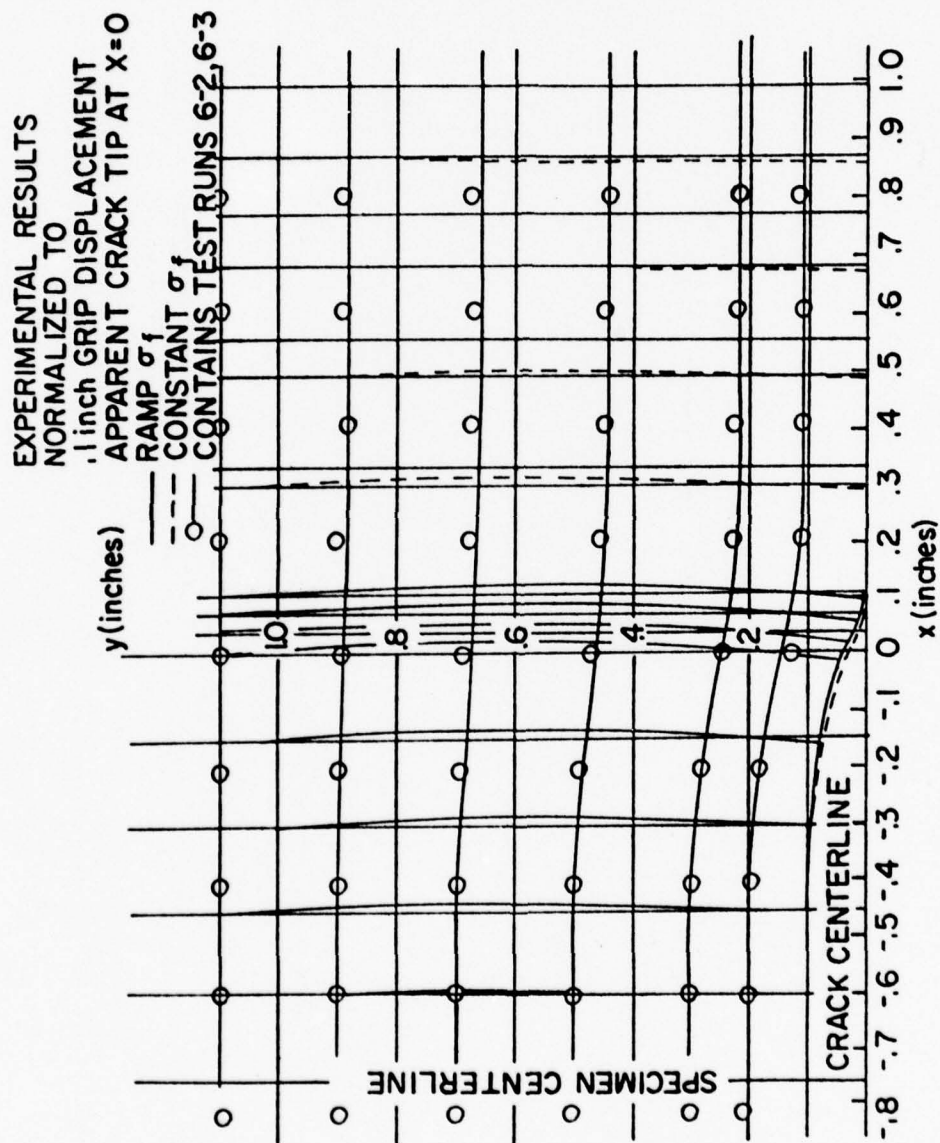


Figure 26. Modified Williams' grid deformations (TEXGAP solutions) for the quarter biaxial strip compared with measured deformations (○ contains data points) for both constant (dashed curves) and ramp (solid curves) failure stresses.

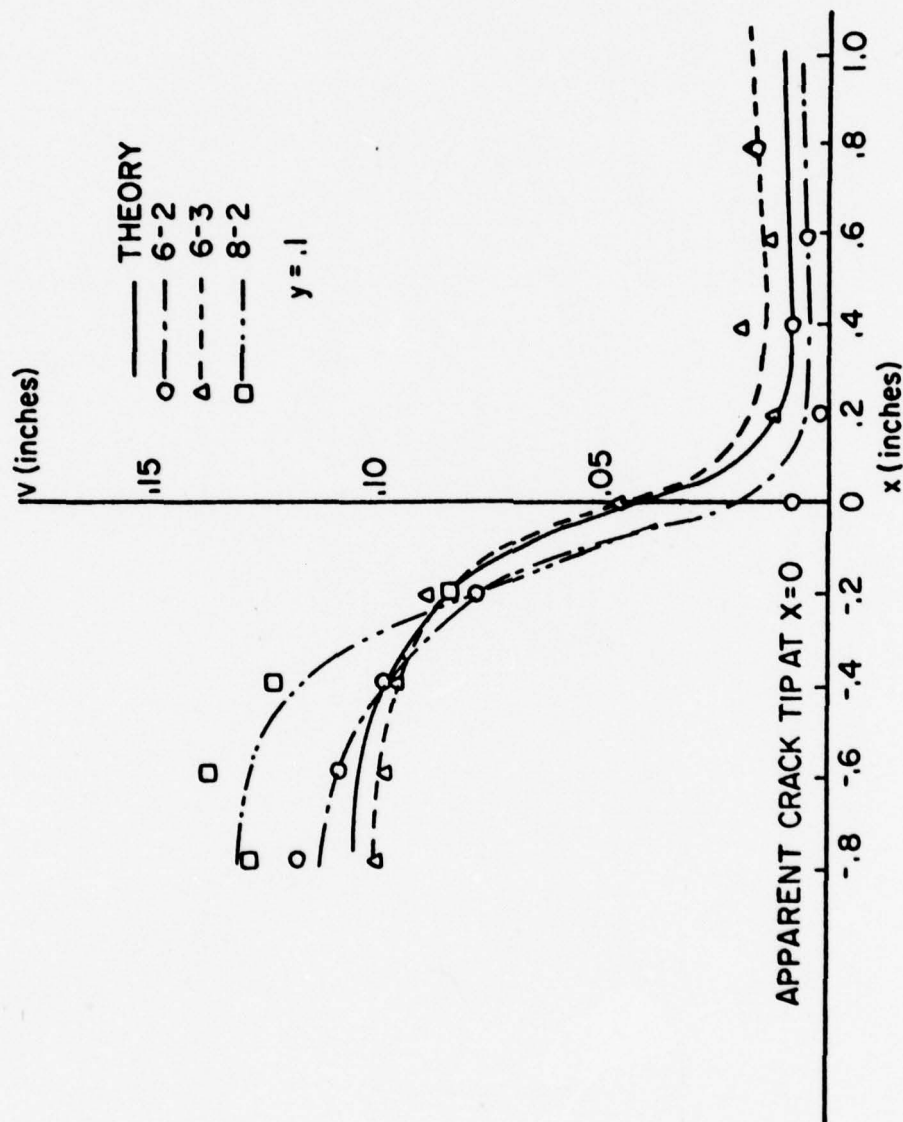


Figure 27. Modified Williams' displacements for the quarter biaxial strip compared with measured displacements @ $y = .1$ inches with the vertical scale expanded by a factor of 10.

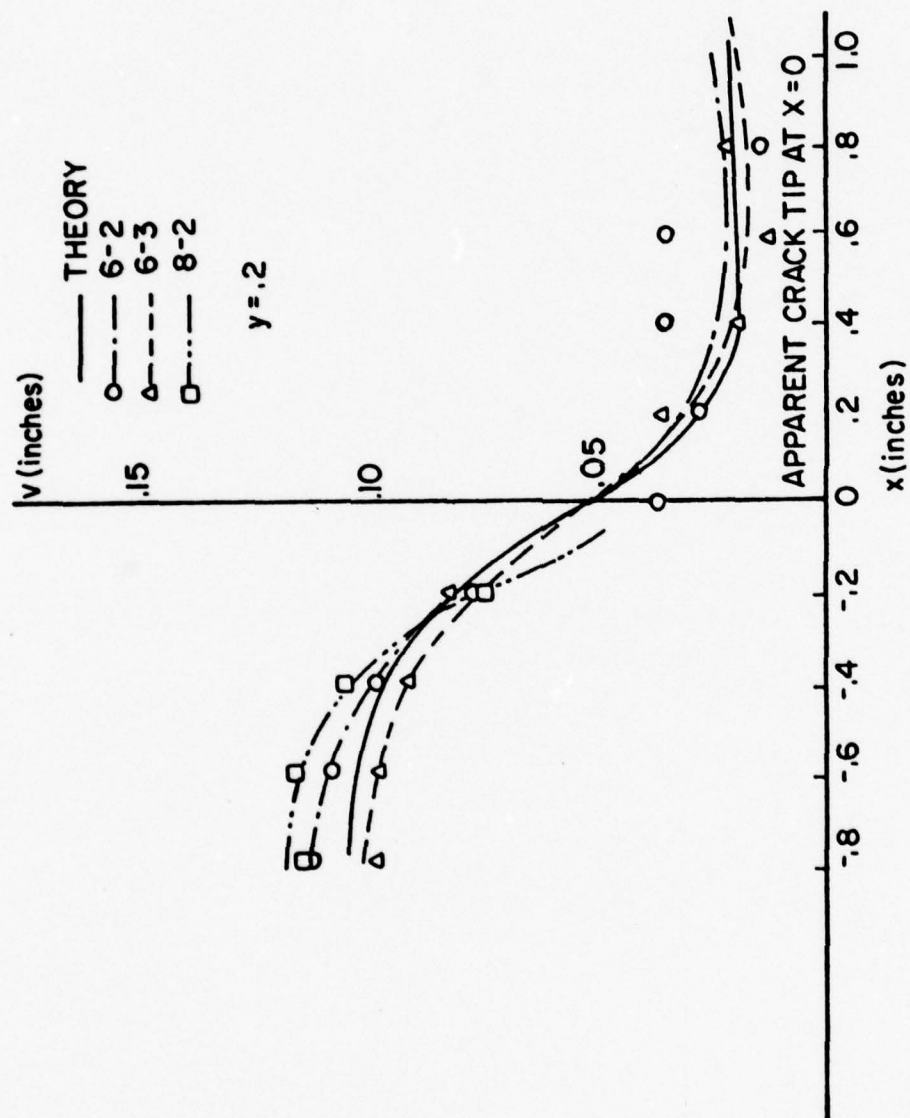


Figure 28. Modified Williams' displacements for the quarter biaxial strip compared with measured displacements @ $y = .2$ inches with the vertical scale expanded by a factor of 10.

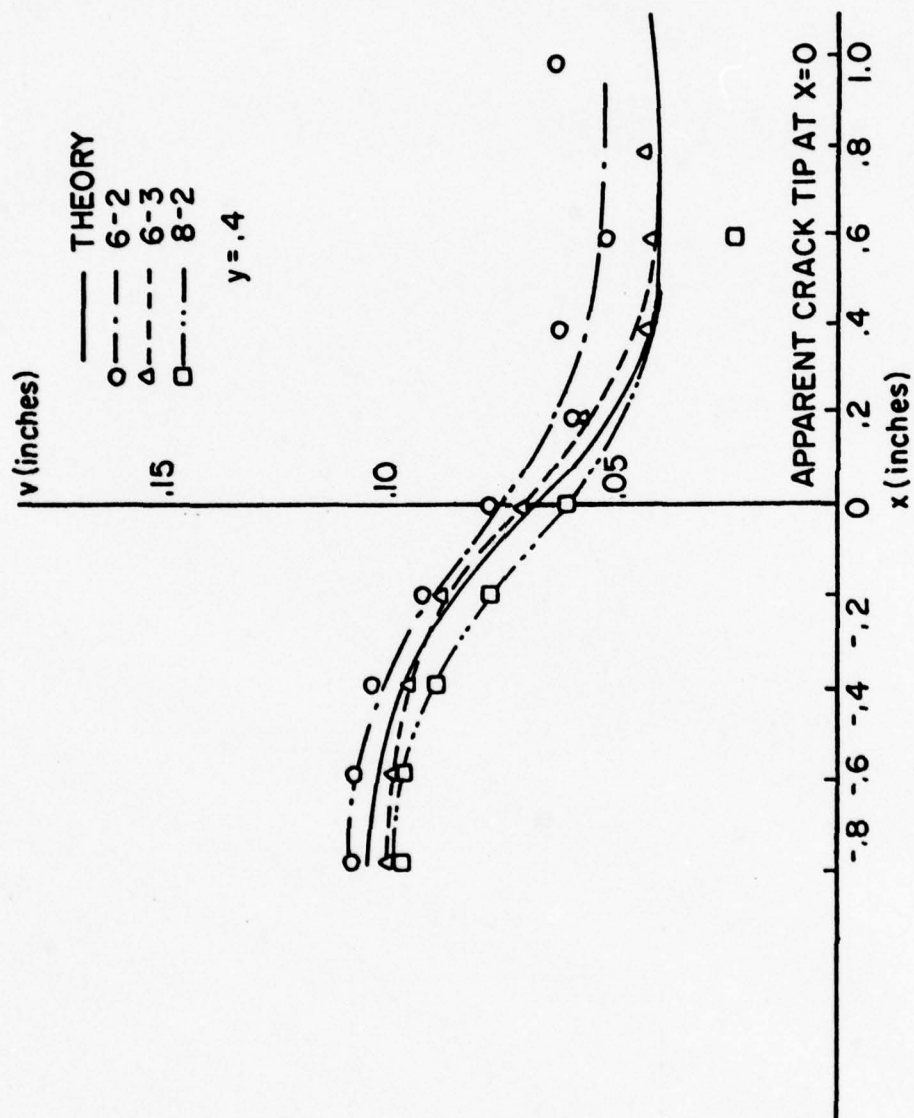


Figure 29. Modified Williams' displacements for the quarter biaxial strip compared with measured displacements @ $y = .4$ inches with the vertical scale expanded by a factor of 10.

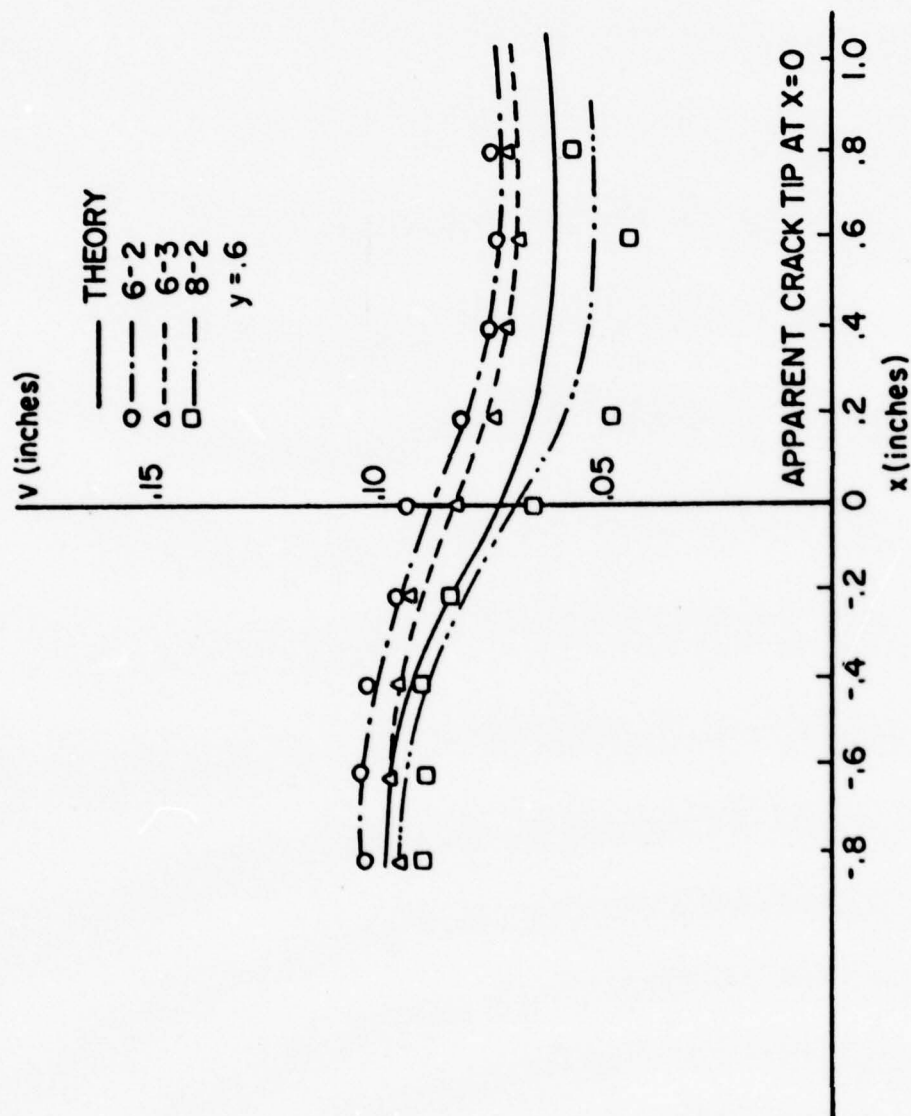


Figure 30. Modified Williams' displacements for the quarter biaxial strip compared with measured displacements @ $y = .6$ inches with the vertical scale expanded by a factor of 10.

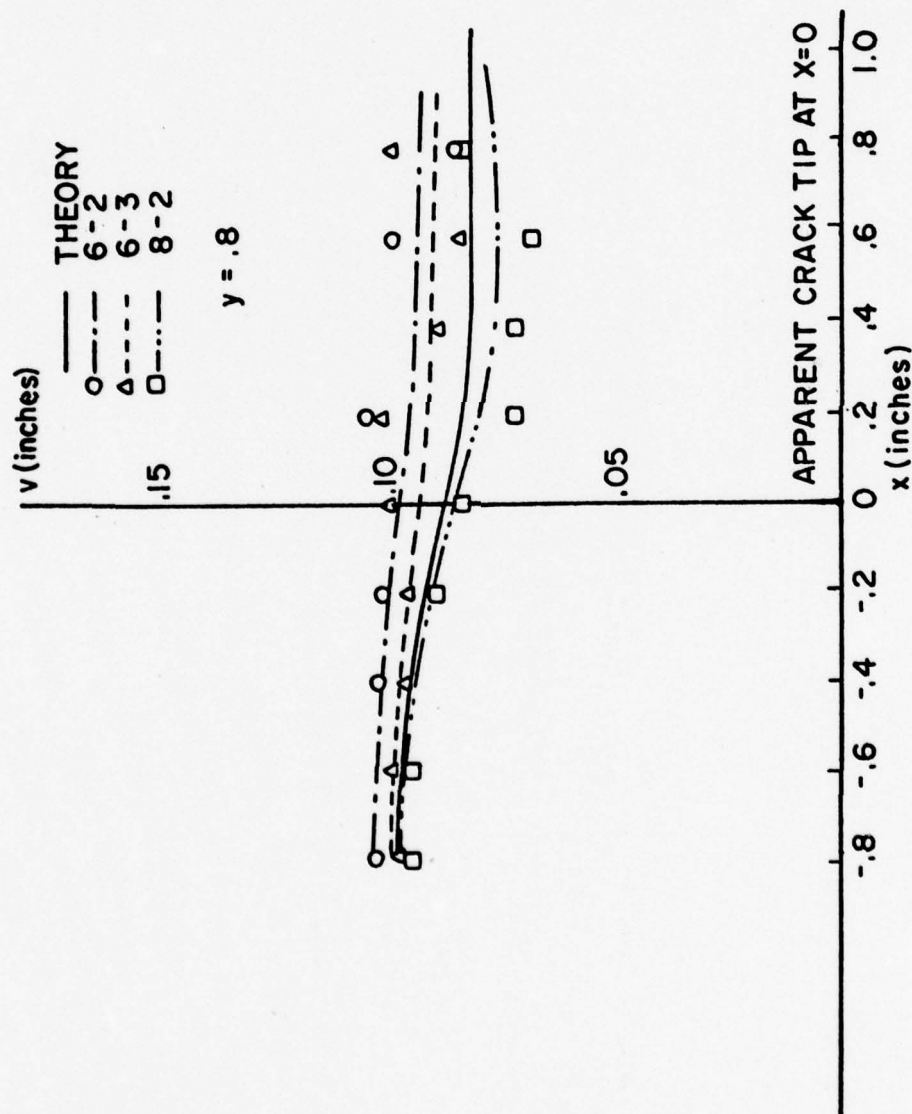


Figure 31. Modified Williams' displacements for the quarter biaxial strip compared with measured displacements @ $y = 0.8$ inches with the vertical scale expanded by a factor of 10.

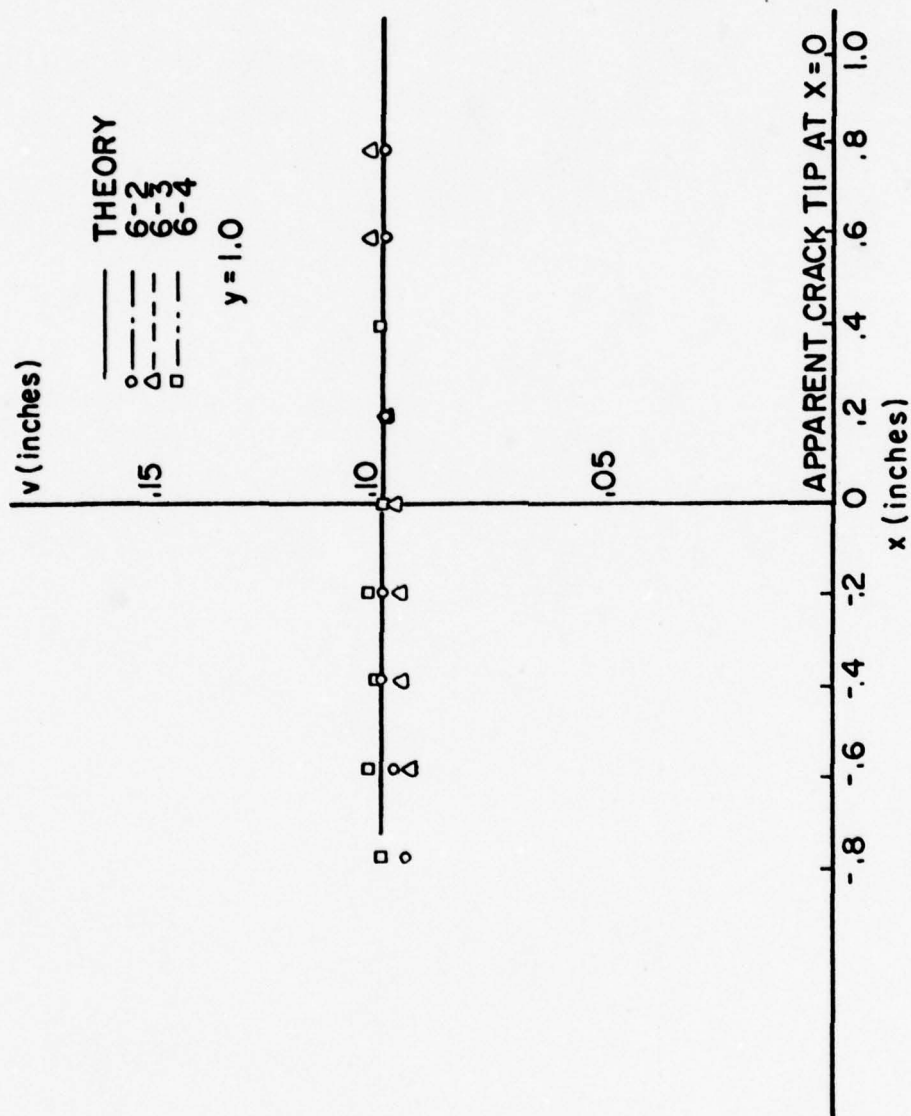


Figure 32. Modified Williams' displacements for the quarter biaxial strip compared with measured displacements @ $y = 1.0$ inches with the vertical scale expanded by a factor of 10.

ing frame shifts were between 5% and 10% of applied grip displacements.

Four possible causes of the relatively high vertical displacements were investigated: 1) sample thickness effect, 2) different Poisson's ratios, 3) different failure zone lengths, and 4) nonlinear material behavior.

From a strictly theoretical point of view, one would suspect, all else being equal; the thinner the biaxial strip, the more closely approximated the plane stress hypothesis. This contradicts the experimental results recorded in Figures 27-32 (pp. 64-69). Notice in particular for $y = .1, .2$ inches, the trend of the thinner sample's (test run 8-2) displacements is definitely higher than the displacements recorded from the thicker samples (test runs 6-2, 6-3); however, as we move farther away from the crack centerline, we record a closer agreement between the thinner .125 inch thick material (test run 8-2) and the theoretically obtained curve than between the thicker .2 inch thick material (test runs 6-2, 6-3) and the theoretically obtained curve. Thus, the recorded phenomenon cannot be explained as a sample thickness effect.

It is well established that Poisson's ratio for propellant is approximately equal to .5, i.e., propellant behaves as an incompressible material. Propellant castings can contain large internal voids, thereby exhibiting compressible behavior with effective Poisson's ratios substantially lower than .5. Accordingly, Poisson's ratios of .45, .4, .3, and .2 were used in additional calculations. The resulting theoretical displacements in both the horizontal and vertical directions were nominally 10% smaller for a Poisson's ratio of

.45, with a similar trend continuing (an additional 4% displacement reduction for each reduction in Poisson's ratio) as smaller Poisson's ratios were tested. We can conclude that the high vertical displacements were not due to a Poisson's ratio effect.

Finally, an investigation of the effect of varying failure zone lengths was conducted. Figures 24 (p. 61) and 26 (p. 63) illustrate the cracked biaxial strip with failure zone lengths of 0 and .1 inches, respectively. The failure zone length was felt to be less than .2 inches because of the speckle decorrelation effect mentioned earlier. A failure zone length of .2 inches (not shown) was tested. The trend established by Figures 24 (p. 61) and 26 (p. 63) continued; i.e., the effect was limited to the crack tip neighborhood with the theoretically predicted vertical values higher than those shown in Figure 26. For all of the above failure zone lengths the measured vertical displacement field away from the crack tip remained high. Evidently, the high experimentally obtained vertical displacements cannot be theoretically explained by varying failure zone lengths.

The sensitivity of the experimental technique, as stated previously, is ± 1 micron, which, for the displacements used in this experiment, represent an accuracy of approximately 2% — not sufficiently large enough to account for the observed phenomenon.

We are left to conclude that the displacement field behavior cannot be explained through linear theory, and must represent a nonlinear behavior.

A QUESTION OF UNIQUENESS

Motivation

There remain several open questions concerning crack problems, and among these are: 1) is the Barenblatt solution unique, and 2) are the displacements the smoothest we can hope for, i.e., $u \in C(\bar{\Omega})$ with derivatives failing to hold throughout the problem's domain, $\bar{\Omega}$?

Knowles and Pucik [64] address the question of uniqueness of solution to the traction boundary value problem for the two-dimensional linear elastostatic problem for a bounded domain containing a crack. In addition to the standard hypotheses in the Kirchhoff uniqueness theorem (cf. Love [65]), Knowles and Pucik require the displacement field to be bounded. With these hypotheses, Knowles and Pucik show that the strain energy in a neighborhood of the crack tip remains finite, and then prove uniqueness.

In the following section we address the question of uniqueness of solution to the traction boundary value problem for the three-dimensional linear elastostatic problem for a class of bounded regions (that will be made precise later in the chapter) by relaxing the Kirchhoff stress and displacement smoothness hypotheses. As a special result, uniqueness for the three-dimensional crack problem is obtained.

The uniqueness theorem of the next section does not preclude solutions with infinite strain energy. The stresses need only be absolutely integrable in the Lebesgue sense, whereas finite strain energy implies square integrability.

Our formulation requires that $u \in C(\bar{\Omega})$, which implies bounded displacements for bounded domains.

Classical Elastostatic Results

We begin with a review of some classical elastostatics results; however, before we begin with the review, some necessary notation will be described. Ordinary lower case letters represent scalars, while letters with a tilde placed under them represent tensors of positive order. We designate $\underline{\epsilon} \cdot \underline{\gamma}$ as the fully contracted outer product and write

$$\underline{\epsilon} \cdot \underline{\gamma} = \epsilon_{ij} \gamma_{ij}$$

where repeated indices imply summation. Furthermore, we define $\|\underline{\omega}\|$ of any order tensor to be the square root of the fully contracted outer product of $\underline{\omega}$. We write $R_n = \prod_{i=1}^n R_i$ where R is the real line, and (R_n, U) the usual topological space, where U is the topology generated by the projection mappings. By a domain in R_n we mean an open connected subset in R_n , by a region we mean a connected subset in R_n . Let $\Omega \subset R_n$ then $\partial\Omega$, $\overset{\circ}{\Omega}$, $\bar{\Omega}$ denote the boundary, interior and the closure of Ω respectively.

Let $\Omega \subset R_n$, then $C(\Omega)$ is the set of all tensor valued functions continuous on Ω , and $C^m(\Omega)$ is the set of all tensor valued functions continuous on Ω and with all partial derivatives up to order m , a positive integer, existing and coinciding with functions $C(\Omega)$. We further write

$$C^\infty(\Omega) = \bigcap_{n=1}^{\infty} C^n(\Omega).$$

Let $\Omega \subset R_n$ be a region. The scalar field, ϕ , is a function

defined on Ω with range in R . We write $\phi: \Omega \rightarrow R$. We use the standard covariant differentiation symbols, i.e.,

$$\underbrace{\phi_{,ij\dots k}}_{m \text{ indices}} = \frac{\partial^m \phi}{\partial x_k \dots \partial x_j \partial x_i}$$

Here the covariant differentiation raises ϕ to an m th order tensor. Similarly, let u be a first order tensor in $C^1(\Omega)$, then we write ∇u for $u_{i,j}$ where $u_{i,j}$ is a second order tensor.

We now state the Divergence Theorem [66] for regular regions, where regular region is an adoption of Kellogg's [67] notation.

Divergence Theorem - Let Ω be a bounded or unbounded regular region. Let ϕ be a scalar field, u a vector field, and T a tensor field, and let ϕ , u , and T be continuous on Ω , differentiable almost everywhere on Ω , and of bounded support. Then

$$\int_{\partial\Omega} \phi n_i dS = \int_{\Omega} \phi_{,i} dV$$

$$\int_{\partial\Omega} u_i n_i dS = \int_{\Omega} u_{i,i} dV$$

$$\int_{\partial\Omega} u_i n_j dS = \int_{\Omega} u_{i,j} dV$$

$$\int_{\partial\Omega} \epsilon_{ijk} n_j u_k dS = \int_{\Omega} \epsilon_{ijk} u_{k,j} dV$$

$$\int_{\partial\Omega} T_{ij} n_j dS = \int_{\Omega} T_{ij,j} dV$$

whenever the integrand on the right is piecewise continuous on $\bar{\Omega}$.

We now state some classical results from the linearized theory of elasticity (cf. [68]).

Definition (State: regular elastostatic state.) Let R be a bounded domain in R_3 , and $D \subset \bar{R}$. If u is a vector-valued and σ a second-ordered tensor-valued function on D , the ordered pair $S = [u, \sigma]$ is called a state on D with the displacement field u and the stress field σ .

Suppose that f is a vector field on D and c a fourth order tensor field on \bar{R} . Then, $S = [u, \sigma]$ is said to be a regular elastostatic state on D corresponding to the body-force field f and the elasticity field c , provided:

$$i) f \in C(D); c \in C(\bar{R}) \text{ with}$$

$$c_{ijkl} = c_{jikl} = c_{klij} \text{ on } R$$

and c invertible on R , i.e., the six by six matrix associated with c has nonvanishing determinant on R .

$$ii) u \in C^2(\overset{\circ}{D}) \cap C^1(D), \sigma \in C^1(\overset{\circ}{D}) \cap C(D)$$

$$iii) \sigma_{ij} = c_{ijkl} u_{k,l} \text{ in } \overset{\circ}{D}$$

$$\sigma_{ij,j} + f_i = 0 \text{ in } \overset{\circ}{D}$$

We write $E(f, c; D)$ for the set of all regular elastostatic states with the above f , c , and D .

Let $S' = [u', \sigma']$ and $S = [u, \sigma]$ be in $E(f, c; D)$ and let $\alpha \in R$. We define addition and scalar multiplication of two states in $E(f, c; D)$ through:

$$S + S' = [u, \sigma] + [u', \sigma'] = [u + u', \sigma + \sigma']$$

and

$$\alpha S = \alpha[u, \sigma] = [\alpha u, \alpha \sigma],$$

implying $E(f, c; D)$ is a linear vector space. Regular regions are composed of a finite number of regular surfaces, which may have in common a single point (a vertex for both), or a single regular arc (an edge for both), but no other points. At these common points there may not be a definable normal. With the preceding as motivation, we define the regular part of ∂R , designated $\partial^* R$, as that subset of ∂R at which a normal is definable. Let R be a regular region, $S = [u, \sigma]$ a state on \bar{R} , and n the unit outward normal on ∂R , then the traction vector, s , of S on $\partial^* R$ is defined by

$$s_i = \sigma_{ij} n_j \text{ on } \partial^* R$$

We now state the traction problem for regular elastostatic states (classical traction problem). Let $\Omega \subset R$ be a regular region. We wish to find

$$S = [u, \sigma] \in E(f, c; \bar{\Omega})$$

given the data f and c subjected to the boundary conditions

$$s = \xi^* \text{ on } \partial^* R$$

where ξ^* is a prescribed function.

The uniqueness of the solution to the classical traction problem, due to Kirchhoff, is now given (cf. Love [65]),

Theorem (Uniqueness theorem of classical elastostatics: Kirchhoff). Let Ω be a regular region, and suppose

$$\alpha) S' = [\underline{u}', \underline{q}'], S'' = [\underline{u}'', \underline{q}''] \in E(\underline{f}, \underline{c}; \bar{\Omega})$$

$$\beta) \underline{\xi}' = \underline{\xi}'' \text{ on } \partial\Omega$$

$\gamma) \underline{c}$ is positive definite on Ω , i.e.,

$$c_{ijkl}(\underline{x}) \gamma_{ij}(\underline{x}) \gamma_{kl}(\underline{x}) > 0 \text{ on } \Omega \text{ for all } \underline{x} \in \Omega$$

and for every non-zero symmetric two-tensor, $\underline{\gamma}$. Then $S' = S''$ on \bar{R} modulo a rigid displacement.

Now we relax the previous regularity assumptions on the solution to the traction problem of elastostatics and deal with the attending problem of uniqueness. After dealing with necessary preliminaries, we cast the traction problem in its proper setting, and then prove an appropriate uniqueness theorem. The resulting arguments closely follow the spirit of Brockway [68], who looks at the uniqueness of solutions to the traction problem for "weak elastodynamic states".

Mathematical Preliminaries

The following requires liberal usage of functional analysis results. Functional analysis rests heavily on two pillars of mathematics, Topology and Algebra. As such, the following definitions and results, albeit not complete, will aid the engineering reader through the maze of terminology [69-74].

A collection, τ , of subsets of a set X is said to be a topology in X provided:

- i) $\phi \in \tau$ and $X \in \tau$
- ii) If $0_i \in \tau$ for $i=1, \dots, n$; then $\bigcap_{i=1}^n 0_i \in \tau$

iii) If $0_\alpha \in \tau$, for all $\alpha \in I$, then $\bigcup_{\alpha \in I} 0_\alpha \in \tau$.

Special note should be made of the finite number of intersections in ii) and of the finite, countable, or uncountable number of sets in iii).

A family of sets is countable provided there exists a bijection (one-to-one correspondence) between a subset of the positive integers and the collection of sets, i.e., we can label the sets $0_1, 0_2, \dots$.

If τ is a topology in X , then (X, τ) is called a topological space. Let (X, τ_X) , (Y, τ_Y) be topological spaces, and f a mapping (function) of X into Y . Then f is said to be continuous provided $f^{-1}(v) \in \tau_X$ for every $v \in \tau_Y$. By function we mean "single-valued" function in the standard mathematical sense.

Let M be a collection of subsets of the set X , then M is called a σ -algebra provided:

- i) $X \in M$
- ii) if $A \in M$ then $X \setminus A = \{x \in X \mid x \notin A\} \in M$
- iii) if $\{A_n\}$ is a countable number of sets, then $\bigcup_{n=1}^{\infty} A_n \in M$.

Let M be a σ -algebra in X , then the ordered pair (X, M) is called a measurable space and the members of M the measurable sets in X . If (X, M) is a measurable space and (Y, τ) a topological space, then a mapping, f , of X into Y is said to be measurable provided $f^{-1}(v) \in M$ for every $v \in \tau$.

A positive measure, μ , is a function defined on a σ -algebra, M , whose range is in $[0, \infty]$ and which is countably additive, i.e., if $\{A_i\}$ is a countable number of disjoint sets in M ($A_i \cap A_j = \emptyset$ whenever $i \neq j$) then $\mu(\bigcup_{i=1}^{\infty} A_i) = \sum_{i=1}^{\infty} \mu(A_i)$. To avoid trivial cases we

will further assume there exists at least one $A \in M$ such that $\mu(A) < \infty$.

We define a measure space as the ordered triple (X, M, μ) . We now state, without proof, some facts of positive measure.

Let μ be a positive measure on a σ -algebra M . Then

- a) $\mu(\phi) = 0$.
- b) $\mu(A_1 \cup \dots \cup A_n) = \mu(A_1) + \dots + \mu(A_n)$ if A_1, \dots, A_n are pairwise disjoint members of M .
- c) $A \subset B$ implies $\mu(A) \leq \mu(B)$, $A, B \in M$.
- d) $\mu(A_n) \rightarrow \mu(A)$ as $n \rightarrow \infty$ where $A = \bigcup_{n=1}^{\infty} A_n$,

$A_n \in M$ and $A_i \subset A_j$ whenever $i < j$.

- e) $\mu(A_n) \rightarrow \mu(A)$ as $n \rightarrow \infty$ if $A = \bigcap_{n=1}^{\infty} A_n$, $A_n \in M$ and $A_i \supset A_j$ whenever $i < j$ and $\mu(A_1) < \infty$.

Let (X, M) be a measurable space. The function $s: X \rightarrow [0, \infty)$ such that the range of s consists of only a finite number of points in $[0, \infty)$ is called a simple function. Suppose $\alpha_1, \dots, \alpha_n$ are the distinct values of a simple function, s . Set $A_i = \{x | s(x) = \alpha_i\}$, define χ_{A_i} through

$$\begin{aligned} \chi_{A_i}(x) &= 1 & x \in A_i \\ &= 0 & \text{otherwise} \end{aligned}$$

we characterize s through

$$s(x) = \sum_{i=1}^n \alpha_i \chi_{A_i}(x)$$

and denote χ_{A_i} as the characteristic function of A_i , clearly, s is

measurable if and only if A_i is measurable.

We are now in a position to define Lebesgue integral.

Let (X, M) be a measurable space and s be a measurable simple function on X , we write

$$s = \sum_{i=1}^n \alpha_i \chi_{A_i}$$

further, let $E \in M$, then define

$$\int_E s d\mu = \sum_{i=1}^n \alpha_i \mu(A_i \cap E)$$

We use the convention $0 \cdot \infty = 0$ (note, some α_i might be 0 and $\mu(A_i \cap E) = \infty$)

If $f: X \rightarrow [0, \infty]$ is measurable, and $E \in M$, we define

$$\int_E f d\mu = \sup_{0 \leq s \leq f} \int_E s d\mu$$

Occasionally it is desirable to define the integral for measurable functions, f , with range in $[-\infty, \infty]$, the obvious result is, (provided at least one of the integrals $\int_E f^+ d\mu$, $\int_E f^- d\mu$ is finite);

$$\int_E f d\mu = \int_E f^+ d\mu - \int_E f^- d\mu$$

where $f^+(x) = \max \{f(x), 0\}$ and $f^-(x) = \max \{-f(x), 0\}$.

An easy result to show, for non-negative f and s is

$\phi(E) = \int_E s d\mu$ and $\phi(E) = \int_E f d\mu$ define positive measures on M .

Let Ω be a bounded subset of R_3 , and $0 < p < \infty$. Define $L^p(\Omega)$ by

$$L^p(\Omega) = \{f \mid f \text{ is tensor valued and measurable on } \Omega \text{ and}$$

$$\int_{\Omega} |f_{ij\dots k}|^p d\mu < \infty \text{ where } d\mu \text{ is the Lebesgue measure in } R_3\}.$$

We must now turn our attention to regular surfaces in order to clarify the divergence theorem and extend the classical (Riemann) integrals to Lebesgue integrals.

A surface is a mapping $\vartheta: \Pi \rightarrow R_3$ where $\Pi \subset R_2$. The trace of a surface is the range of ϑ . In our work we deal with regular surfaces and regular regions in the sense of Kellogg (Kellogg's surfaces coincide with the above definition of trace). As such, given a regular surface S , there exists a Cartesian frame in R_3 such that S admits the representation

$$x_3 = G(x_1, x_2) \text{ for all } (x_1, x_2) \in \Pi, G \in C^1(\Pi)$$

where Π is a closed region in the (x_1, x_2) -plane. By an integral over the surface, S , of a function, we mean

$$\iint_{G(\Pi)} f(y) \cdot \underline{n} dy = \iint_{\Pi} f(G(x_1, x_2)) |J_G(x_1, x_2)| dx$$

where $\underline{f} \equiv (0, 0, f)$ and \underline{n} is the unit normal to the surface and $J_G(x_1, x_2) \in C(\Pi)$, and $J_G(\underline{x})$ is the Jacobian of G at \underline{x} (cf. Buck [72], Rudin [71]).

We need more mathematics, consider R_k , then a set of the form

$$W = \{\underline{x} \in R_k \mid \alpha_i \leq x_i \leq \beta_i, 1 \leq i \leq k \text{ where } \underline{x} = (x_1, \dots, x_k), \leq \in \{<, \leq\}\}$$

is called a k -cell. Its volume is defined to be

$$\text{vol}(W) = \prod_{i=1}^k (\beta_i - \alpha_i)$$

We call a set of the form

$$Q(a; \delta) = \{x \in R_k \mid \alpha_i \leq x_i < \alpha_i + \delta, 1 \leq i \leq k\}$$

a δ -box with a corner at $a = (\alpha_1, \dots, \alpha_n)$.

Let (x, M, μ) be a measure space, with μ a positive measure.

We then say (x, M, μ) is complete or μ is a positive complete measure on M provided given any $A \in M$ such that $\mu(A) = 0$, and $E \subset A$ then $E \in M$.

We now state a familiar result of real analysis [71]. There exists a positive complete measure, μ , defined on a σ -algebra, M , in R_k , with the following properties:

- i) $\mu(W) = \text{vol}(W)$ for all k -cells W
- ii) μ is translate invariant, i.e.

$$\mu(E + x) = \mu(E) \text{ for all } E \in M, x \in R_k.$$

We call the members of M the Lebesgue measurable sets in R_k and μ the Lebesgue measure. We now state the divergence theorem in a relaxed setting, the proof of which is given in Appendix C.

Let Ω be a bounded regular region (hence a Lebesgue measurable set), and ϕ , \underline{u} , \underline{T} a scalar, vector, and second order tensor field, respectively, differentiable almost everywhere on Ω with derivatives in $L^1(\Omega)$. Then the results of the classical divergence theorem hold on Ω with the surface integral interpreted as defined on page 81.

Uniqueness of Solution to the Traction Problem
for Weak Elastostatic States

Let Ω be a bounded domain in R_n . Define $\hat{C}^n(\bar{\Omega}) = \{f \in C^n(\bar{\Omega}) \mid \text{supp } f \subset \Omega\}$, where $\text{supp } f = \overline{\{x \in \Omega \mid f(x) \neq 0\}}$. Clearly, if $f \in \hat{C}^n(\bar{\Omega})$ then f vanishes in a neighborhood of $\partial\Omega$.

Definition (generalized gradient): Let \underline{f} be a vector field, $\underline{f} \in L^1(\Omega)$ where Ω is a bounded domain in R_3 . If there exists a two-tensor field $\underline{\omega} \in L^1(\Omega)$ such that for every $\phi \in \hat{C}^1(\bar{\Omega})$

$$\int_{\Omega} \phi_{i,j} f_i = - \int_{\Omega} \phi_i \omega_{ij} \quad i, j \in \{1, 2, 3\}$$

we say \underline{f} has generalized gradient $\underline{\omega}$ on $\bar{\Omega}$ and we write

$$\partial \underline{f} = \underline{\omega}$$

Suppose there exists $\underline{\omega}'$ and $\underline{\omega}''$ in $L^1(\Omega)$ that satisfy the above definition. Then

$$\int_{\Omega} \phi_{i,j} (f_i - f_i) = 0 = - \int_{\Omega} \phi_i (\omega'_{ij} - \omega''_{ij}) \text{ for all } \phi \in \hat{C}^1(\bar{\Omega}).$$

Therefore $\phi_i (\omega'_{ij} - \omega''_{ij}) = 0$ almost everywhere (a.e.), i.e., zero except on a set of measure zero. The arbitrariness of ϕ dictates $\omega'_{ij} = \omega''_{ij}$ almost everywhere.

Now suppose $q \in \hat{C}^1(\bar{\Omega})$. We wish to show $\nabla q = \partial q$. Applying the divergence theorem to the first integral on the right we get

$$\int_{\Omega} \phi_{i,j} q_i = \int_{\partial\Omega} \phi_i q_i n_j - \int_{\Omega} \phi_i q_{i,j} ,$$

but $\int_{\partial\Omega} \phi_i q_i n_j = 0$ since $\phi \in \hat{C}^1(\bar{\Omega})$,

and by the uniqueness of ∂q the result follows.

Definition ($W_2^1(\bar{\Omega})$): Let Ω be a bounded domain in R_3 ,

$X = \{q \in L^2(\bar{\Omega}) \mid q \text{ is vector-valued, } \partial q \text{ exists}\}$, and

$$W_2^1(\bar{\Omega}) = (X, \|\cdot\|_S)$$

where

$$\|q\|_S^2 = \int_{\Omega} \{|q|^2 + |\partial q|^2\}.$$

Remarks

1. X is a vector space over the real field, where the elements of the space are sets of functions that are equal except on sets of Lebesgue measure zero.

2. $\|\cdot\|_S$ is a norm, i.e.

i) $\|q\|_S \geq 0$ and $\|q\|_S = 0$ iff $q = 0$ a.e. for all $q \in W_2^1(\bar{\Omega})$

ii) $\|q + p\|_S \leq \|q\|_S + \|p\|_S$ for all $p, q \in W_2^1(\bar{\Omega})$

iii) $\|\alpha q\|_S = |\alpha| \|q\|_S$ for all $q \in W_2^1(\bar{\Omega})$, $\alpha \in \mathbb{R}$

3. $W_2^1(\bar{\Omega})$ is a complete normed linear space, i.e., every Cauchy sequence in the space converges. $\{f_n\}$ is a Cauchy sequence provided given any $\epsilon > 0$ there exists $M \in \mathbb{P}$, the positive integers, such that $m, n > M$ implies $\|f_n - f_m\| < \epsilon$. A complete normed linear space is called a Banach Space (the proof of completeness is established by the standard argument of selecting a candidate in $W_2^1(\bar{\Omega})$ for a sequence's

limit and then showing the convergence of the sequence to the limit, cf Smirnov [75]

To motivate the definition of weak elastostatic state about to be introduced, consider the following. Let Ω be a regular region and

$$S = [u, \sigma] \in E(f, c; \bar{\Omega}),$$

We wish to show

$$\int_{\Omega} (-\phi_{i,j} \sigma_{ij} + \phi_i f_i) + \int_{\partial\Omega} \phi_i s_i = 0 \quad (28)$$

or

$$\int_{\Omega} (-\nabla \phi \cdot \sigma + \phi \cdot f) + \int_{\partial\Omega} \phi \cdot s = 0$$

for all $\phi \in C^1(\bar{\Omega})$.

Let $p_j(x) = -\phi_i(x) \sigma_{ij}(x)$ for all $x \in \Omega$. The smoothness of p implies

$$p_{j,j}(x) = -\phi_{i,j}(x) \sigma_{ij}(x) - \phi_i(x) \sigma_{ij,j}(x).$$

But $S \in E(f, c; \bar{\Omega})$ (the stress equation of motion) implies

$$p_{j,j}(x) = -\phi_{i,j}(x) \sigma_{ij}(x) + \phi_i(x) f_i(x).$$

The smoothness of $p_{j,j}$ allows us to apply the classical divergence theorem,

$$\begin{aligned} \int_{\Omega} p_{j,j} &= - \int_{\Omega} \phi_{i,j} \sigma_{ij} + \int_{\Omega} \phi_i f_i = \int_{\partial\Omega} p_i n_i = - \int_{\partial\Omega} \phi_j \sigma_{ij} n_i = \\ &= - \int_{\partial\Omega} \phi_i s_i, \end{aligned}$$

the result follows. \blacksquare

Definition (Weak elastostatic state). Let Ω be a regular region, and c as defined before, and f a vector field measurable on $\bar{\Omega}$. Then $S = [u, \sigma]$ is said to be a weak elastostatic state on $\bar{\Omega}$ corresponding to the body-force field f and elasticity field c , provided:

- i) $f \in L^2(\bar{\Omega})$, $u \in W_2^1(\bar{\Omega})$
- ii) $\sigma_{ij}(x) = c_{ijkl}(x) \partial_l u_k(x)$
- iii) $\int_{\Omega} (-\phi_{i,j} \sigma_{ij} + \phi_i f_i) = 0$ for all $\phi \in \hat{C}^1(\bar{\Omega})$

For the set of all such states, we write

$$E_w(f, c; \bar{\Omega})$$

What is the relationship between $E(f, c; \bar{\Omega})$ and $E_w(f, c; \bar{\Omega})$?

Proposition: $E(f, c; \bar{\Omega}) \subset E_w(f, c; \bar{\Omega})$; furthermore if $S \in E_w(f, c; \bar{\Omega})$ with $u \in C^2(\Omega) \cap C^1(\bar{\Omega})$, and $\sigma \in C^1(\Omega) \cap C(\bar{\Omega})$, then $S \in E(f, c; \bar{\Omega})$ where

$$\int_{\Omega} |f - f'|^2 = 0, \text{ i.e. } \|f - f'\|_{L^2} = 0$$

Proof: $E(f, c; \bar{\Omega}) \subset E_w(f, c; \bar{\Omega})$ follows trivially from the smoothness condition of $E(f, c; \bar{\Omega})$ and equation (28). Now let $S \in E_w(f, c; \bar{\Omega})$ together with the hypothesis as stated above.

Define f' through

$$f' = - \nabla \cdot \sigma \quad (f'_i = - \sigma_{ij,j}) \text{ on } \bar{\Omega}$$

then clearly

$$S = [u, \sigma] \in E(f', c; \bar{\Omega}) \subset E_w(f', c; \bar{\Omega})$$

AD-A059 526

TEXAS A AND M UNIV COLLEGE STATION MECHANICS AND MAT--ETC F/G 11/4
STUDIES ON THE MECHANICAL RESPONSE AND FRACTURE OF VISCOELASTIC--ETC(U)
JUL 78 R A SCHAPERY, J H SCHMIDT AFOSR-74-2697

UNCLASSIFIED

MM-3064-78-6

AFOSR-TR-78-1257

NL

2 of 2

AD
A069 526



END

DATE

FILMED

-12-78

DDC

therefore

$$\int_{\Omega} (-\phi_{ij} \sigma_{ij} + \phi_i f_i) = 0 = \int_{\Omega} (-\phi_{ij} \sigma_{ij} + \phi_i f'_i) \text{ which implies}$$

$$\int_{\Omega} \phi_i (f_i - f'_i) = 0, \text{ which implies}$$

$$f = f' \text{ a.e. iff } \| \underline{f} - \underline{f}' \|_2 = 0.$$

Theorem: Let Ω be a bounded, locally star-shaped domain in R_3 . Then $C^1(\Omega)$ is dense in $W_2^1(\bar{\Omega})$.

Proof: (Smirnov [75] proves this for bounded star-shaped domains, this proof is due to Brockway [68]).

NOTE: If (X, τ) is a topological space, then $A \subset X$ is dense in X provided $\bar{A} = X$. Here, $W_2^1(\bar{\Omega})$ together with the usual topology defined through $\| \cdot \|_S$ is a topological space; indeed it is a Hilbert space and we need only show given any $p \in W_2^1(\bar{\Omega})$ that there exists a sequence $\{p^n\} \subset C^1(\bar{\Omega})$ such that $p^n \xrightarrow{\| \cdot \|_S} p$ i.e. $\| p^n - p \|_S \rightarrow 0$ as $n \rightarrow \infty$.

If $x \in \bar{\Omega}$, then, there exists a neighborhood $N(x)$ such that $\bar{\Omega} \cap N(x)$ is star-shaped. Now $(R_3, \| \cdot \|_2)$ is a finite dimensional normed linear space (note: $\| x \|_2^2 = x_1^2 + x_2^2 + x_3^2$).

We state the following result [73].

Proposition: If $(V, \| \cdot \|)$ is a normal linear space over the field Φ , then the following are equivalent:

- i) $(V, \| \cdot \|)$ is finite dimensional
- ii) If $E \subset V$ is a closed bounded set, then E is compact.

Definition: Let (X, τ) be a topological space, then $A \subset X$ is compact provided every open cover of A is reducible to a finite cover.

Let $\Gamma = \{G_i | G_i \in \tau, i \in I\}$, we say Γ is an open cover of $A \subset X$ provided $\bigcup_{i \in I} G_i \supset A$. By the preceding proposition, $\bar{\Omega}$ is compact, therefore there exists a finite subcovering from $\Gamma = \{N(x) | x \in \bar{\Omega}\}$, namely,

$$\{N(x^1), N(x^2), \dots, N(x^m)\}$$

such that

$$\bigcup_{k=1}^m N(x^k) \supset \bar{\Omega} \text{ and such that } N(x^i) \text{ is not contained in } \bigcup_{\substack{j=1 \\ j \neq i}}^m N(x^j).$$

Next, let $N_k \equiv N(x^k) \quad k = 1, 2, \dots, m$.

Define

$$D_k = N_k \cap \Omega \quad k = 1, 2, \dots, m.$$

Now each D_k is star-shaped. If $p \in W_2^1(\bar{\Omega})$ then p_k is in $W_2^1(\bar{D}_k)$ for all $k = 1, \dots, m$ where p_k is the restriction of p to \bar{D}_k .

Then by Smirnov there exists $\{p_k^n\} \subset C^1(\bar{D}_k)$ such that

$$p_k^n \xrightarrow{\|\cdot\|_{s_k}} p \text{ as } n \rightarrow \infty \quad (\|\cdot\|_{s_k} \text{ is the restriction of } \|\cdot\|_s \text{ to } \bar{D}_k).$$

Define $\Xi(\Omega) = \{f \in C^\infty(\Omega) | f \text{ has compact support in } \Omega\}$.

We state the following well known theorem [70];

Theorem: If Λ is a collection of open sets in R_n , whose union is Ω , then there exists a sequence $\{\psi_i\} \subset \Xi(\Omega)$ with $\psi_i \geq 0$, such that

- a) each ψ_i has its support in some member of Λ ,
- $\beta)$ $\sum_{i=1}^{\infty} \psi_i = 1$ for all $x \in \Omega$
- $\gamma)$ to every compact $K \subset \Omega$ corresponds an integer, m , and an open

set $W \subset K$ such that

$$\psi_1(x) + \psi_2(x) + \dots + \psi_m(x) = 1 \text{ for all } x \in W.$$

Such a collection, $\{\psi_i\}$ is called a locally finite partition of unity in Ω subordinate to the open cover Λ of Ω .

Corollary: If Λ is a finite collection of open sets in the above theorem, then there exists a sequence $\{\psi_i\} \subset \Xi(\Omega)$ with $\psi_i \geq 0$ such that

- a) each ψ_i has support in some member of Λ
- b) $\sum_{i=1}^n \psi_i = 1$ for all $x \in \Omega$, where there are n open sets in Λ .

Proof: Let $\{D_1, \dots, D_m\}$ be the open cover of Ω . Then corresponding to each D_i there exists a compact set K_i such that $K_i \subset D_i$. Then from the above theorem there exists

$$\psi_{1i} + \dots + \psi_{p_i i} = 1 \text{ for all } x \in W_i \supset K_i, W_i \dots \text{ open and } W_i \subset \Omega.$$

At least one of the ψ_{ji} has support in D_i since there exists $x \in D_i, x \notin \bigcup_{\substack{j=1 \\ j \neq i}}^m D_j$ and by choosing K_i such that $x \in K_i$. Now

$$\frac{1}{m} \sum_{i=1}^m \sum_{j=1}^{p_i} \psi_{ij} = 1 \text{ and by defining } \psi_i = \sum \psi_{ij} \text{ such that } \text{supp } \psi_{ij} \subset D_i.$$

The result follows. \blacksquare

Introduce a partition of unity $\{\psi_1, \dots, \psi_m\}$ subordinate to $\{D_1, D_2, \dots, D_m\}$, where

$$\sum_{k=1}^m \psi_k(x) = 1 \text{ for all } x \in \Omega \text{ and } \text{supp } \psi_k \subset D_k \text{ (} k = 1, \dots, m \text{),}$$

Define $q_k^n = \psi_k p_k^n$ on D_k (no sum on k)
 $= 0$ on $\bar{\Omega} \setminus D_k$ ($k=1, \dots, m; n=1, 2, \dots$),

clearly $q_k^n \in C^1(\Omega)$.

Define $p_n = \sum_{k=1}^m q_k^n$ on $\bar{\Omega}$,

clearly $p_n \in C^1(\bar{\Omega})$ ($n = 1, 2, \dots$).

We need only show

$$p^n \xrightarrow{\|\cdot\|_s} p$$

$$\text{Now } \|p - p^n\|_s = \left\| p - \sum_{k=1}^m \psi_k - \sum_{k=1}^m q_k^n \right\|_s \leq \sum_{k=1}^m \|\psi_k p - q_k^n\|_s,$$

$$\text{but } \|\psi_k p - q_k^n\|_s = \|\psi_k(p - p_k^n)\|_{s_k}$$

$$\text{since } \psi_k q_k^n = 0 \text{ on } \bar{\Omega} \setminus D_k \text{ and } q_k^n = \psi_k p_k^n \text{ on } \bar{\Omega}.$$

$$\text{Now } \|\psi_k(p - p_k^n)\|_{s_k}^2 = \int_{D_k} [|\psi_k(p - p_k^n)|^2 + |\partial(\psi_k(p - p_k^n))|^2]$$

Simirnov shows the product rule applies to generalized differentiation of functions in W_2^1 . Since $\psi_k \in C^\infty(\bar{\Omega})$, ψ_k and $\nabla \psi_k$ are bounded on $\bar{\Omega}$, therefore there exists $M \in \mathbb{R}$ such that

$$\|\psi_k(p - p_k^n)\|_{s_k}^2 \leq M^2 \int_{D_k} \{|p - p_k^n|^2 + |\partial(p - p_k^n)|^2\} \text{ for all } k=1, \dots, m.$$

$$\text{Therefore } \|\psi_k(p - p_k^n)\|_{s_k} \leq M \|p - p_k^n\|_{s_k}.$$

$$\text{But } \|p - p_k^n\|_{s_k} \rightarrow 0 \text{ as } n \rightarrow \infty,$$

which implies $\|p - p^n\|_S \rightarrow 0$ as $n \rightarrow \infty$.

Therefore $p \in C^1(\bar{\Omega})$ and $C^1(\bar{\Omega}) \supset W_2^1(\bar{\Omega})$.

But by definition of $W_2^1(\bar{\Omega})$, $W_2^1(\bar{\Omega}) \supset C^1(\bar{\Omega})$, the result follows. \square

We formulate the weak elastostatic traction problem. Given a regular locally star-shaped region, Ω , find

$$S = [u, \sigma] \in E_W(f, c; \bar{\Omega})$$

corresponding to data f, c and subjected to the generalized boundary conditions

$$\int_{\Omega} (-\phi_{i,j} \sigma_{ij} + \phi_i f_i) + \int_{\partial\Omega} \phi_i \bar{s}_i^* = 0 \text{ for all } \phi \in C^1(\bar{\Omega})$$

where \bar{s}^* is $L^1(\partial\Omega)$ as discussed previously (p. 81).

That this is a generalization of the classical elastostatic problem follows by assuming enough smoothness on S .

Theorem: (Uniqueness of solution for the traction problem of weak elastostatic states): Let Ω be a regular locally star-shaped region and

$$\alpha) S' = [u', \sigma'] \in E_W(f, c; \bar{\Omega})$$

$$S'' = [u'', \sigma''] \in E_W(f, c; \bar{\Omega})$$

$$\beta) \text{ for all } \phi \in C^1(\bar{\Omega})$$

$$\int_{\Omega} (-\phi_{i,j} \sigma'_{ij} + \phi_i f_i) + \int_{\partial\Omega} \phi_i \bar{s}_i^* = 0$$

$$\int_{\Omega} (-\phi_{i,j} \sigma''_{ij} + \phi_i f_i) + \int_{\partial\Omega} \phi_i \bar{s}_i^* = 0 \text{ where } \bar{s} \in L^1(\partial\Omega).$$

Furthermore, assume

γ) c is positive definite on Ω , so that

$$c_{ijkl}(x) \gamma_{ij}(x) \gamma_{kl}(x) > 0 \text{ for all } x \in \Omega$$

for all symmetric two-tensors, $\gamma \neq 0$. Then $u' = u''$ modulo a rigid displacement, and $\sigma' = \sigma''$ almost everywhere on $\bar{\Omega}$.

Proof: Define a state $S = [u, \sigma]$ through $u = u' - u''$, $\sigma = \sigma' - \sigma''$ on $\bar{\Omega}$

according to α), β) and the definition of weak elastostatic state,

$$S = [u, \sigma] \in E_W(0, c; \bar{\Omega}), \int_{\Omega} -\phi_{i,j} \sigma_{ij} = 0 \text{ for all } \phi \in C^1(\bar{\Omega}). \quad (A)$$

We show that (A) holds for $\phi \in W_2^1(\bar{\Omega})$ with $\phi_{i,j}$ replaced by $\partial_j \phi_i$.

If $\phi \in W_2^1(\Omega)$, then since $C^1(\bar{\Omega})$ is dense in $W_2^1(\Omega)$, there exists a net $\{\phi^n\} \subset C^1(\bar{\Omega})$ such that $\phi^n \xrightarrow{\|\cdot\|_S} \phi$ a.e. on Ω .

Define Δ through

$$\Delta = \int_{\Omega} (\partial_j \phi_i - \phi_{i,j}^n) \sigma_{ij}.$$

Now

$$|\Delta| \leq \int_{\Omega} |\sigma_{ij} (\partial_j \phi_i - \phi_{i,j}^n)| = \int_{\Omega} |\sigma_{ij}| |\partial_j \phi_i - \phi_{i,j}^n|,$$

and an application of Hölder's inequality implies

$$|\Delta| \leq \left\{ \int_{\Omega} |\sigma_{ij}|^2 \right\}^{1/2} \left\{ \int_{\Omega} |\partial_j \phi_i - \phi_{i,j}^n|^2 \right\}^{1/2}.$$

But $\phi, \phi^n \in W_2^1(\bar{\Omega})$, and $\|\phi^n - \phi\|_S \rightarrow 0$ as $n \rightarrow \infty$, i.e.

$$\int_{\Omega} \{ |\phi - \phi^n|^2 + |\partial \phi - \nabla \phi^n|^2 \} \rightarrow 0 \text{ as } n \rightarrow \infty.$$

Therefore $\int_{\Omega} |\partial \phi - \nabla \phi^n|^2 \rightarrow 0$ as $n \rightarrow \infty$

and $|\Delta| \rightarrow 0$ as $n \rightarrow \infty$. That is to say, given $\phi \in W_2^1(\Omega)$, there exists $\phi^n \in C^1(\bar{\Omega})$ such that

$$\int_{\Omega} \nabla \phi \cdot \underline{\sigma} \rightarrow \int_{\Omega} \partial \phi \cdot \underline{\sigma} \text{ as, i.e. } \int_{\Omega} \phi_{i,j}^n \sigma_{ij} \rightarrow \int_{\Omega} \partial_j \phi_i \sigma_{ij} \text{ as } n \rightarrow \infty.$$

But (A) implies $\int_{\Omega} \phi_{i,j}^n \sigma_{ij} = 0$ for all $\phi^n \in C^1(\bar{\Omega})$,

therefore $\int_{\Omega} \partial_j \phi_i \sigma_{ij} = 0$.

Now

$$\int_{\Omega} (\partial_j \phi_i) \sigma_{ij} = 0 \text{ for all } \phi \in W_2^1(\bar{\Omega}),$$

in particular, $u \in W_2^1(\Omega)$, therefore

$$\int_{\Omega} (\partial_j u_i) \sigma_{ij} = 0.$$

But $S = [u, \sigma]$ is a weak elastostatic state, therefore

$$\sigma_{ij} = C_{ijkl} \partial_l u_k$$

and

$$\int_{\Omega} C_{ijkl} \partial_j u_i \partial_l u_k = 0.$$

A prudent look at the definition of generalized gradient indicates the symmetry of the generalized gradient; therefore, since c is positive definite, $\partial u = 0$ almost everywhere, and by $\sigma_{ij} = C_{ijkl} \partial_l u_k$ we have $\sigma = 0$ a.e. Since $\partial u = 0$ a.e., u is unique modulo a rigid displacement.

Among the types of singularities admissible by the preceding theorem are any stress fields in $L^2(\bar{\Omega})$ (this includes the crack problem

which has stresses of order $O(r^{-1/2})$ as $r \rightarrow 0$), however, $u \in W_2^1(\bar{\Omega})$ precludes finite discontinuities, indeed Smirnov [75] shows if $u \in W_2^1(\bar{\Omega})$, then u is absolutely continuous almost everywhere in $\bar{\Omega}$. Obviously, absolutely continuous implies continuity.

If μ is a positive measure function on (X, M) , then $\phi: D \rightarrow Y$, where $(Y, \|\cdot\|)$ is a normed linear space and $D \subset M$, is a set function on D . We say ϕ is absolutely continuous with respect to μ , provided given any $\epsilon > 0$ there exists $\delta > 0$ such that

$$|\phi(E)| < \epsilon \text{ whenever } \mu(E) < \delta, E \in D.$$

CONCLUSIONS AND RECOMMENDATIONS

This work has produced three main results—failure zone effects on isochromatic lines, feasibility of laser interferometric techniques in the measurement of displacement fields near crack tips in solid propellant, and uniqueness of solution to a broad class of elastostatic problems.

Studies of the isochromatic fringe patterns in an infinite sheet with a semi-infinite crack under equal biaxial loadings indicate that failure zones induce tilting of isochromatic fringe patterns. Additional problems, such as a finite sheet with a small, centered crack (small relative to sheet dimensions) under equal biaxial loadings, need to be solved (numerically) to determine the extent of failure zone effects.

The experimental results observed and recorded herein closely agree (6%-10%) with theoretical results from linear theories and partially confirm results observed by others [8]. There were, however, apparent nonlinearities, or at least observations not explainable through linear theory. To further substantiate these observations, additional experimental data should be obtained in a more controlled environment. A loading frame that would eliminate out-of-plane and in-plane translational displacements is desirable. Different loadings on the sample should be scrutinized, e.g., the combined Mode I and Mode II problem, and compared to analytical solutions.

The uniqueness of solution to the traction boundary value problem proved here applies to a variety of traction boundary value problems. Many authors [76-78] treat elliptic boundary value problems using a

modern approach. (Uniqueness for the generalized Dirichlet problem is given, for example, in [76].) It is the way the boundary conditions β (p. 91) of the uniqueness theorem (as opposed to normal derivatives which are specified in the generalized Dirichlet problem) that separate this treatment from previous work [76-78].

In summary, it is the view of this author that: 1) further study determining the extent of failure zone effects should be conducted, 2) further refinements are needed in the interferometric technique, whose feasibility has been established in the present work, and 3) uniqueness of the displacement boundary value problem should be investigated.

REFERENCES

- [1] L. Holliday, Composite Materials, Elsevier Publishing Co., (1969).
- [2] R. A. Schapery, "A Theory of Crack Initiation and Growth in Viscoelastic Media - I Theoretical Development," Int. J. Fract. Mech., 11 (1975) 141.
- [3] R. A. Schapery, "A ... Media - II Approximate Methods of Analysis," Int. J. Fract. Mech., 11 (1975) 369.
- [4] R. A. Schapery, "A ... Media - III Analysis of Continuous Growth," Int. J. Fract. Mech., 11 (1975) 549.
- [5] L. R. Cornwell and R. A. Schapery, "SEM Study of Microcracking in Strained Solid Propellant," Metallography, 8 (1975) 445.
- [6] W. G. Knauss, "The Mechanics of Polymer Fracture," Applied Mechanics Reviews, 26 (1973) 1.
- [7] W. G. Knauss, "Fracture of Solids Possessing Deformation Rate Sensitive Material Properties," A.S.M.E. - A.M.D., 19 (1976) 69.
- [8] S. R. Swanson, "An Application of Schapery's Theory of Viscoelastic Fracture to Solid Propellant," (submitted for publication to AIAA J, 1975).
- [9] R. J. Farris and J. E. Fitzgerald, "Deficiencies of Viscoelastic Theories as Applied to Solid Propellants," Bulletin JANNAF Mech. Beh. Wkg. Group, 8th Meeting, CPIA Pub. 193, (March, 1970).
- [10] R. J. Farris and R. A. Schapery, "Development of a Solid Rocket Propellant Nonlinear Viscoelastic Constitutive Theory," Final Report AFRPL-TR-73-50, (June, 1973).
- [11] R. A. Schapery, "A Nonlinear Constitutive Theory for Particulate Composites Based on Viscoelastic Fracture Mechadics," JANNAF Operational Serviceability and Structures and Mechanical Behavior Working Groups, CPIA Pub. 253, (July, 1974).
- [12] Barenblatt, "The Mathematical Theory of Equilibrium Cracks in Brittle Fracture," Advances in Applied Mechanics, 7 (1962) 55.
- [13] M. L. Williams, "On the Stress Distribution at the Base of a Stationary Crack," J. Applied Mech., 24 (1957) 109.
- [14] P. C. Paris and G. C. Sih, "Stress Analysis of Cracks," Fracture Toughness Testing and its Application, ASTM, STP381, (1965) 30.
- [15] G. R. Irwin, "Fracture Mechanics," Structural Mechanics, Proceedings of the First Symposium on Naval Structural Mechanics, (1960) 557.

- [16] I. S. Sokolnikoff, Mathematical Theory of Elasticity, McGraw-Hill, 2nd Ed., (1956).
- [17] G. R. Irwin, J. H. Kies, and H. L. Smith, "Fracture Strengths Relative to Onset and Arrest of Crack Propagation," Proc. American Society for Testing and Materials, (1958) 640.
- [18] S. P. Timoshenko and J. N. Goodier, Theory of Elasticity, McGraw-Hill, 3rd Ed., (1970).
- [19] H. M. Westergaard, "Bearing Pressures and Cracks," Journal of Applied Mech., 6 No. 2 (1939) A-49.
- [20] G. R. Irwin, "Analysis of Stresses and Strains Near the End of A Crack Traversing a Plate," J. Applied Mech. 24 No. 3 (1957) 361.
- [21] G. R. Irwin, "Relation of Stresses Near a Crack to the Crack Extension Force," Proc. Ninth Congress of Applied Mech. (1957) 245.
- [22] G. R. Irwin, "Fracture," Handbuch der Physik, VI, Springer-Verlag, (1958) 551.
- [23] N. I. Muskhelishvili, Some Basic Problems of the Mathematical Theory of Elasticity, Noordhoff, 4th Ed., (1954).
- [24] G. C. Sih, "On the Westergaard Method of Crack Analysis," Int. J. of Fract. Mech., 2 (1966) 628.
- [25] J. Eftis and H. Liebowitz, "On the Modified Westergaard Equations For Certain Plane Crack Problems," Int. J. Fract. Mech., 8 No. 4 (1972) 383.
- [26] C. E. Inglis, "Stresses in a Plate Due to the Presence of Cracks and Sharp Corners," Transaction Institute of Naval Arch., 55 (1913) 219.
- [27] A. A. Griffith, "The Phenomena of Rupture and Flow in Solids," Philosophical Transactions of the Royal Society, A 221 (1920) 861.
- [28] M. L. Williams, "Stress Singularities Resulting from Various Boundary Conditions in Angular Corners of Plates in Extension," Journal of Applied Mech., 19 (1952) 526.
- [29] E. G. Coker and L. G. N. Filon, A Treatise on Photoelasticity, Cambridge University Press, (1931).
- [30] G. C. Sih and H. Liebowitz, "Mathematical Theories of Brittle Fracture," Fracture, an Advanced Treatise, Academic Press, 2 (1968) 67.
- [31] J. R. Rice, "Mathematical Analysis in the Mechanics of Fracture," Fracture, an Advanced Treatise, Academic Press, 2 (1968) 191.

- [32] J. N. Goodier, "Mathematical Theory of Equilibrium Cracks, Fracture, an Advanced Treatise, Academic Press, 2 (1971) 1.
- [33] E. Sternberg, "Three-Dimensional Stress Concentrations in the Theory of Elasticity," Applied Mechanics Reviews, 24 No. 1 (1958) 1.
- [34] E. Sternberg and W. T. Koiter, "The Wedge Under a Concentrated Couple: A Paradox in the Two-Dimensional Theory of Elasticity," J. Applied Mech., 25 (1958) 575.
- [35] A. H. England and A. J. M. Spencer, "On stress Singularities in Linear Elasticity," Int. J. Eng. Sci., 9 (1971) 571.
- [36] D. S. Dugdale, "Yielding of Steel Sheets Containing Slits," J. of the Mechanics and Physics of Solids, 8 (1960) 100.
- [37] J. R. Rice, "A Path Independent Integral and the Approximate Analysis of Strain Concentration by Notches and Cracks," J. of Applied Mech., 35 (1968) 379.
- [38] A. S. Kobayashi, "Photoelastic Studies of Fracture," Fracture, an Advanced Treatise, Academic Press, 3 (1971) 311.
- [39] A. A. Wells and D. Post, "The Dynamic Stress Distribution Surrounding a Running Crack - A Photoelastic Analysis," Proc. Soc. Exp. Stress Analysis, 16 No. 1 (1958) 69.
- [40] G. R. Irwin, "Discussion," Proc. Soc. Exp. Stress Analysis, 16 No. 1 (1958) 93.
- [41] N. Conrad, "On Microcrack Growth and Arrest in Simulated Fibrous Composites," Mech. and Mat. Res. Center, Texas A&M University, MM 3168-76-10, (1976).
- [42] R. S. Dunham and E. B. Becker, TEXGAP - The Texas Grain Analysis Program, University of Texas, TICOM 73-1, (1973).
- [43] P. M. Prenter, Splines and Variational Methods, John Wiley & Sons, (1975).
- [44] G. Strang and G. J. Fix, An Analysis of the Finite Element Method, Prentice-Hall, (1973).
- [45] J. T. Oden and J. N. Reddy, An Introduction to the Mathematical Theory of Finite Elements, John Wiley & Sons, (1976).
- [46] A. J. Durelli and V. J. Parks, Moire' Analysis of Strain, Prentice-Hall, (1970).
- [47] W. D. Hart, "Moire' Method for the Measurement of Strains in Solid Propellants," Lockheed Propulsion Company Research Division T.N. 115, (16 July, 1964).

- [48] "Moire' Method of Stress Analysis," Technical Data Bulletin TDG-2, Photoelastic Inc., Malvern, Pa.
- [49] Manuscript, "Microdensitometry Procedures and Rationale," Obtained from NASA in Houston.
- [50] P. Lorain and D. R. Corson, Electromagnetic Fields and Waves, Freeman and Co., 2nd Ed., (1970).
- [51] C. E. Taylor and Y. Y. Hung, "Holography in Experimental Stress Analysis," The Engineering Science Perspective, 1 No. 1 (March/April, 1976) 4.
- [52] M. Francon, Holography, Academic Press, (1974).
- [53] D. Gabor, "Holography, 1948-1971," Science, 177 No. 4046 (1972) 299.
- [54] R. Brown, Lasers: Tools of Modern Technology, Doubleday and Co., (1968).
- [55] A. E. Ennos, "Speckle Interferometry," Topics in Applied Physics, 9(1975) 203.
- [56] K. A. Stetson, "A review of Speckle Photography and Interferometry," Optical Engineering, 14 No. 5 (1975) 482.
- [57] Air Force Flight Dynamics Laboratory Publication, Photomechanics Facility, 2nd Ed., (March, 1976).
- [58] E. Archbold, J. M. Burch, and A. E. Ennos, "Recording of In-Plane Surface Displacements by Double-Exposure Speckle Photography," Optica Acta, 17 No. 12 (1970) 883.
- [59] F. D. Adams and G. E. Maddux, "On Speckle Diffraction Interferometry for Measuring Whole Field Displacements and Strains," Technical Report AFFDC-TR-73-123, (December, 1973).
- [60] J. A. Leendertz, "Interferometric Displacement Measurements on Scattering Surfaces Utilizing Speckle Effect," J. Phys. E. (J. Scient. Instrument), 3(1970) 214.
- [61] F. D. Adams and G. E. Maddux, "Dual Plate Speckle Photography," Technical Memorandum AFFDL-TM-75-57-FBR, (April, 1975).
- [62] G. E. Maddux, Air Force Flight Dynamics Laboratory, Wright-Patterson Air Force Base, private communication, (1977).
- [63] E. Archbold and A. E. Ennos, "Displacement Measurement from Double-Exposure Laser Photographs," Optica Acta, 19 (1972) 253.

- [64] J. K. Knowles and T. A. Pucik, "Uniqueness for Plane Crack Problems in Linear Elastostatics," J. of Elasticity, 3 No. 3 (1973) 155.
- [65] A. E. H. Love, A Treatise on the Mathematical Theory of Elasticity, Dover Publications, (1944).
- [66] M. E. Gurtin, "The Linear Theory of Elasticity," Handbuch der Physik, VI a/2, Springer-Verlag, (1972) 1.
- [67] O. D. Kellog, Foundations of Potential Theory, Dover Publications, (1953).
- [68] G. S. Brockway, "On the Uniqueness of Singular Solutions to Boundary-Initial Value Problems in Linear Elasticity," Archive for Rational Mechanics and Analysis, 48 No. 3 (1972) 213.
- [69] G. Klambauer, Real Analysis, American Elsevier Co., (1973)
- [70] W. Rudin, Functional Analysis, McGraw-Hill, (1973).
- [71] W. Rudin, Real and Complex Analysis, McGraw-Hill, (1974)
- [72] R. C. Buck and E.F. Buck, Advanced Calculus, McGraw-Hill, (1965).
- [73] R. Larsen, Functional Analysis an Introduction, Dekker, (1973).
- [74] T. M. Apostol, Mathematical Analysis A Modern Approach to Advanced Calculus, Addison-Wesley, (1964).
- [75] V. I. Smirnov, A Course of Higher Mathematics, V, Addison-Wesley, (1964).
- [76] S. Agmon, Lectures on Elliptic Boundary Value Problems, Van Nostrand, (1965).
- [77] G. Fichera, "Existence Theorems of Elasticity," Handbuch der Physik, VI a/2, Springer-Verlag, (1972) 347.
- [78] R. J. Knopps and L. E. Payne, Uniqueness Theorems in Linear Elasticity, Springer-Verlag, (1971).
- [79] D. Broek, Elementary Engineering Fracture Mechanics, Noordhoff (1974).

APPENDIX A

The Equivalence of the Singular Terms of Williams and Irwin

MODE I

From equation (23)

$$\sigma_x = \sigma_r \cos^2 \theta + \sigma_\theta \sin^2 \theta - 2\sigma_{r\theta} \sin \theta \cos \theta. \quad (\text{A.1})$$

Equation (7) implies

$$\begin{aligned} \sigma_r &= \frac{a_1}{4r^{1/2}} \left[-5 \cos \frac{\theta}{2} + \cos \frac{3}{2} \theta \right] \\ \sigma_\theta &= \frac{a_1}{4r^{1/2}} \left[-3 \cos \frac{\theta}{2} - \cos \frac{3}{2} \theta \right] \end{aligned} \quad (\text{A.2})$$

$$\tau_{r\theta} = \frac{a_1}{4r^{1/2}} \left[-\sin \frac{\theta}{2} - \sin \frac{3}{2} \theta \right].$$

Equations (A.1) and (A.2) give

$$\begin{aligned} \sigma_x &= \frac{a_1}{4r^{1/2}} \left[-5 \cos \frac{\theta}{2} \cos^2 \theta + \cos \frac{3}{2} \theta \cos^2 \theta \right. \\ &\quad \left. - 3 \cos \frac{\theta}{2} \sin^2 \theta - \cos \frac{3}{2} \theta \sin^2 \theta \right. \\ &\quad \left. + 2 \sin \theta \cos \theta \left(\sin \frac{\theta}{2} + \sin \frac{3}{2} \theta \right) \right]. \end{aligned} \quad (\text{A.3})$$

Using

$$\begin{aligned} \cos \frac{3}{2} \theta &= \cos \theta \cos \frac{\theta}{2} - 2 \sin^2 \frac{\theta}{2} \cos \frac{\theta}{2} \\ \sin \frac{\theta}{2} + \sin \frac{3}{2} \theta &= 2 \sin \theta \cos \frac{\theta}{2} \\ \sin^2 \frac{\theta}{2} &= \frac{1}{2}(1 - \cos \theta), \end{aligned} \quad (\text{A.4})$$

equation (A.3) and (A.4) give

$$\sigma_x = -\frac{a_1}{r^{1/2}} \cos \frac{\theta}{2} \left[1 - \sin \frac{\theta}{2} \sin \frac{3}{2} \theta \right]. \quad (\text{A.5})$$

Recalling equation (1),

$$\sigma_x = \frac{K_I}{(2\pi r)^{1/2}} \cos \frac{\theta}{2} \left[1 - \sin \frac{\theta}{2} \sin \frac{3}{2} \theta \right]. \quad (\text{A.6})$$

Equations (A.5) and (A.6) imply

$$a_1 = -\frac{K_I}{\sqrt{2}\pi} \quad (\text{A.7})$$

Equation (A.7) could be found by using the expression for σ_y or τ_{xy} from equation (23).

MODE II

From Williams [13],

$$\begin{aligned} \sigma_\theta &= \frac{b_1}{4r^{1/2}} \left[-5 \sin \frac{\theta}{2} + 3 \sin \frac{3}{2} \theta \right] \\ \sigma_r &= \frac{b_1}{4r^{1/2}} \left[-3 \sin \frac{\theta}{2} - 3 \sin \frac{3}{2} \theta \right] \\ \tau_{r\theta} &= \frac{b_1}{4r^{1/2}} \left[-3 \sin \frac{\theta}{2} - 3 \sin \frac{3}{2} \theta \right]. \end{aligned} \quad (\text{A.8})$$

Equations (A.1) and (A.8) give

$$\begin{aligned} \sigma_x &= \frac{b_1}{4r^{1/2}} \left[-5 \sin \frac{\theta}{2} \cos^2 \theta + 3 \sin \frac{3}{2} \theta \cos^2 \theta \right. \\ &\quad \left. - 6 \sin^3 \theta \cos \frac{\theta}{2} - 4 \sin \frac{\theta}{2} \cos \frac{\theta}{2} \cos \theta (\cos \frac{\theta}{2} + \cos \frac{3}{2} \theta) \right] \end{aligned} \quad (\text{A.9})$$

where

$$\sin \frac{3}{2} \theta = \sin \frac{\theta}{2} \cos \theta + \sin \theta \cos \frac{\theta}{2}. \quad (\text{A.10})$$

Equations (A.4) (A.9) (A.10) imply

$$\sigma_x = - \frac{b_1}{r^{1/2}} \left(\sin \frac{\theta}{2} \right) \left[2 + \cos \frac{\theta}{2} \cos \frac{3}{2} \theta \right]. \quad (\text{A.11})$$

Recalling equation (1),

$$\sigma_x = - \frac{K_{II}}{(2\pi r)^{1/2}} \sin \frac{\theta}{2} \left[2 + \cos \frac{\theta}{2} \cos \frac{3}{2} \theta \right]. \quad (\text{A.12})$$

Equations (A.11), (A.12) imply

$$b_1 = \frac{K_{II}}{(2\pi)^{1/2}}. \quad (\text{A.13})$$

APPENDIX B

Linking the Failure Stress Distribution with TEXGAP

The following material properties will be used in this analysis,

$$E(\mu) \dots \text{Young's (shear) modulus} \quad (\text{B.1})$$

$$\nu \dots \text{Poisson's ratio.}$$

The constants in (B.1) are related through [18]

$$2\mu = \frac{E}{1+\nu} \quad (\text{B.2})$$

Using dimensional analysis for a quarter biaxial strip of width w , height h , crack length a , and grip displacement v_g ,

$$K_I = \lambda \mu \frac{v_g}{\sqrt{a}} \left(\frac{h}{w} \right) \quad (\text{B.3})$$

where λ is a constant of proportionality.

From equations (25a) and (25b) corresponding to the constant and ramp failure stresses,

$$K_I = 2 (2 \alpha / \pi)^{1/2} \sigma_m \quad (\text{constant stress}) \quad (\text{B.4})$$

$$K_I = \frac{4}{3} (2 \alpha / \pi)^{1/2} \sigma_m \quad (\text{ramp stress})$$

For plane stress [79]

$$G = K_I^2 / (3\mu), \quad (\text{B.5})$$

where G is the energy release rate and may be calculated through [30]

$$G \approx \frac{1}{2} \Delta W / \Delta a, \quad (\text{B.6})$$

and W is the strain energy per unit thickness, and is obtained from TEXGAP. Equations (B.3) and (B.5) combine to give

$$G = \frac{\lambda^2 v_g^2 h^2}{3 a w^2} \mu \quad (\text{B.7})$$

where $\frac{\lambda^2 v g^2 h^2}{3 a w^2}$ is constant for a given problem.

We seek an expression for σ_m . Equations (B.3), (B.4) give

$$\frac{\lambda \mu v g h}{w/a} = 2 (2 \alpha / \pi)^{1/2} \sigma_m$$

$$\frac{\lambda \eta v g h}{w/a} = \frac{4}{3} \left\{ \frac{2\alpha}{\pi} \right\}^{1/2} \sigma_m \quad (B.8)$$

now equations (B.7), (B.8) combine to give

$$\sigma_m = \sqrt{\{3G\mu\pi/(8\alpha)\}} \quad (B.9)$$

for the constant failure zone stress distribution and

$$\sigma_m = \sqrt{\{27G\mu\pi/(32\alpha)\}} \quad (B.10)$$

for the ramp failure zone stress distribution.

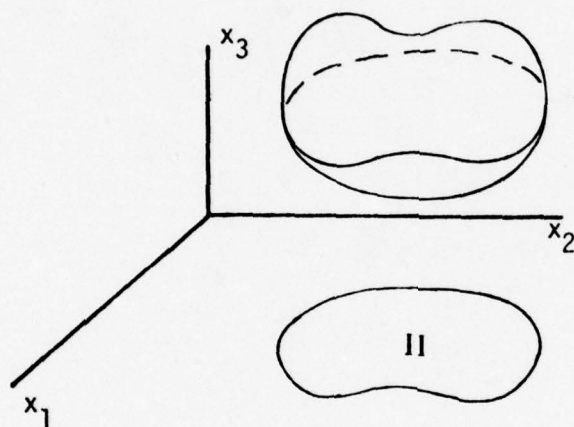
APPENDIX C

The Extended Divergence Theorem

Let Π be a closed region in R_2 whose boundary, $\partial \Pi$, is a rectifiable Jordan curve and let

$$\Omega = \{(x_1, x_2, x_3) | \psi(x_1, x_2) \leq x_3 \leq \phi(x_1, x_2), (x_1, x_2) \in \Pi\},$$

where $\psi, \phi \in C^1(\Pi)$. Further assume $\psi = \phi$ if and only if $(x_1, x_2) \in \partial \Pi$



Let S_1 and S_2 be the trace of the surfaces described respectively through

$$S_1(x) = x_1 e_1 + x_2 e_2 + \phi(x_1, x_2) e_3$$

$$S_2(x) = x_1 e_1 + x_2 e_2 + \psi(x_1, x_2) e_3$$

for all $(x_1, x_2) \in \Pi$

and let $S = S_1 \cup S_2$.

Theorem. (The Extended Divergence Theorem). Let Ω be a bounded regular region (hence a Lebesgue measurable set), and ϕ, u, σ a scalar, vector, and second-order tensor field, differentiable almost

everywhere on Ω with derivatives in $L^1(\Omega)$, then the results of the classical divergence theorem hold with the proper interpretations of the surface integral.

Proof

We need only consider Ω as defined in the preceeding paragraph, and will only show the proof for the two-tensor field σ as different order tensor fields are proved in a similar fashion.

Now Ω is a Lebesgue measurable subset of R ; therefore, by restricting μ , the Lebesgue measure on R_3 , to the measurable subsets of Ω , a new measure space is obtained in the obvious fashion; indeed, we may think of Ω as a product space and apply Fubini's Theorem to obtain

$$\int_{\Omega} \sigma_{i3,3} d\mu = \int_{\Pi} \int_{\psi(x_1, x_2)}^{\phi(x_1, x_2)} \sigma_{i3,3} d\lambda d\sigma$$

where λ is the Lebesgue measure on the line segment between $\phi(x_1, x_2)$ and $\psi(x_1, x_2)$ and σ the Lebesgue measure on Π . By Fubini's Theorem $\int_{\psi}^{\phi} \sigma_{i3,3}$ exists and is $L^1(\Pi)$ therefore

$$\int_{\Omega} \sigma_{i3,3} d\mu = \int_{\Pi} [\sigma_{i3}(x_1, x_2, \phi(x_1, x_2)) - \sigma_{i3}(x_1, x_2, \psi(x_1, x_2))] d\sigma$$

by the smoothness of S_i we obtain

$$\int_{\Omega} \sigma_{i3,3} d\mu = \int_{\Pi} \{(\sigma_{i3} \circ S_1) |J_{S_1}| - (\sigma_{i3} \circ S_2) |J_{S_2}|\} d\sigma.$$

Define the vector $\sigma_{i3} = (0, 0, \sigma_{i3})$ then by the convention established in the uniqueness chapter,

$$\int_{\Pi} (\sigma_{i3} \circ S_1) |J_{S_1}| = \int_{S_1} \sigma_i \cdot \vec{n}_1$$

and

$$-\int_{\Pi} (\sigma_{i3} \circ S_2) |J_{S_1}| = \int_{S_2} \sigma_i \cdot \hat{n}_2$$

where \hat{n}_1, \hat{n}_2 are the unit normals of S_1 and S_2 respectively, i.e..

$$\hat{n}_1 = \frac{D_1 S_1 \times D_2 S_1}{\|D_1 S_1 \times D_2 S_1\|} \quad \text{and} \quad \hat{n}_2 = \frac{D_1 S_2 \times D_2 S_2}{\|D_1 S_2 \times D_2 S_2\|}$$

The result follows.

ACKNOWLEDGMENTS

The author wishes to express his deep gratitude to his chairman and advisor, Dr. R. A. Schapery, for his guidance and understanding. Many thanks are also due Dr. T. J. Kozik, Dr. J. T. Tielking, Dr. L. B. Treybig, Dr. H. W. Pu, and Dr. P. W. Smith for their helpful suggestions and for examining the dissertation.

Additional acknowledgments are due Dr. G. S. Brockway of Bell Laboratories for answering many questions and giving helpful suggestions.

Acknowledgment is gratefully extended to Mr. G. E. Maddux of the AFFDL — Photomechanics Facility, Wright-Patterson AFG, Ohio for his constant help with the holographic equipment and experiments.

Further acknowledgment is given Dr. S. B. Raju and Dr. D. D. Hardin for their help with computer programming.

ON THE MECHANICAL BEHAVIOR OF SOLID PROPELLANT
UNDER TRANSIENT TEMPERATURES

R. A. Schapery

ABSTRACT

The effect of simultaneous cooling and straining on composite solid propellant is studied experimentally and theoretically. It is shown that the use of isothermal viscoelastic relaxation data and the linear viscoelastic theory for thermorheologically simple materials results in stresses which greatly underpredict the actual stresses in propellant under this important type of loading. An improved constitutive equation for predicting the mechanical response of propellant is then proposed. It is based on theoretical results obtained from non-equilibrium thermodynamics and a viscoelastic theory of microcrack growth. Some aspects of the calculated response are described and shown to be in qualitative agreement with experimental data. However, additional experimental results are needed in order to assess the accuracy and range of validity of the theory.

INTRODUCTION

Composite solid propellant consists of a viscoelastic rubber matrix which is highly filled with a broad size distribution of hard particles of ammonium perchlorate and aluminum; the volume percent filler is typically 75%. The weak rubber matrix together with high internal stress concentrations produced by the filler are largely responsible for causing highly nonlinear behavior over practically the entire range of service-induced stresses. Fortunately, there now exist verified engineering methods of characterizing and stress analyzing propellant in terms of "effective" linear properties for many types of loading [1]. Also, linear viscoelastic fracture mechanics has met with considerable success when the correct stresses are employed [2]. However, it is not yet possible to predict the correct stresses in rocket motors subjected to a large temperature drop with any reasonable degree of confidence. A few ad hoc methods exist for predicting stresses during cooling, but their accuracy is highly dependent on the strain and temperature history and the particular propellant investigated [1].

The magnitude of the discrepancy between linear theory and actual nonlinear nonisothermal behavior is not well-documented in the literature, and therefore we discuss this aspect of the problem in the next section. A generalized constitutive model, which is believed to correctly account for the main physical mechanisms of deformation, is then developed and discussed in the last section.

EXPERIMENTAL RESULTS

A series of biaxial tensile tests on 1/8" thick strip specimens, which are shown in Fig. 1, and uniaxial tensile tests was conducted

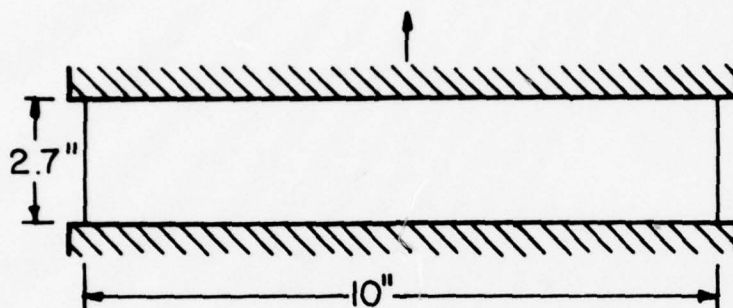


Figure 1. The strip-biaxial sample.

under the direction of Francis [3]. The specimens were subjected to the constant strain and cooling rates shown in Fig. 2; the rates were applied simultaneously in order to simulate the type of loading which is experienced by propellant when in a case-bonded motor under cooling conditions. The abscissa in Fig. 2 is a non-dimensional temperature defined as

$$\Delta T_n \equiv \frac{T_0 - T}{T_0 - T_a} \quad (1)$$

where T_0 is the initial temperature ($\approx 70^\circ\text{F}$), T is the instantaneous temperature and T_a is a constant ($\approx -145^\circ\text{F}$); ΔT_n is a parameter which is employed in the linear theory. The ordinate is the ratio of the experimentally derived engineering stress, σ , to the stress, σ_T , predicted from linear theory for a thermorheologically simple material.

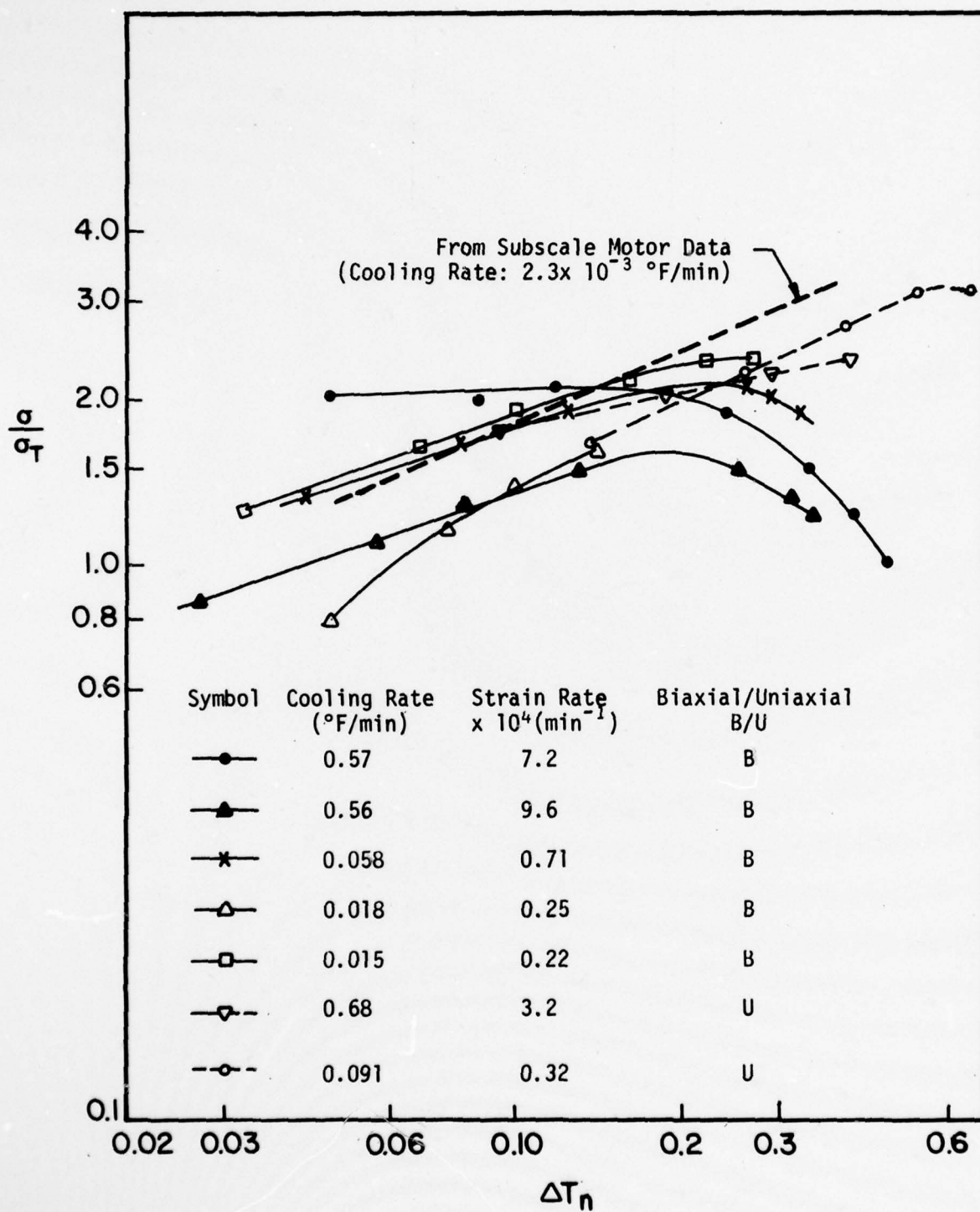


Figure 2. Ratio of experimental to predicted stresses in HTPB solid propellant under simultaneous cooling and straining.

Also shown in Fig. 2 is this stress ratio at the case bond line; the stress σ is an average quantity obtained from stress gages in small steel-cased motors (4.5 inch outside diameter x 24 inches long with approximately 1 inch diameter circular port).

The stress σ_T was calculated using the method in Section 5.5.3.3 of [1]. This method employs the uniaxial relaxation modulus $E = E(\xi)$ and time-temperature shift factor $a_T = a_T(T)$; $\xi \equiv t/a_T$ is "reduced time". The modulus and shift factor are shown in Fig. 3 and Fig. 4 respectively; the crack growth data cited in Fig. 4 are discussed in [2].

It is indicated in Fig. 3 that the relaxation modulus was obtained at a strain of 3%. Inasmuch as variable straining tests [3] revealed that the material is nonlinear at this strain level (by checking against the superposition principle), two other types of tests were conducted at Texas A&M to obtain the relaxation modulus. The duomorph test [4] consisted of placing a thin piezoelectric sandwich disc against a block of propellant and noting the effect of the propellant on vibrational bending strain; linear viscoelastic analysis yielded the relaxation modulus [4]. The other type of test consisted of resting long circular cylinders under constant load on the same block of material and observing the amount of time-dependent indentation; again, linear analysis yielded the desired modulus [5]. The average strains in the propellant for the duomorph and indentation tests were approximately 0.01% and 3%, respectively. The data from all three tests are in excellent agreement, as shown in Fig. 3. That the duomorph data were obtained at very small values of time at room temperature, and the fact that they agree out to the low temperature end ($\approx -65^\circ\text{F}$) of the relaxation modulus, serves as

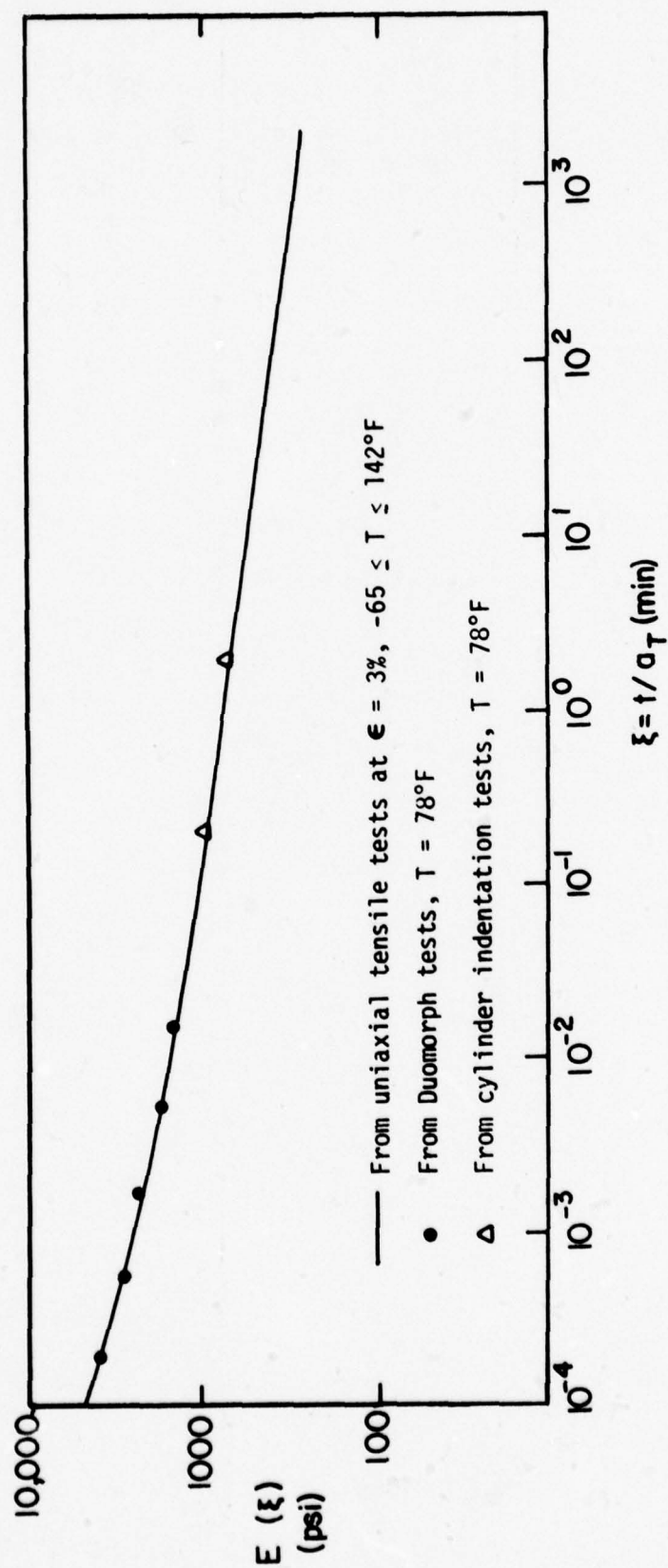


Figure 3. Uniaxial relaxation modulus of HTPB propellant.

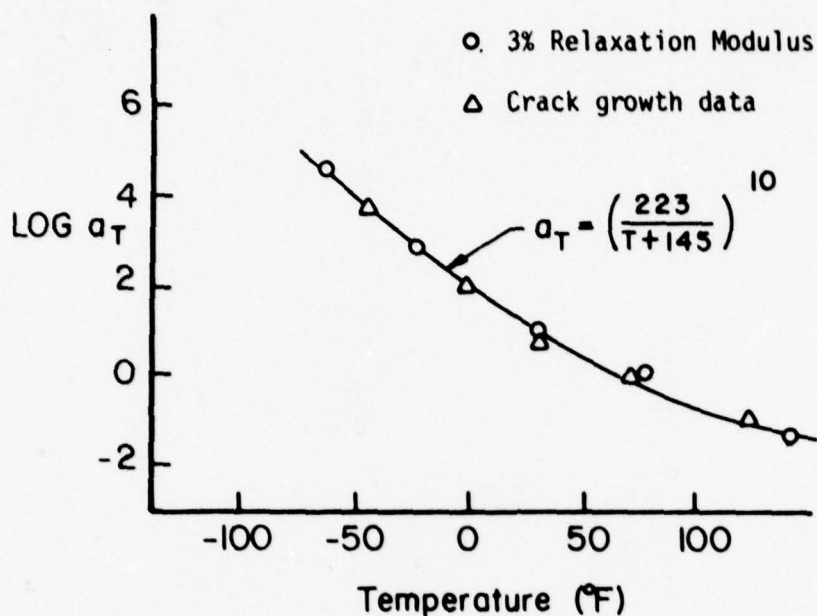


Figure 4. Shift factor for HTPB propellant.

a direct check on the validity of the shift factor in Fig. 4. This agreement between the results of all three tests is very surprising; but it can be "explained" by using the constitutive equation discussed in the next section.

Returning to Fig. 2, it is seen that the experimentally obtained stress greatly exceeds the predictions. There appears to be considerable specimen - to - specimen property variation (cf. the first two tests in the table), but it is clearly not sufficient to account for the discrepancy between theory (σ_T) and experiment (σ).

We shall discuss next a constitutive equation which is believed to be sufficient for removing this difference.

A CONSTITUTIVE EQUATION FOR TRANSIENT TEMPERATURES

Let us first consider a linear, uniaxial stress-strain equation for a special type of thermorheologically complex behavior [6], which was originally derived from thermodynamic principles:

$$\sigma = a_G \int_0^t E(\xi - \xi') \frac{d\xi}{d\tau} d\tau \quad (2)$$

where

$$\xi = \xi(t) \equiv \int_0^t dt' / a_T \quad , \quad \xi' \equiv \xi(\tau) \quad (3)$$

(Note that the reduced time ξ reduces to that used in Fig. 3 for constant temperature.) Also ϵ_σ is the total strain less that due to thermal expansion,

$$\epsilon_\sigma = \epsilon - \alpha(T - T_0) \quad (4)$$

where α is the expansion coefficient, and $a_G = a_G(T)$ is a temperature-dependent material function. If one were to use a mechanical model consisting of springs and dashpots to represent Eq. (2), it can be easily shown that all of the spring moduli would be proportional to a_G and all of the dashpot viscosities would be proportional to the product $a_T a_G$. If $a_G = 1$ these moduli are independent of temperature, and Eq. (2) reduces to the constitutive equation for a thermorheologically simple material.

For an isothermal relaxation test, Eq. (2) becomes

$$\sigma = a_G E(\xi) \epsilon_\sigma \quad (5)$$

where $\xi = t/a_T$. If we assume that

$$E(\xi) = E_1 \xi^{-n} \quad (6)$$

where E_1 and n are constants, then Eq. (5) can be written as

$$\sigma = E(\hat{\xi}) \epsilon_\sigma \quad (7)$$

where

$$\hat{\xi} \equiv t/(a_T a_G^{1/n}) \quad (8)$$

Thus, as observed previously [6], if one obtains experimental values of the relaxation modulus, σ/ϵ_σ , at different temperatures, the standard procedure of shifting data to obtain a master curve will yield only a composite shift factor, $a_c \equiv a_T a_G^{1/n}$; thus, for power law materials, isothermal data are not sufficient to evaluate all material functions in Eq. (2). On the other hand for many transient temperature conditions, such as a constant cooling rate, one finds that the stress, Eq. (2), is sensitive to the values of a_G and a_T separately; therefore, nonisothermal testing may be employed to complete the characterization.

These observations are highly relevant to solid propellant since its modulus can be approximated by a power law over a wide range of reduced time; e.g., the slope of the log-log plot in Fig. 3 is a very weak function of ξ . Furthermore, a study of Eq. (2) reveals that it is possible to select functions a_G for which $\sigma/\sigma_T \gg 1$ by letting a_G

increase with decreasing temperatures; this can be achieved without difficulty without affecting the isothermal behavior. We conclude, therefore, that at least a portion of the discrepancy between experiment and the commonly used theory (i.e. $a_G = 1$) may be due to a type of thermorheological complexity for which elastic moduli increase as the material is cooled.

This type of generalization is apparently not sufficient since the stress ratio in Fig. 2 varies with the straining and cooling rates; some of the differences between the curves is due to material variability, as discussed above, but probably not all. Also, as noted previously, isothermal tests reveal that the material is nonlinear.

A significant if not major portion of this nonlinear behavior may be due to microcracking [7,8]. Here we shall draw upon the model developed in [9] in order to incorporate this phenomenon in the nonisothermal constitutive theory. From [9], as generalized by means of Eq. (2),

$$\epsilon_\sigma = \int_0^t D(\xi - \xi') \frac{d(\sigma F/a_G)}{d\tau} d\tau \quad (9)$$

where $D(\xi)$ is the uniaxial creep compliance, and for a non-aging material F is a function of the "damage" parameter

$$S_0 \equiv \int_0^\xi \sigma^q d\xi \quad (10)$$

where q is a positive constant. The microstructure serves to define F through the distribution of initial stress intensity factors for the microflaws and their softening effect during growth; however, in practice, F can be found from experimental stress-strain data. It is shown

in [9] that $dF/dS_0 > 0$ in view of its relation to the microcracking.

Each microcrack was assumed to obey the growth rate equation,

$$\frac{da}{d\xi} = AK_I^q \quad (11)$$

where A and q are positive constants, and K_I is the opening mode stress intensity factor.

Equation (9) may be inverted exactly to find

$$\sigma = \frac{a_G}{F} \int_0^t E(\xi - \xi') \frac{d\epsilon_\sigma}{d\tau} d\tau \quad (12)$$

Thus, we see that Eq. (2) is contained in nonlinear Eq. (12).

One further generalization of Eq. (2) will be made to account for the effect of strain on Eq. (11). Specifically, Eq. (11) was found to apply to macrocracks if a retarding effect of tensile strain is incorporated in the form [2],

$$\frac{da}{d\xi} = A(K_I/f)^q \quad (13)$$

where $f = f(\epsilon_\sigma)$ is an increasing function of overall specimen strain; for a large amount of data it was found that

$$f = \begin{cases} C \epsilon_\sigma^\beta, & 0 < \epsilon_\sigma < 0.085 \\ \text{constant}, & \epsilon_\sigma > 0.085 \end{cases} \quad (14)$$

where $\beta \approx 0.7$. It will be assumed that strain affects microcrack growth in the same way, and therefore f must be included in the constitutive theory. A review of the derivation in [9] shows that the only modification needed is the replacement of S_0 by the more general damage parameter,

$$S \equiv \int_0^{\xi} \left(\frac{\sigma}{F} \right)^q d\xi \quad (15)$$

So far we have discussed Eq. (9) as if it were limited to uniaxial tensile loading of a specimen containing only opening-mode cracks. However, our results are actually more general than this. Specifically, if proportional loading exists and if mixed-mode crack growth obeys an equation of the same form as Eq. (13), but with K_I^q replaced by any homogeneous function of the three stress-intensity factors, then Eq. (2) still applies. In this more general case, ϵ_0 and σ may be interpreted as the maximum principal strain and stress, respectively, and $E(\xi)$ is the linear viscoelastic relaxation modulus for the particular ratio of principal stresses under consideration. (This interpretation will be used in the rest of the analysis.) The function F is also dependent on the stress ratios; but, for given ratios, $F = F(S)$ and $dF/dS > 0$. Proportional loading may not be exactly satisfied for the strip geometry in Fig. 1, but because the lateral strain vanishes, the results apply to this problem. Of course, there is no basis for assuming F is the same for uniaxially stressed bar and strip specimens.

Let us now rewrite Eq.(12) in a more useful form by solving for stress in terms of strain and temperature history. First, define

$$\sigma_\ell \equiv \int_0^t E(\xi - \xi') \frac{d\epsilon_\sigma}{d\tau} d\tau \quad (16)$$

which is the stress for a linear viscoelastic, thermorheologically simple material. Also, define the ratio,

$$R \equiv \sigma_\ell / \sigma \quad (17)$$

Introduce Eqs. (16) and (17) in Eq. (12) and then solve for S ,

$$S = G(\lambda) \quad (18)$$

where, by definition,

$$\lambda \equiv Ra_G \quad (19)$$

and G is the inverse of F ; viz. $F(G(\lambda)) = \lambda$. Now, differentiate Eq. (18) with respect to ξ and introduce the definition,

$$S_\ell \equiv \int_0^\xi \left(\frac{\sigma_\ell a_G}{f} \right)^q d\xi \quad (20)$$

After rearrangement and integration we find

$$S_\ell = \int_1^\lambda \lambda^q \frac{dG}{d\lambda} d\lambda \quad (21)$$

where, without loss in generality, we have normalized a_G such that $a_G(T_0) = 1$; also, use of the fact that $F = 1$ without damage ($S = 0$) has been made. In view of the definition of G , it follows that

$$\frac{dG}{d\lambda} = \left(\frac{dF}{dS} \right)^{-1} > 0 \quad (22)$$

and $\lambda \geq 1$. Solve Eq. (21) for $\lambda = \lambda(S_\ell)$ and then use Eqs. (17) and (19) to find

$$\sigma = \frac{a_G}{F_\ell} \sigma_\ell \quad (23)$$

where $F_\ell = F_\ell(S_\ell)$ and $dF_\ell/dS_\ell > 0$.

Equation (23) is the desired result as it expresses the stress in terms of the strain and temperature histories; these histories appear in Eqs. (16) and (20). The function $F_\ell(S_\ell)$ is directly related to the initial microstructural state of the material; it is to be found by applying Eq. (23) to experimental data rather than carrying out detailed calculations from microstructural information. We should add that on the basis of some existing data the function f was assumed to be a function of applied strain but not of temperature [2]. If, however, the shift factor for microcracks is different from that for overall mechanical behavior and/or if a function analogous to a_G is used in the prediction of crack speed from creep compliance information [9], then f will depend on temperature. Consequently, for the sake of generality, we shall suppose $f = f(\epsilon_\sigma, T)$.

Let us now discuss the previously reported experimental data in light of Eq. (23). First introduce the secant moduli,

$$E_n \equiv \sigma/\epsilon_\sigma, \quad E_\ell \equiv \sigma_\ell/\epsilon_\sigma \quad (24)$$

and obtain

$$E_n = \frac{a_G}{F_\ell} E_\ell \quad (25)$$

Now, if $f \sim \epsilon_\sigma$, Eqs. (20) and (25) show that the nonlinear secant modulus E_n is a function of the history of E_ℓ but is independent of the strain level. Thus, for example, the relaxation modulus is predicted to be independent of strain even though the material is nonlinear; this behavior often exists for solid propellant at small strains. Also, for a constant amount of softening due to damage (i.e. $F_\ell = \text{constant}$),

Eq. (25) shows that linear viscoelastic modulus interrelationships apply to the nonlinear modulus, which was found to be true for the HTPB propellant (cf. Fig. 3). This type of behavior will exist, at least as an approximation, if there is a range for which F_ℓ is a weak function of damage (i.e., a range for which there is a negligible or only a small change with the number and size of microcracks). For this situation the ratio of the measured relaxation modulus to the linear viscoelastic modulus is constant. The modulus in Fig. 3, for example, would then be a constant fraction of the true linear modulus. Inasmuch as σ_T (cf. Fig. 2) was calculated using the data in Fig. 3, we conclude that $\sigma_\ell/\sigma_T = K$, where $K \geq 1$ is a constant. The theory, Eq. (23), corresponding to Fig. 2 then is written

$$\frac{\sigma}{\sigma_T} = \frac{a_G K}{F_\ell} \quad (26)$$

If the softening due to damage were the same for all data in both Figs. 2 and 3, we would have $\sigma/\sigma_T = a_G$; the spread in the data in Fig. 2 would then be due solely to material variability, and all dependence on temperature could be attributed to a_G . On the other hand, F_ℓ is probably not constant and, in fact, is believed to be the cause of the decrease in some of the data in Fig. 2 at large values of ΔT_n . Most of the propellant in the subscale motor is at relatively very low distortion, and for this case S should exhibit much less of an increase than for the strip tests; this observation is consistent with the data in Fig. 2.

Another interesting phenomenon is observed when a tensile bar of solid propellant is held at a constant, positive strain for a period of time and then cooled at a constant rate: the rate of stress

increase is often much greater than when the strain is zero [3]. This behavior is predicted by Eq. (23) if the factor a_G increases significantly with decreasing temperature. Furthermore, the data from such tests are very useful for obtaining this material function. Indeed, various data are now being generated by Francis [3] in order to establish both functions a_G and F_ℓ and check the predictions of the constitutive equation (23).

REFERENCES

- [1] Anon, JANNAF Solid Propellant Structural Integrity Handbook, CPIA Pub. No. 230 (Sept. 1972).
- [2] R. A. Schapery, "Fracture Mechanics of Solid Propellants," Proc. ONR Int. Symposium on Fracture Mechanics, George Washington Univ., (Sept., 1978).
- [3] E. C. Francis, "Predictive Techniques for Failure Mechanisms in Solid Rocket Motors," Contract No. F04611-75-C-0027 with United Technologies, Chemical Systems Division.
- [4] R. A. Schapery, "Analysis of the Duomorph Gage," Section 4 in Design and Test of the Operational In-situ Gage for Solid Propellant Surveillance, Air Force Report No. AFRPL 1064-26-F (June 1976).
- [5] K. Y. Chan, "The Development of a Cylindrical Indentor Test Apparatus for the Determination of Linear Viscoelastic Properties," M.S. Thesis, Texas A&M University, August 1978.
- [6] R. A. Schapery, "Viscoelastic Behavior and Analysis of Composite Materials," Mechanics of Composite Materials, Vol. 2, G.P. Sendeckyj, ed., Academic Press, New York, 1974, pp. 85-168.
- [7] L. R. Cornwell, and R. A. Schapery, "SEM Study of Microcracking in Strained Solid Propellant," Metallography, 8, 1975, pp. 445-452.
- [8] R. J. Farris, "The Influence of Vacuole Formation on the Response and Failure of Highly Filled Polymers," Trans. Soc. Rheol., 12., 1968, pp. 315-334.
- [9] R. A. Schapery, "A Nonlinear Constitutive Theory for Particulate Composites Based on Viscoelastic Fracture Mechanics," Proc. of JANNAF Structures & Mechanical Behavior Working Group, 12th. Meeting, Jan. 1974, CPIA Publication No. 253.

SOME VISCOELASTIC CRACK GROWTH RELATIONS FOR ORTHOTROPIC
AND PRESTRAINED MEDIA*

by G. S. Brockway and R. A. Schapery

ABSTRACT

Equations are developed for predicting opening and sliding modes of crack growth along planes of geometric symmetry in viscoelastic orthotropic media with and without large prestrains. Except for the small failure zone at the crack-tip, the material is assumed to be linearly viscoelastic with respect to the changes in stress and strain which occur during crack propagation. For an orthotropic body in plane strain, an observation of Biot relating the Fourier transformed tractions and displacements on the surface of any homogeneous, elastic half-space is used in conjunction with Graham's extended correspondence principle to generate the viscoelastic crack face displacements. Application of a suitable energy criterion for failure leads to a nonlinear integro-differential equation for the crack tip speed in terms of material and loading parameters. The resulting equation is of the same generic form as in the previously published isotropic case except that the isotropic creep compliance is replaced by effective compliances formed from orthotropic moduli. Thus, just as in the isotropic case, a much simpler, approximate crack growth rate equation is deduced from the assumption these effective

*Published originally as Texas A&M Univ. Rept. No. MM-3064-75-3 (AFOSR TR-76-1148) 1975; to be published in Engineering Fracture Mechanics, 1978.

compliances have small curvature when plotted logarithmically against logarithmic time. Included is a numerical sample using constitutive properties of a fiber-reinforced plastic. Extension to fracture of prestrained media and crack growth between certain types of dissimilar media is then made. Again the growth equations have the same basic form, but for a prestrained medium the effective compliances involve the incremental moduli. The results indicate that crack growth is accelerated for initial compressive stress states that create certain surface instabilities ahead of the crack tip. Finally, it is argued that these crack velocity relations can be employed in plane stress problems and in many three-dimensional cases, and, with a small change, can be used to predict the time of fracture initiation.

CONCLUSIONS

Equations for predicting crack growth in opening and sliding modes in orthotropic media have been developed. Although the emphasis was on homogeneous, orthotropic media in plane strain, it was shown that for the opening mode these crack growth relations carry over without change to three-dimensional problems if the material is isotropic in the crack plane. The relations were also extended to problems involving crack propagation between certain types of dissimilar orthotropic media.

Furthermore, by means of an argument analogous to that used previously for isotropic media, one can show that the plane-strain crack growth relations apply even when the global state of the body is one of plane stress; it is only necessary that the failure zone be small enough for the neighborhood of the crack-tip to be in plane strain. The

assumption of crack plane isotropy is not needed.

Except for a small modification, it was demonstrated that the crack growth relations in terms of incremental properties apply to homogeneously prestrained media if linearity exists with respect to the incremental stresses and strains. Although no theoretical limits were placed on the magnitudes of the initial strains, we did assume that the initial maximum shear stress was, at most, of the same order of magnitude as the incremental stresses associated with crack propagation. Allowing for large initial strains, while limiting the initial shear stress and incremental strains, are not necessarily incompatible conditions with viscoelastic materials which undergo cracking. Consider, for example, the situation in which the body is strained very slowly and assume that crack growth does not occur until the strains are quite large and possibly considerable material nonlinearity is exhibited. Then, suppose that the crack grows during an interval of time which is small relative to the time of application of the externally applied strains. The incremental strains associated with the unloading process of crack propagation will be relatively small (except possibly for the material very close to the crack-tip) if these two time scales are far apart and the body is highly viscoelastic; as just one application, we believe these requirements are quite realistic in certain situations encountered with solid propellant rocket fuel.

A THEORY OF TIME-DEPENDENT BONDING
FOR VISCOELASTIC MEDIA*

by R. A. Schapery

ABSTRACT

A theory is developed for the prediction of time-depending bonding of surfaces of similar or dissimilar linear viscoelastic materials. Starting with an extended correspondence principle, viscoelastic stresses and displacements in the neighborhood of a moving contact edge are derived. These results are then employed in a local energy balance which leads to an equation for predicting the rate of bonding as a function of the local displacement intensity factor. A comparison of true and apparent energies for bonding and fracture is made. Finally, criteria are given for determining whether or not bonding can occur, and then the prediction of the time required for complete bonding or healing of cracks is examined.

CONCLUSIONS

A theory of time-depending bonding has been developed which, in certain respects, is described by relations which are similar to those of time-dependent fracture. As one particular result, it was shown that the apparent or pseudo fracture energy, which is dependent on the speed

*Published as Texas A&M Univ. Rept. No. MM 3064-76-4 (AFOSR TR-76-1148) 1976.

of the crack, is typically much larger than the speed-dependent pseudo energy of bonding. Additionally, criteria for bonding or crack healing were derived and compared with the conditions under which crack growth occurs.

A simple extended correspondence principle was employed in the development of the theory which permitted the direct use of elasticity solutions in predicting viscoelastic stresses and displacements. Although this principle limits us to certain types of boundary conditions, it is believed the theory is applicable to a large number of practical problems dealing with microcrack healing in composites and adhesion phenomena.

A METHOD FOR PREDICTING CRACK GROWTH IN
NONHOMOGENEOUS VISCOELASTIC MEDIA*

by R. A. Schapery

ABSTRACT

Equations are developed for predicting crack growth in the opening mode for quite general situations, including many quasi-static and dynamic problems involving moisture and temperature gradients in monolithic and composite materials. Except for the small zone of failing material at the crack tip, the body is assumed to be linearly viscoelastic. A method for obtaining viscoelastic stresses and displacements from elastic solutions is first described. The traction boundary condition for the crack faces is not in general satisfied by these results. However, it is shown that by modifying the failure zone this condition can be met. An integral equation for the stress in the modified failure zone is then derived. Approximate analysis similar to that used previously by the author in stress analysis is then employed to solve the integral equation and develop relatively simple equations for predicting crack speed; these equations relate crack speed to the stress intensity factor in a suitably defined elastic body.

*Published originally in Proceedings of Conference - Environmental Degradation of Engineering Materials, Oct. 10-12, 1977, College of Engineering Virginia Tech; to be published in Int. J. Fracture, 1978.

CONCLUSIONS

The problem of predicting crack speed in nonhomogeneous viscoelastic bodies has been reduced to quasi-elastic analysis through a series of approximations. The primary result is analogous to that derived previously for situations in which the stress intensity factor is independent of compliance. For composite materials and/or when the viscoelastic properties vary throughout the body (due to, for example, moisture and temperature) the speed controlling compliance $C_v(t_\alpha)$ is that for the material in the neighborhood of the crack tip. Through a proper selection of this compliance the present results will apply to cohesive cracks in locally isotropic media and to cohesive and adhesive cracks in certain locally isotropic and orthotropic media.

The far-field viscoelastic properties affect crack growth through the quasi-elastic stress intensity factors $K_I^e(t_\alpha)$ and $K_I^e(3t_\alpha)$; these factors are the instantaneous values for an elastic material having the applied loads defined in the paper and compliances equal to viscoelastic creep compliances which are evaluated at the "local" times t_α and $3t_\alpha$.

The functions C_v and K_I^e may depend on actual time t in addition to local time t_α , although the former time-dependence is not explicitly shown in these results. This dependence on actual time may, for example, be due to changes in applied loads, temperature, and moisture and/or changes in crack size and speed. However, any changes which do occur should be small during the time required for the crack to propagate a distance of approximately five to ten times the length of the failure zone, a ; further study is needed to determine the effect of relaxing this condition.

Inertia effects associated with very high crack speed have been neglected in the development of explicit results. It is anticipated, however, that effects of high speed can be taken into account using the procedure described herein because the dynamic crack-tip stress field for an elastic material is completely characterized by a time-dependent stress intensity factor.

The present analysis enables one to use experimental crack growth data, $\dot{a} = \text{function}(K_I^e)$, obtained with special loading histories and uniform temperature and moisture conditions, in the prediction of growth in complex structures under quite general loading histories and nonuniform conditions. However, in contrast to problems for which K_I^e does not depend on compliances, the size of the failure zone α is explicitly needed because it affects the value of the stress intensity factor.